DESIGN OF TANDEM SOLAR CELL TO ENHANCE THE CONVERSION EFFICIENCY USING FDTD SIMULATION

by

Al-Amin Patwarty

16321155

Mohammad Ahmed Feroz

16221055

Salik Bin Saif

17121019

Supervised by Dr. Abu S.M. Mohsin Assistant Professor

Department of Electrical and Electronic Engineering, Brac University, Dhaka.

A thesis submitted to the Department of Electrical and Electronic Engineering in partial fulfillment of the requirements for the degree of Bachelor of Science in Electrical and Electronic Engineering.

Department of Electrical and Electronic Engineering

BRAC University

January, 2021

© 2021. BRAC University

All rights reserved.

Declaration

It is hereby declared that

1. The thesis submitted is our own original work while completing degree at Brac University.

2. The thesis does not contain material previously published or written by a third party, except where this is appropriately cited through full and accurate referencing.

3. The thesis does not contain material which has been accepted, or submitted, for any other degree or diploma at a university or other institution.

4. We have acknowledged all main sources of help.

Student's Full Name & Signature:

Al-Amin Patwary
16321155

Mohammad Ahmed Feroz
16221055

Salik Bin Saif
17121019

Approval

The thesis/project titled "Design Of Tandem Solar Cell To Enhance The Conversion Efficiency Using FDTD Simulation" submitted by

1. Al-Amin Patwary (16321155)
2. Mohammad Ahmed Feroz (16221055)
3. Salik Bin Saif (17121019)

of Fall, 2020 has been accepted as satisfactory in partial fulfillment of the requirement for the degree of Bachelor of Science in Electrical and Electronic Engineering on 13th of January.

Examining Committee:

Supervisor:
(Member)

____

Dr. Abu S.M. Mohsin, PhD
Assistant Professor, Department of Electrical and Electronic Engineering
BRAC Univeristy

Program Coordinator:
(Member)

____

Dr. Abu S.M. Mohsin, PhD
Assistant Professor, Department of Electrical and Electronic Engineering
BRAC University

Head of Department:
(Chair)

____

Dr. Md. Mosaddequr Rahman, PhD
Professor and Chairperson, Department of Electrical and Electronic Engineering
BRAC University

Executive Summary

One of the major problem the world is facing today is the scarcity of the resources to produce electrical energy using non-renewable resources. To overcome this limitation, renewable energy sources such as solar energy are the best alternative. Hence, solar cells are used to convert this bulk amount of energy into electrical energy. The maximum efficiency obtained for a six-junction III-V tandem solar cell is around 47%. However, to obtain the mentioned efficiency is costly as the fabrication process is complex. Therefore, a two-junction III-V tandem solar cell is designed with Indium Phosphide (InP) as the base material. This design would be much simpler as there are less materials used and the complexity is thus reduced. The research consisted of couple of finite difference time domain (FDTD) simulations to analyze the optical properties by changing the physical parameter like varying the material of the substrate (GaAs/InP). Upon getting the best results, the proposed model is constructed which an improved absorption due to the material has used. Besides, the CHARGE simulation also yielded better current density of 39.1479 mA/cm2 and an increased conversion efficiency of 36.9373 %.

Dedication

Dedicated to our parents and supervisor, Dr.Abu S.M. Mohsin who diligently guided us all throughout the entire research process.

Acknowledgement

In the first place, we express our innermost gratefulness to the Almighty Allah for the good health and well-being which was necessary to work and complete this thesis book. Despite of many obstacles due to COVID-19, and unfavorable situation to meet with group members physically, we overcome the difficulties and adapt the new way of working. We would like to thank and express sincere appreciation to our supervisor Dr. Abu S.M. Mohsin, Assistant Professor, Department of Electrical and Electronic Engineering at Brac University, for constant support, motivation, sharing his knowledge and giving an excellent hand in guiding. We are grateful to Sir for recommending us this growing area to explore and work on it. He supported us to think critically and trained us to work professionally. We would like to express our deepest gratitude and dedicate our work to our beloved parents who gave steady support mentally and financially, and provided thorough understanding into our study.

Table of Contents

Declaration **i**

Approval **ii**

Executive Summary **iii**

Dedication **iv**

Acknowledgment **v**

Table of Contents **vi**

List of Figures **ix**

List of Tables **xiii**

List of Acronym **xiv**

1 Introduction **1**

1.1 Introduction 1

1.2 The motivation and challenges of this work 1

1.3 Literature review 2

1.4 Semiconductor junction 3

1.5 Solar cell operation 6

1.5.1 Structure 7

1.6 General and optical features 10

1.6.1 General Property of Indium Phosphide (InP) 10

1.6.2 Optical Properties of Indium Phosphide (InP) 11

1.7 Doping 13

1.8 Spectral and theoretical efficiency 15

1.8.1 Spectral efficiency 15

1.8.2 Theoretical efficiency 16

1.9 The history of solar cells 17

1.9.1 Different type of solar cells 18

1.10 Objective and Methodology 24
1.11 Thesis layout 25
1.12 Conclusion 28

2 Theory 29

2.1 Introduction 29
2.2 Light trapping 29
2.3 Doping Mechanism 30
2.4 Theoretical study of optical and electrical quantities 32
2.4.1 Optical Simulation 34
2.4.2 Electrical simulation 36
2.5 Fundamental of FDTD and CHARGE 39
2.5.1 FDTD 39
2.5.2 Implementing FDTD technique 41
2.5.3 CHARGE 42
2.5.4 Implementing CHARGE technique 44
2.6 Simulation road-map 45
2.7 Conclusion: 47

3 Aluminium Gallium Arsenide ($Al_xGa_{(1-x)}As$)/Gallium Arsenide ($GaAs$) Tandem Solar Cell 48

3.1 Introduction 48
3.1.1 Background study of GaAs Tandem Solar Cell 49
3.2 Modeling and Simulation 49
3.2.1 FDTD Model 49
3.2.2 Device Model 52
3.3 Optical simulation 53
3.3.1 Introduction 53
3.3.2 Results and Discussions 54
3.4 Electrical Simulation 57
3.4.1 Introduction 57
3.4.2 Results and Discussions 57
3.5 Comment and Conclusion 68

4 Aluminium Gallium Arsenide ($Al_xGa_{(1-x)}As$)/Indium Phosphide (InP) Tandem Solar Cell 70

4.1 Introduction 70

4.1.1 Background study of InP Tandem Solar Cell 70
4.2 Modeling and Simulation 71
4.2.1 FDTD Model 71
4.2.2 DEVICE Model 74
4.3 Optical simulation 75
4.3.1 Introduction 75
4.3.2 Result and discussion 76
4.4 Electrical simulation 79
4.4.1 Introduction 79
4.4.2 Result and discussion 79
4.5 Comment and conclusion 90

5 Thesis Findings 92

5.1 Introduction 92
5.2 Comparison of GaAs and InP TSC 92
5.3 Results and Discussions 96
5.3.1 Results from Optical Simulation 96
5.3.2 Results from Electrical Simulation 100
5.4 Conclusion 113

6 Conclusion and Future Work 114

6.1 Introduction 114
6.2 Thesis Summary 114
6.3 Challenges 115
6.4 Future Work 116

Bibliography 120

List of Figures

1.1 A circuit diagram of solar cell including shunt and series resistance. . 9
1.2 I-V and P-V curve of a solar cell. 9
1.3 Refractive index and Photon Energy (eV) of InP. 12
1.4 Absorption Coefficient of InP. 12
1.5 Reflection coefficient (r) of InP. 13
1.6 Reflectance (R) of InP. 13
1.7 “n-type” semiconductor. 14
1.8 “p-type” semiconductor. 15
1.9 Process of Transmission and Thermalization. 16
1.10 Theoretical efficiency vs Bandgap energy. Shockley-Queisser limit for the efficiency of solar cell. 17
1.11 The evolution and the conversion efficiency of the different generations of solar cells since 1976. 18
1.12 Monocrystalline silicon solar cell and Polycrystalline solar cell sample. 19
1.13 CdTe panel sample (left) and an amorphous silicon cell panel (right). 20
1.14 Absorption and loss of solar spectrum in a multi-junction solar cell. . 21
1.15 Schematic design of monolithic and tandem solar cell devices. (a)- Monolithic tandem device and (b) - Stacked tandem device. 22
1.16 Organic solar panel sample. 23
1.17 Perovskite solar panel sample. 24
1.18 Dye-sensitized solar panel sample. 24
1.19 The thesis layout. 27

2.1 Doping concentration. 31
2.2 Energy-band diagram of a PV cell. 32
2.3 Grid cell, considering for solving field components. 40
2.4 Simulation road-map. 46

3.1 Efficiency vs Band-gap of a single junction solar cell.[24] 49
3.2 2D Design of GaAs TSC. 50
3.3 FDTD 2D Planar GaAs TSC design. 51
3.4 FDTD 3D Planar GaAs TSC design. 51
3.5 DEVICE 2D Planar GaAs TSC design. 52
3.6 DEVICE 3D Planar GaAs TSC design. 53
3.7 Absorption per unit volume vs Wavelength for GaAs. 54
3.8 Total Absorption per unit volume vs Wavelength for GaAs. 55
3.9 Current density (J_{SC}). 55
3.10 Absorption enhancement factor. 56
3.11 Generation Rate. 56
3.12 Current density vs Voltage for shadow less. 58
3.13 Efficiency vs Voltage for shadow less. 58
3.14 Total Absorption per unit volume vs Wavelength for GaAs. 59
3.15 Current density vs Voltage with shadow loss. 60
3.16 Efficiency vs Voltage with shadow loss. 60
3.17 Current density vs Voltage when trap-assisted is disabled. 61
3.18 Efficiency vs Voltage when trap-assisted is disabled. 61
3.19 Current density vs Voltage with trap-assisted re-enabled. 62
3.20 Efficiency vs Voltage with trap-assisted re-enabled. 62
3.21 Recombination rate (Radiative, Auger, and Trap-Assisted) vs depth. . 63
3.22 Current density vs Voltage with RSE enabled. 63
3.23 Efficiency vs Voltage with RSE enabled. 64
3.24 Current density vs Voltage with a decrease in radiative recombination rate. 65
3.25 Efficiency vs Voltage with a decrease in radiative recombination rate. 65
3.26 Comparison of Current Density vs Voltage. 66
3.27 Comparison of Efficiency vs Voltage. 67
3.28 Result obtained for different simulation settings. 68

4.1 Efficiency vs Band-gap of a single junction solar cell. 71
4.2 2D Design of InP TSC. 72
4.3 FDTD 2D Planar InP TSC design. 73
4.4 FDTD 3D Planar InP TSC design. 73

4.5 DEVICE 2D Planar InP TSC design. 74
4.6 DEVICE 3D Planar InP TSC design. 75
4.7 Absorption per unit volume vs Wavelength for InP. 76
4.8 Total Absorption per unit volume vs Wavelength for InP. 77
4.9 Current density (J_{SC}). 77
4.10 Absorption enhancement factor. 78
4.11 Generation Rate. 78
4.12 Current density vs Voltage for shadow less. 80
4.13 Efficiency vs Voltage for shadow less. 80
4.14 Band structure monitor. 81
4.15 Current density vs Voltage with shadow loss. 82
4.16 Efficiency vs Voltage with shadow loss. 82
4.17 Current density vs Voltage when trap-assisted is disabled. 83
4.18 Efficiency vs Voltage when trap-assisted is disabled. 83
4.19 Current density vs Voltage with trap-assisted re-enabled. 84
4.20 Efficiency vs Voltage with trap-assisted re-enabled. 84
4.21 Recombination rate (Radiative, Auger, and Trap-Assisted) vs depth. . 85
4.22 Current density vs Voltage with RSE enabled 85
4.23 Efficiency vs Voltage with RSE enabled. 86
4.24 Current density vs Voltage with a decrease in radiative recombination rate. 87
4.25 Efficiency vs Voltage with a decrease in radiative recombination rate. 87
4.26 Comparison of Current Density vs Voltage. 88
4.27 Comparison of Efficiency vs Voltage. 89
4.28 Result obtained for different simulation settings. 90

5.1 Power absorbed when GaAs is the base material. 96
5.2 Power absorbed when InP is the base material. 96
5.3 Total power absorbed for GaAs and InP. 97
5.4 Short-Circuit Current Density for GaAs and InP. 98
5.5 Absorption Enhancement Factor for GaAs. 99
5.6 Absorption Enhancement Factor for InP. 99
5.7 Exported Generation Rate for GaAs. 100
5.8 Exported Generation Rate for InP. 100

5.9 Current-Density vs Voltage for GaAs and InP. 101
5.10 Efficiency vs Voltage for GaAs and InP. 102
5.11 Band Structure for GaAs. 102
5.12 Band Structure for InP. 103
5.13 Current Density vs Voltage for GaAs and InP. 103
5.14 Efficiency vs Voltage for GaAs and InP. 104
5.15 Current Density vs Voltage for GaAs and InP when Trap-Assisted is disabled. 105
5.16 Efficiency vs Voltage for GaAs and InP when Trap-Assisted is disabled. 105
5.17 Current density vs Voltage for GaAs and InP with Trap-Assisted re-enabled. 106
5.18 Efficiency vs Voltage for GaAs and InP with Trap-Assisted re-enabled. 106
5.19 Recombination rate (Radiative, Auger, and Trap-Assisted) vs depth for GaAs. 107
5.20 Recombination rate (Radiative, Auger, and Trap-Assisted) vs depth for InP. 108
5.21 Current Density vs Voltage for GaAs and InP with RSE enabled. . . 109
5.22 Efficiency vs Voltage for GaAs and InP with Rse enabled. 109
5.23 Current Density vs Voltage for GaAs and InP incorporating radiative recombination rate coefficient. 110
5.24 Efficiency vs Voltage for GaAs and InP incorporating radiative recombination rate coefficient. 110
5.25 Current Density vs Voltage for both the models. 111
5.26 Efficiency vs Voltage for both the models. 112

List of Tables

1.1 General properties of InP. [18][19][20][21] 11

1.2 Features of a semiconductor. [23] 14

5.1 Comparing FDTD dimensions of each model. 94

5.2 Comparing DEVICE dimensions of each model. 96

5.3 Comparison of key parameters. 113

List of Acronyms

TW- Terawatt

EPH- Energy of photon

I_{SC}- Short-Circuit Current

R_{SH}- Shunt Resistance

CIGS- copper indium gallium diselenide

CdTe- cadmium telluride

$CH_3NH_3PbX_3$ - Methylammonium lead trihalide

TE- Transverse Electric

TM- Transverse Magnetic

m- metre

mA- milli Ampere

mW- milli Watt

S-Q- Shockley-Queisser

PV- photo-voltaic

fs- femto second

InP- Indium Phosphide

AlGaAs- Aluminium Gallium Arsenide

GaAs- Gallium Arsenide

TSC- Tandem Solar Cell

ARC- Air Reflective Coating

TIR- Total Internal Reflection

EHP- Electron-Hole Pair

J_{SC}- Short-Circuit Current Density

V_{OC}- Open Circuit Voltage

η- Efficiency

PML- Perfectly Matched Layer

μm- micro metre

LASER- Light Amplification by Stimulated Emission of Radiation

LED- Light Emitting Diode

DFT Monitor- frequency Domain Field profile monitor

RSE- Series Resistance

FDTD- Finite Difference Time Domain

InGaP- Indium Gallium Phosphide

IoT- Internet of Things

Chapter 1

Introduction

1.1 Introduction

A tandem solar cell technology has been a revolutionary approach to exceed the efficiency limits of single-material solar cells. In the following chapter, a tandem solar cell has been introduced which can reduce the thermalization of surplus energy of high-energy photons and transparency to low energy photons. These two main losses restrict to enhance the efficiency of single-material solar cells. However, tandem solar cells are layers of p-n junctions. Each of these p-n junctions is made of a semiconductor of dissimilar bandgap energy and they respond to a different portion of solar spectrum. This factor helps to enhance the efficiency of a tandem solar cell. Further in this chapter, the motivation that influences to research in this sector has been discussed followed by a brief analysis on literature review. Moreover, an overview on semiconductor junction, solar cell operation and the material feature of Indium Phosphide (InP) have also been analyzed. This is a depiction of history expressing the legacy of increasing efficiency of solar efficiency. At the end of this chapter, the objective of this research and its methodology along with thesis layout has been discussed.

1.2 The motivation and challenges of this work

The high price of solar cell modules has been the main obstacles that came in the way of broad expansion of photovoltaic (PV) systems and large-scale production. To reduce this steep cost, researchers invented one of the solutions by developing thin-film solar cells. The tough challenges to develop such thin film solar cell with higher efficiency and economical has influenced to work on this research for many. One of toughest challenges is to have the eco-friendly energy as well as cost-effective

in today's world which can meet the demand of huge population. Photovoltaic energy source can fulfill this huge demand if it is being utilized effectively. The total radiation which hits the earth is 1.75E5 TW. However, only 15 TW is being possible to use in recent times [1].Besides, energy produced by other renewable and non-renewable sources such as wind energy, geothermal, hydro-electric, oil, coal, gas etc. are cheaper than photovoltaic module. This factor has worked as a driving force to produce economical and higher efficient thin film tandem solar cell.

Meanwhile, research on nanophotonic particles has brought out its effectiveness optical devices and light. Many micro and macro features of light like absorption, reflection, di-electric property, coupling effect etc. can be guided by altering the nanoparticles. Therefore, application of nanophotonic technology in tandem solar cell can lead to enhance its efficiency and to have more stable solar energy.

However, a thin film solar cell is not very well light absorber in comparison with a typical thicker solar cells made of identical materials with equivalent absorption coefficient. Using different differ light trapping techniques, applying doping mechanism and different mole fraction of materials, can enhance its overall light absorption as well as its efficiency.

1.3 Literature review

A number of research papers has been studied about the function of Tandem Solar Cell (TSC) and their mechanism for increasing the efficiency of solar cell. Photons which have broader range of solar spectrum cannot be absorbed by single junction solar cell. For instance, a photon which has a wavelength more than 100 nm cannot be absorbed by Silicon solar cell [2]. In consequences of limitations of single junction solar cell, multi-junction solar cell (TSC) have been focused. Theoretical and experimental analysis are being performed by researchers from last few decades [3]. Thin-film solar cell that are made of polycrystalline materials are found to be more efficient [4]. AlxGa1-xAs which has a broader range of absorption coefficient and cubic crystal structure, has a great contribution to enhance the efficiency of

solar cell [5]. The materials band gap changes with the mole fraction value (x). Experimental theoretical calculations of TSC proved that bandgap of 1.70-1.85 eV for top cell, and 1.1 eV bandgap of rear cells are finest composition [6]. The light gets absorbed more effectively when the top material has greater bandgap than the lower one. On experimental basis, multi junction solar cells which are made from III-V semiconductor materials, such as GaAs, InP are demonstrated to be highly efficient [6]. When the number of junctions increased, InP lattice constant is found to be more suitable. InP substrate has been used in the quarter junction solar cell which gave the world record efficiency [7]. For a single junction InP solar cell, efficiency is found to be 33.2% [8]. Through the research, it can be concluded that InP in tandem solar cell could give high efficiency, with certain alterations in material parameters.

1.4 Semiconductor junction

Semiconductor is a class of crystalline solids with electrical conductivity ranging between a conductor and an insulator and a band-gap of less than or equal to 5 eV [9]. A semiconductor can be either of a single element, such as Si or Ge, a compound, such as GaAs, InP or CdTe, or an alloy, such as SixGe(1-x) or AlxGa(1-x)As, where x is the mole fraction of the particular element and ranges from 0 to unity. Although semiconductor materials come from different groups in the periodic table, yet they share certain similarities. The atoms in a semiconductor are materials from either group IVA of the periodic table, or from a combination of group IIIA and group VA (called III-V semiconductors), or of combinations from group IIA and group VIA (called II-VI semiconductors). The properties of each semiconductor varies owing to the fact that different semiconductors are made up of elements from different groups in the periodic table [10]. Besides, band-gap energy is the minimum energy required to break the bonding of electrons which also determines the magnitude of solar energy required for conduction. When the electron leaves its original position, a hole is generated and thus participates in conduction as well. These electrons and holes are also called intrinsic carriers and is an important factor in improving the solar cell efficiency as they are dependent on the temperature and band-gap.

A mechanism known as doping is used to vary the number of electrons and holes in a semiconductor. Thus, the total number of carriers in the conduction and valence band varies due to doping and is known as equilibrium carrier concentration. For example, if a semiconductor is doped with group-VA atoms of the periodic table, then "n-type" doped material is formed. On the contrary, if the same semiconductor is doped with group-IIIA atoms, then P-type doped material is formed. In "n- type" material, electrons, while in "p-type" materials, holes, are the majority carriers. This is because the electrons in "n-type" and holes in "p-type" materials have higher concentration than their counterparts. Conversely, holes and electrons are the minority carrier in "n-type" and "p-type" materials, respectively.

When the energy of incoming photon (E_{PH}) exceeds the band-gap energy (E_G), absorption takes place. The absorbed photon excites the electron in the valence band and causes it to transit to conduction band, leaving behind a hole in the valence band. As a result, majority and minority carriers are generated. This event is the foundation of the production of PV energy. Moreover, absorption coefficients plays an important role in the production of this energy. It varies from material to material and relates directly with the absorption of photon. Hence, materials with high absorption coefficient are favored for efficient solar cell design. On the flip side, absorption depth in inversely related to absorption coefficient. Mathematically, it can be.1 [11].

$$\delta = \frac{1}{\alpha} \tag{1.1}$$

Where,
δ: absorption depth and
α: absorption coefficient

It explains how deep the light or photon would penetrate or travel before it gets absorbed. A high energy photon has small wavelength and thus lower absorption depth. Therefore, the thickness of the semiconductor is of great importance in designing with the favorable absorption depth. However, most of the light is absorbed at the surface of the semiconductor. As a result, Electron-Hole Pair (E_{PH}) gen-

eration is maximum at the surface. In addition to that, E_{PH} generation is also dependent on the wavelength of the incoming photon. As discussed earlier, solar spectrum consists of range of wavelengths, therefore, variable generation rates must be accommodated when designing the solar cell.
On the other hand, when the electron de-excites and loses its energy, the electron transit down in energy to valence band from conduction band and releases its absorbed energy in the form of light or heat. This phenomenon, where the electron meets the hole and annihilate, is called recombination. This can be categorized into:

1. Radiative Recombination (R_{opt})
2. Shockley-Read-Hall Recombination (R_{SRH})
3. Auger Recombination (R_{Au}).

Furthermore, minority carrier lifetime and minority carrier diffusion length are the parameters that can manipulate recombination rate. Minority carrier lifetime is the average time a carrier takes before it recombines. On the contrary, minority carrier diffusion length is the average length the carrier would diffuse before it recombines. As similar as they sound, they are related by the following equations (1.2 and 1.3) [11].

$$L_n = (D_n \tau_n)^{\frac{1}{2}} \tag{1.2}$$

$$L_p = (D_p \tau_p)^{\frac{1}{2}} \tag{1.3}$$

Where: $L_{n,p}$ is the minority carrier diffusion length, $\tau_{n,p}$ is the minority carrier lifetime and $D_{n,p}$ is the diffusion coefficient for electron and hole, respectively.

As seen from the equation, carrier lifetime and diffusion length are proportionally related, hence higher carrier lifetime indicates a material have greater diffusion length. In solar cells, surface recombination is high which decreases diffusion length. Therefore, care must be taken to design the desired efficient solar cell.

In a semiconductor lattice, the carriers are in spontaneous motion with non-uniform velocity that varies with the temperature and it's mass. The carrier continues to

move in a haphazard way unless experiences a collision with the neighboring atom, hence, there is no net movement in any specific direction. In spite of the mentioned factor, two more events are seen within the semiconductor. They are the drift and diffusion. As mentioned earlier, E_PH generation is higher at the surface of the material, so there is a diffusion gradient of concentration. As a result, carriers diffuse from high concentration area to low concentration area. On the flip side, drift occurs due to the electric field present on the solar cells that causes holes to move along the direction of this electric field and electrons in the opposite direction, ceteris paribus.

In order to create the voltage difference in a PV cell, the carriers are partitioned by a p-n junction. When n-type and p-type materials are combined together, surplus electrons from n-type and holes from p-type diffuses to the other side of the material, exposing the positive and negative ions on either side. This creates the p-n junction and induces an electric field across it producing the depletion region. This electric field generates voltage and plays an important role in carrier transport, generation, recombination, and is a basis of the working principle of all electronic devices. Majority carriers diffuse across the opposing electric field in depletion region while the minority carriers drift away across the p-n junction depletion region. When equilibrium is reached, the net current is zero as the current due to diffusion is equal and opposite of the drift current. When a forward bias voltage is applied, the electric field within the depletion region decreases. This restricts the carrier diffusion and hence increases the diffusion current. As the external circuitry provides the continuous flow of majority carriers, recombination rate increases, thus increasing the diffusion and the current across the depletion region. Alternately, when the solar cell is reverse biased, the electric field increases, thereby, decreasing the diffusion current.

1.5 Solar cell operation

A solar cell, which is also known as PV cell, converts light energy into electrical energy. Semiconductor are the major materials which are used in solar cell. When light hits the solar cell, electrical parameters like current, voltage or resistance can

be manipulated.

In 1954, Chapin invented the first practical solar cell, with the efficiency around 6% [12]. Till date, plenty of techniques are applied to increase the efficiency. Currently, the preferring model to convert photon energy into electrical energy in most efficiently is achieved from multi junction from solar cell known as Tandem Solar Cell TSC composed of several semiconductor materials consist multiple p-n junction will generate current by absorbing different wavelengths of light [13]. The basic TSC arrangement is composed of heavily doped materials, p^+-type and n^+-type material. There are electrodes, emitter and base working as cathode and anode respectively. Emitter is attached to n^+ typed material and base is attached with to p^+- typed material. Both emitter and base are made of Aluminum, and are interconnected. A flow of current is induced when photons generates electrons and holes, and they transport to electrodes. A battery is used to preserve this current.

1.5.1 Structure

The major principle of solar cell is to transform light energy into electrical energy. Solar cell received the photons in the form of light. These photons are absorbed by electrons. It increases electron's energy for which they transit to higher energy level from lower energy level. These excited electrons then flow to external circuit. These movement of electrons generates current which is called "light-generated current". Voltage is also induced and power is given as output. The electron-hole pair generation from absorption influences the amount of current. EHP tends to recombine immediately when they are generated. This will not produce the desired current. The EHP recombination can be block by the p-n junction which barricades the minority carriers to pass the semiconductor/metal boundary.

The light-generated current will flow along the external circuit when the solar cell has been short circuited. This can be done by interconnecting the solar cell base and emitter. The circulating current is known as short circuit current (I_{sc}).

Beside the short circuit current, there is another important parameter known as open circuit voltage V_{oc}. In tandem solar cell, total open circuit voltage is the sum-

mation of the open circuit voltage of individual sub cells. In open circuit condition, the forward bias diffusion current is equal to line current. When the solar cell is short circuited, it will lead the carriers to escape from the device, leaving zero charge. If these escaping carriers are stop to leave, carrier concentration would increase in p-side and n-side of the junction. A second electric field is produced against the existing electric field. The decreased in overall electric field will lead the forward bias diffusion current to raise.

Alongside the short circuit current, there is another important parameter known as open circuit voltage (V_{OC}). In tandem solar cell, total open circuit voltage is the summation of the open circuit voltage of individual sub cells. In open circuit condition, the forward bias diffusion current is equal to line current. When the solar cell is short circuited, it will lead the carriers to escape from the device, leaving zero charge. If these escaping carriers are prevented to leave, carrier concentration would increase in p-side and n-side of the junction. A second electric field is produced against the existing electric field. The decreased in overall electric field will lead the forward bias diffusion current to rise.
There are two major resistances which impact in solar cell circuit. Shunt resistance (R_{SH}) and series resistance (R_{SE}). Shunt resistance decreases the fill factor and solar cell efficiency, also called "parasitic resistance". The construction of the circuit is shown in

The solar cell function with highest power at the characteristic resistance. It is given by [11]

$$R_{CH} = \frac{V_{MP}}{I_{MP}} \cong \frac{V_{oc}}{I_{sc}} \tag{1.4}$$

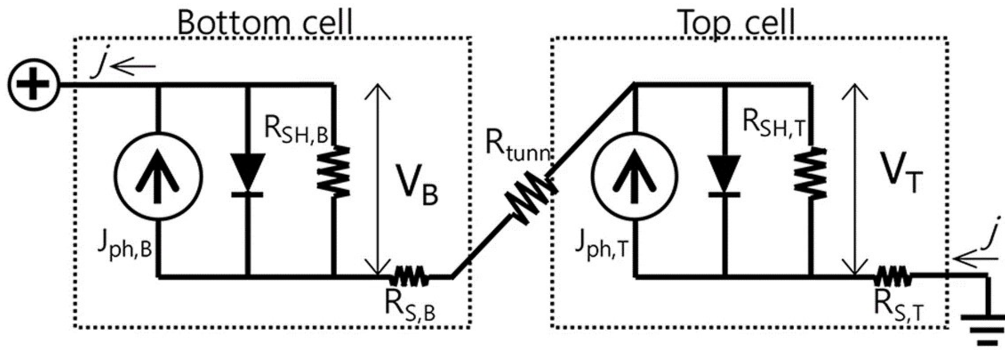

Figure 1.1: A circuit diagram of solar cell including shunt and series resistance.[14]

The series resistance has more impact on the operation of solar cell when the intensity of the light is low, and shunt resistance has more impact when the intensity is high. Therefore, with the variation in density of light, parasitic resistances impact on solar cell operation also varies. Intensity of incident light is the most significant feature for solar cell operation. Light intensity which falls on solar cell refer as number of suns. The standard illumination of 1 sun is AM1.5G or $1kW/m^2$ [15]. Concentrators are those solar cells, which needs more than 1 sun illumination to operate, they are low in cost and higher in efficiency.

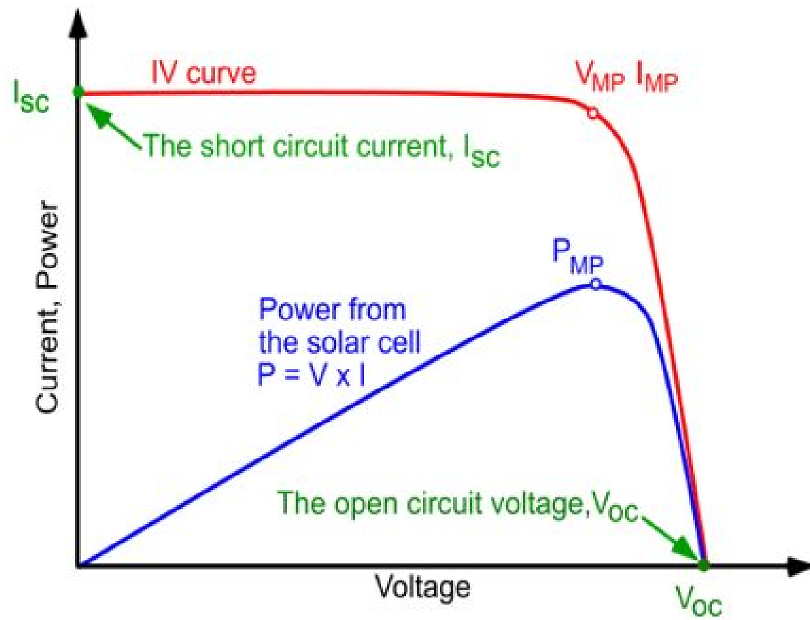

Figure 1.2: I-V and P-V curve of a solar cell. [16]

Solar cell characteristics can be shown by I-V graph, which consist open-circuit voltage, fill factor, short circuit current and efficiency. The light generated current is in superposition with solar cell diode I-V curve under darkness [17]. Figure 1.2 shows a solar cell IV curve. Solar cell has to perform at P_{MP} to give maximum output power, and hence maximum efficiency. Maximum power occurs at current, I_{MP} and voltage, V_{MP}. AT the point I_{sc} and V_{oc}, power is zero.

1.6 General and optical features

1.6.1 General Property of Indium Phosphide (InP)

Indium Phosphide can be compose from white phosphorus and indium iodide reaction. InP use in photovoltaic cells to obtain optimal bandgap composition to transform solar radiation into electrical energy efficiently. Table 1 shows the general properties of InP.

Property	**Value**
Molar mass	145.792 g/mol
Density (ρ) (solid)	4.81 g/cm^3
Energy Bandgap (E_G)	1.35 eV
Electron mobility	5400 cm^2 (V-s) at 300K
Refractive Index (n_D)	3.1 (infrared) 3.55 (632.8nm)
Lattice constant	5.86 Å
Intrinsic carrier concentration (n_i)	$2 \times 10^{16} cm^{-3}$
Hole Mobility	$\leq 200 cm^2 V^{-1} s^{-1}$
Electron Mobility	$\leq 400 cm^2 V^{-1} s^{-1}$
Electron Diffusion Coefficient	$\leq 130 cm^2 s^{-1}$
Hole Diffusion Coefficient	$\leq 5 cm^2 s^{-1}$
Electrical resistivity	$8.6 \times 10^7 \Omega cm$
Melting Point	$1062°C$
Thermal Conductivity	$0.68 W cm$-$^{1°} C^{-1}$
Thermal Expansion Coefficient	4.60×10-$^{6°} C^{-1}$
Effective Valence Band Density of States (N_v)	$1.1 \times 10^{19} cm^{-3}$
Effective Conduction Band Density of States (N_c)	$5.7 \times 10^{17} cm^{-3}$
Relative Permittivity (ϵ_r)	12.4
Electron Affinity	4.38 eV

Table 1.1: General properties of InP. [18][19][20][21]

1.6.2 Optical Properties of Indium Phosphide (InP)

The optical properties of InP such as Refractive index, absorption coefficient, reflection coefficient, reflectance, are observed with respect to photon energy (eV). Energy of photon can be expressed as equation 1.5 [11].

$$E = \frac{\hbar c}{\lambda} \tag{1.5}$$

Where c is the speed of light, $\hbar$ is the plank constant, and λ is the wave length of incident photons.

The refractive index of InP against photon energy is shown in **Figure 1.3**. The highest value of refractive index reached at 4.42 at 3.1 eV.

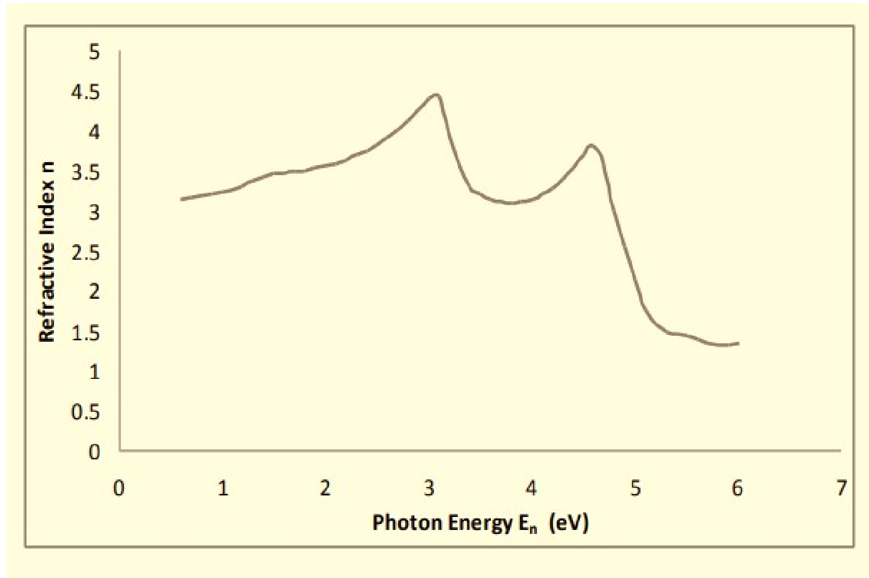

Figure 1.3: Refractive index and Photon Energy (eV) of InP. [22]

The absorption coefficient is plotted against photon energy in Figure 1.4, in the range of $1.3 - 6eV$. The absorption coefficient increases with increase in photon energy. The highest value is $17.8 \times 10^7 m^{-1}$ against at 5.0 eV. There is no absorption below the bandgap energy of InP.

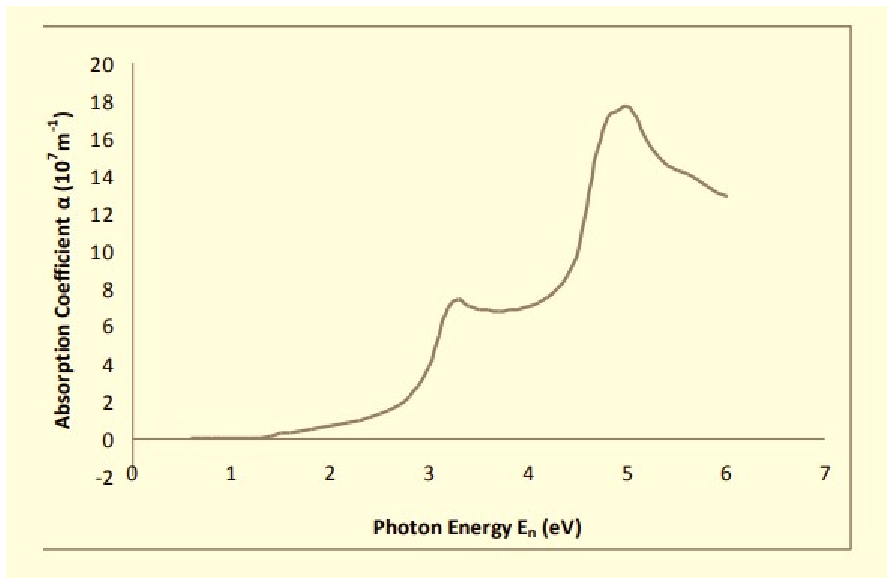

Figure 1.4: Absorption Coefficient of InP.[22]

Reflection Coefficient vs Photon Energy of InP given in Figure 1.5. InP is great absorber, as though from 0.6-5 eV, the reflection coefficient raises, but only reach to peak value of 0.79 at 5.0 eV.

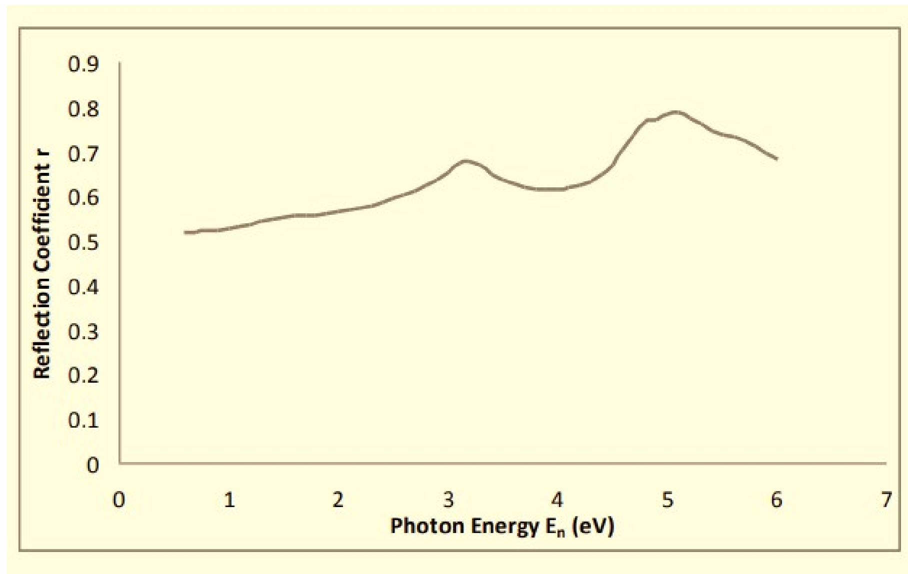

Figure 1.5: Reflection coefficient (r) of InP.[22]

From the Figure 1.6, it can be seen that with the raise of photon energy from 0.6 to 5.1 eV, reflectance increases. The highest value reached 0.62 with corresponded to 5.1 eV.

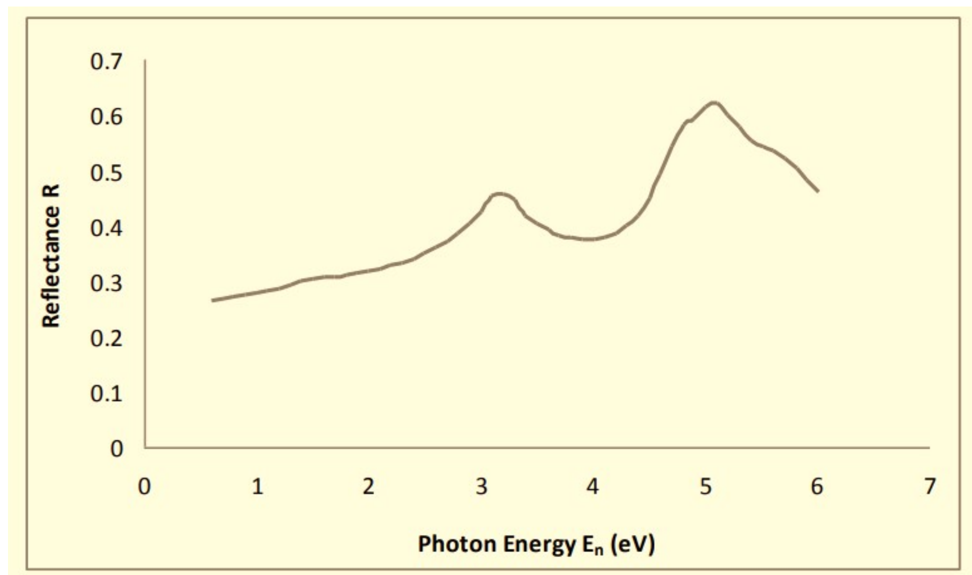

Figure 1.6: Reflectance (R) of InP.[22]

1.7 Doping

A technique used to vary the number of electrons and holes in semiconductors is mainly known as doping. When a semiconductor material is doped with group V atoms, it creates n-type material. On the other hand, p-type materials can be made by doping group III atoms in a semiconductor material. By increasing the number

of available electrons and holes in n-type and p-type materials respectively, the conductivity of the semiconductor can be increased.

The following **Table 1.2** summarizes the features of a semiconductor.

	n-type (negative)	**p-type (positive)**
Dopant	Group V (e.g. Phosphorous)	Group III (e.g. Indium)
Bonds	Excess Electrons	Missing Electron (Holes)
Majority Carriers	Electrons	Holes
Minority Carriers	Holes	Electrons

Table 1.2: Features of a semiconductor. [23]

When the majority carriers are negatively charged electrons and minority carriers are positively charged holes, it is call "n-type" as shown in **Figure 1.7**.

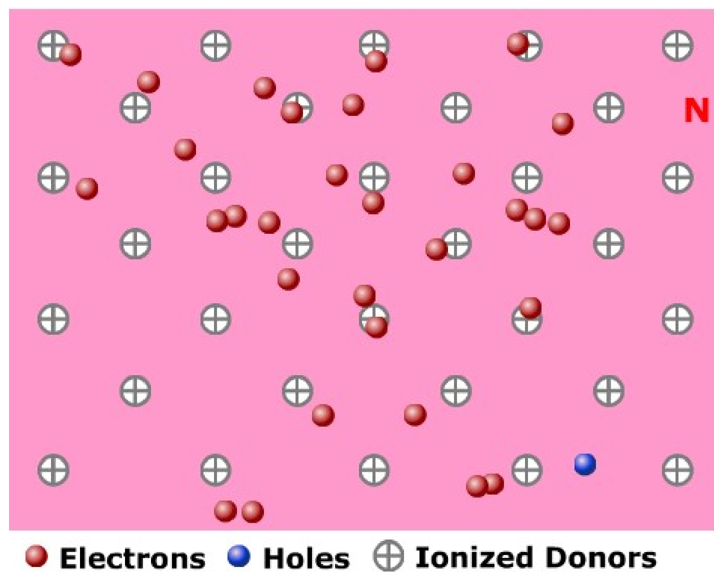

Figure 1.7: "n-type" semiconductor.[23]

Again, when the majority carriers are positively charged holes and minority carriers are negatively charged electrons, it is call "p-type" as shown in **Figure 1.8**.

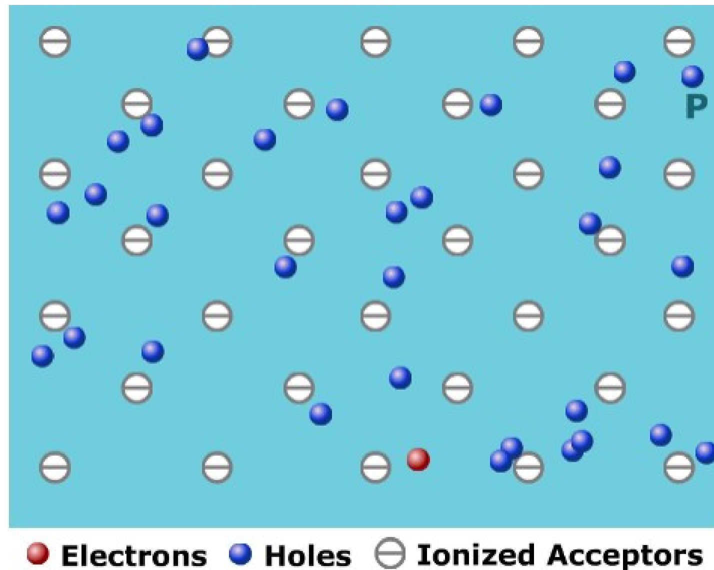

Figure 1.8: “p-type” semiconductor.[23]

Designing a solar cell requires semiconductors whose bandgap energy is very narrow. Hence, even little addition of impurities in the form of dopant can increase the conductivity of the solar cell. As a result, doping plays a major role in solar cell technology.

1.8 Spectral and theoretical efficiency

In the construction of solar cell, its high efficiency is the vital quantity. A number of fields are in await of high efficiency solar cells. An ideal solar cell has 100 percent efficiency, as it considered that each photon generates 1 pair of electron-hole. Practical solar cells have many limitations which decrease its efficiency. Efficiency declines due to efficiency loss by electrical and optical losses. These losses are in the form of contact resistance, trap assisted, reflection, recombination and transmission. Applying various concepts, these quantities can be controlled, despite that some limitations are still exists. Therefore, solar cell theoretical efficiency could be resolute.

1.8.1 Spectral efficiency

Efficiency of solar cells is also dependent on bandgap of different semiconductor materials. A tandem solar cell which consists of multiple bandgap of multiple materials, can enhance the efficiency.

When the incident photon energy is higher than the highest bandgap of TSC material, surplus energy is wasted in the form of thermalization. In contrast, when the incident photon energy is lower than the lowest bandgap of TSC material, it will not be absorbed. Figure 1.9 shows transmission and thermalization.

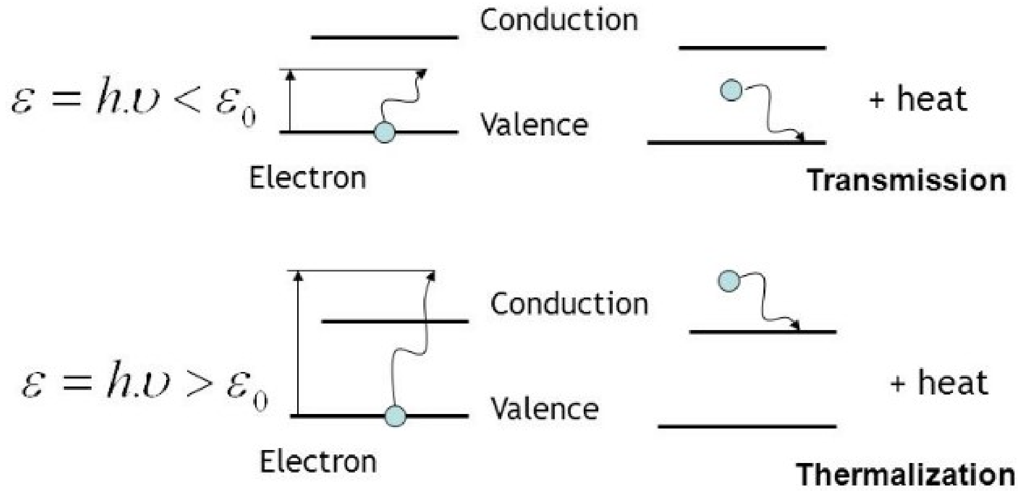

Figure 1.9: Process of Transmission and Thermalization.

The bandgap energy is represented by ϵ_0, and $h.v$ is the energy of photon, h is the plank constant and is the frequency which can be further expressed as $v = \frac{c}{\lambda}$, where c is the speed of light and λ is the wavelength of incident photon. Transmission occurring when photons energy is less than bandgap energy, resulting zero electrical energy. Thermalization is happening when surplus energy of photon is released after the electron moved to lower energy level of conduction band.

1.8.2 Theoretical efficiency

In practical solar cell, fill factor will not be 100% . By means of this, power point current (I) will be lower than short circuit current (I_{sc}), along with, voltage (V) will be lower than open circuit voltage (V_{oc}). Beside this, entire V_{max} which is equals to $\frac{E_G}{q}$ cannot be utilized in practical solar cell. These two major components are not considered in the energy loss of solar cell and spectral study. Solar cell p-n junction is associated with these two hindrances. Theoretical efficiency limit of any material, knowing their bandgap can be found from Figure 1.10 with the assist of stated limits. In this, each and every photon assumed to get absorbed and participated in photon current. There are additional losses as afore mentioned, such as reflection,

partial absorption, recombination sites, contact resistance, transmission and many more.

Theoretical limit of GaAs is 32.8% , and of InP is 33.2% [24] [25]

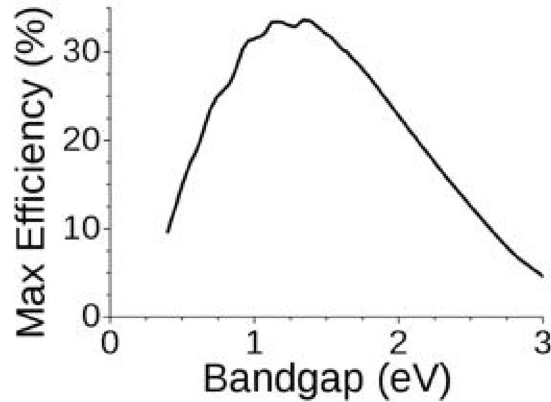

Figure 1.10: Theoretical efficiency vs Bandgap energy. Shockley-Queisser limit for the efficiency of solar cell.[26]

1.9 The history of solar cells

Silicon made typical solar cells are considered to be as the very first generation of solar cell industry. It has higher longevity and high efficiency varying from 15-25% although, to fabricate it requires a large amount of energy. However, the solar cells used in residential and commercial places are most the silicon made solar cells.

Thin film solar cells are known as the second generation of solar cell in the industry. It is thinner than the previous generation as its name suggested and made of semiconductor materials. Its efficiency is ranging from 10-15% and different materials such as CIGS, CdTe and amorphous silicon are used to fabricate thin film solar cells. Using minimum raw material leads to lower cost of manufacturing which acts as a beneficial side of second generation of solar cells.

Enhancing solar cell efficiency is always prime focus in solar cell technology. The third of solar cell came up with the idea of designing it with variety of materials to enhance solar cell efficiency significantly. Organic solar cells, polymer solar cells,

high performance solar cells like perovskite solar cells, multi-junction solar cell etc. all are part of the development of third generation solar cells.

The evolution and the conversion efficiency of the different generations of solar cells are shown in **Figure 1.11**.

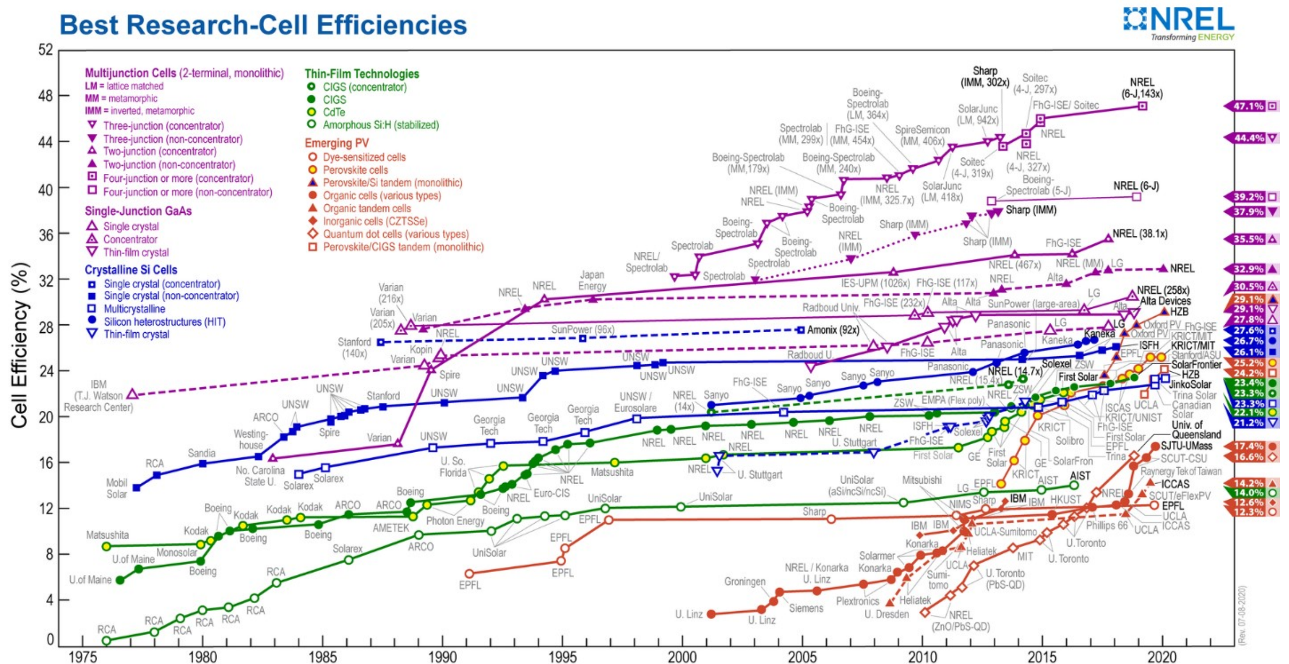

Figure 1.11: The evolution and the conversion efficiency of the different generations of solar cells since 1976. [27]

The most known solar cells are discussed in the following section.

1.9.1 Different type of solar cells

a. Crystalline silicon solar cells

Crystalline silicon solar cell is part of the first generation of solar cell technology. It is delicate in nature which makes it unfeasible for transportation. However, most the solar cells used are made of silicon based and placed on the rooftops. It performs its duty following the same principle just like any other solar cells. Usually, it is illuminated which results in generating EHP (electron-hole pairs). The generated charge carriers are swept apart by the magnetism of the alternate charges. In further step, the electric current is generated by collecting the charge carriers.

Out of many monocrystalline solar cell and polycrystalline solar cell, both belong to the crystalline solar cells family. Firstly, monocrystalline solar cell has high efficiency, energy payback time and more stability. In polycrystalline solar cell, the efficiency, energy payback time and stability rate is comparatively lower than monocrystalline solar cells. However, the materials used for producing both solar cells are easily accessible.

Figure 1.12: Monocrystalline silicon solar cell and Polycrystalline solar cell sample.[28]

b. Thin-film solar cells

Thin film solar cell is crafted from multiple layers of different materials such as semiconductor, metal, glass or plastic. Each of these layers of thin film solar cell contributes to light trapping process. This second generation solar cell layers are composed thinner than its predecessor. Using direct bandgap materials to design thin film solar cell has made it possible. Having this small thickness, it makes the solar cell efficient in terms of mobility and fabricate it in a lower price. The thickness can be varied from ranging nanometers (nm) to micrometers (m) based on the designing parameters.

Cadmium telluride (CdTe), copper indium gallium diselenide (CIGS) and amorphous thin film silicon (a-Si, TF-Si) are the most common thin film solar cell. Among these three, the first two have low energy payback time but materials are hard to find. Moreover, copper indium gallium diselenide (CIGS) solar cell has higher efficiency compare to cadmium telluride (CdTe). However, amorphous thin film silicon (a-Si, TF-Si) has lower efficiency, poor stability and lower energy payback than the

rest of the above mentioned solar cells. Being economical, the lower efficiency has always been a concern of thin film solar cell, comparing to crystalline silicon solar cells. This technology has the potential to increase the production by generating faster output energy and using less amount of materials despite having limited consumers in the field.

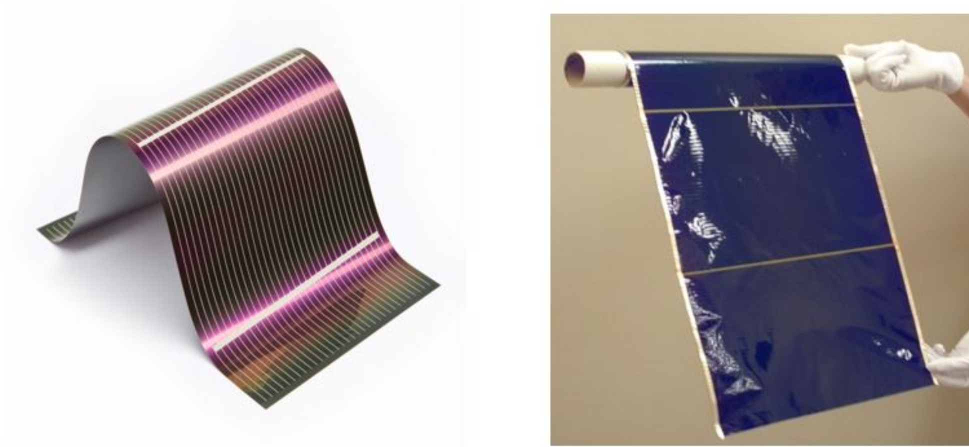

Figure 1.13: CdTe panel sample (left) and an amorphous silicon cell panel (right).[29] [30]

c. Uprising solar cell technologies

The third generation of solar cells also named as uprising solar cell technology, are combination of a wide range of solar cell technologies. The primary focuses of these technologies are enhancing overall efficiency, economical side and dynamics of solar cell production. Multi-junction solar cells tandem solar cells and, organic solar cells, perovskite solar cells, dye-sensitized solar cells and the quantum dot solar cells are the most familiar solar cell in present world. A short discussion about these solar cells technologies are given below.

i. Multi-junction and tandem solar cell

Researchers have found that the solar cell which consists of a single junction, is inadequate to use the solar energy efficiently. Mainly two reasons are there holding its back. To begin with, not absorbing photons are useless for generating current. Each

photon having higher energy than its bandgap energy gives one electron and rest of the excess energy of the photon gets lost,which is considered to be the second reason. Nevertheless, by splitting the solar spectrum into various ranges and designing a cell focusing on separate spectrum ranges, it is possible to solve the above mentioned two problems. Piling two solar cells together is the basic concept of implementation multi-junction solar cells. To get high output voltage, it needs the illumination to hit the very first absorber which has a larger bandgap.

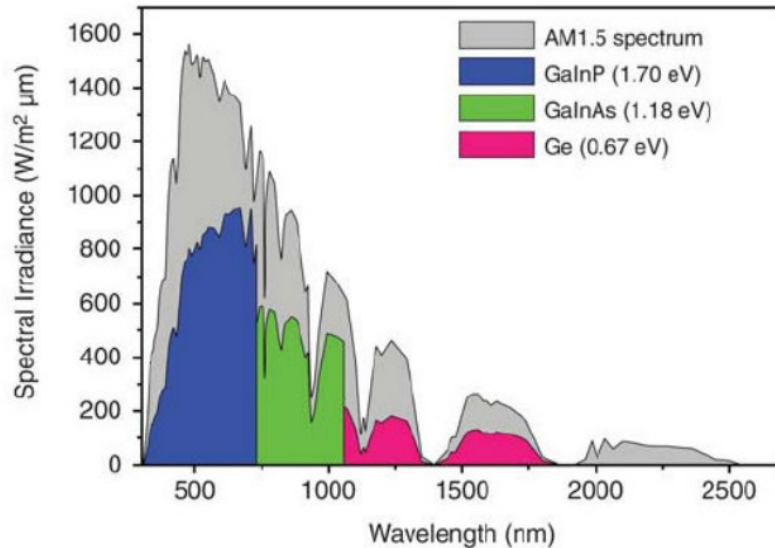

Figure 1.14: Absorption and loss of solar spectrum in a multi-junction solar cell.[31]

Moreover, tandem solar cells has significant amount of current drawing feature hence, it has high demand in solar cell market in recent years. Two different designs consider to fabricate tandem solar cells namely i.) Monolithically integrated tandem and ii.) Mechanically stacked tandem as shown in Figure 1.15. In monolithically integrated cell, two cells are connected in series which causes identical current to flow through each part and photo-current of each layers also remains same.

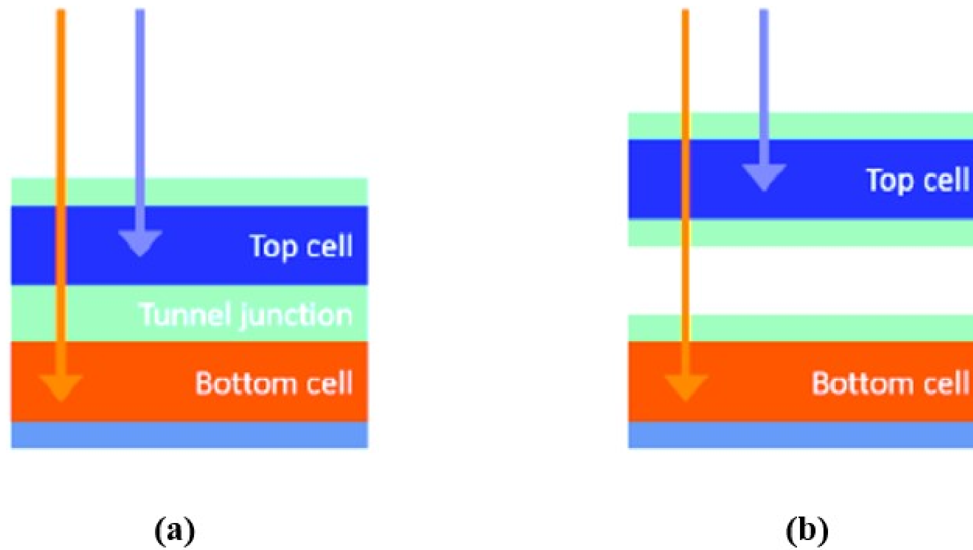

Figure 1.15: Schematic design of monolithic and tandem solar cell devices. (a)- Monolithic tandem device and (b) - Stacked tandem device.[32]

In Figure 1.15, tandem solar cells are illuminated with the solar spectrum. Blue light, which has the high energy photons gets absorbed on the top cell whereas the red light passes through. It gets absorbed on the bottom cell due to having lower photon energy. Mechanically stacked tandem cells are separated from each other while monolithically integrated tandem structure requires a tunnel junction in between the two cells.

On the other hand, stacked solar cell consists of two separated cells and four terminals. There are no identical current present here as such the monolithic tandem device, since there is no series connection between the two cells. Bandgap combination is more flexible here and a transparent contact between two cells helps to transmit the absorbed light. In present time, although multi-junction solar cell is high priced, it has been used in space application for its overall high efficiency rate.

ii. Organic solar cell

Organic solar cell is mainly made of organic materials and has efficiency rate of around 12%. Polymer solar cells and small molecule solar cells are the organic type solar cell. Organic materials and conjugated are used for trapping the light in polymer solar cell. The conjugated materials used in organic solar cell have the similar characteristics of semiconductor. Hideki Shirakawa, Alan J. Heeger and Alan Mac-

Diarmid examined this phenomena [33]. It follows the same methodology to absorb the light and produce electricity even though the materials are not same. It can be used in the form of coating or possible to print as it can be created from solutions unlike any other solar cells. This technology is more flexible, affordable, high production rate and feasible for transportation. However, the lower efficiency rate and the longevity of this technology have always been a concern.

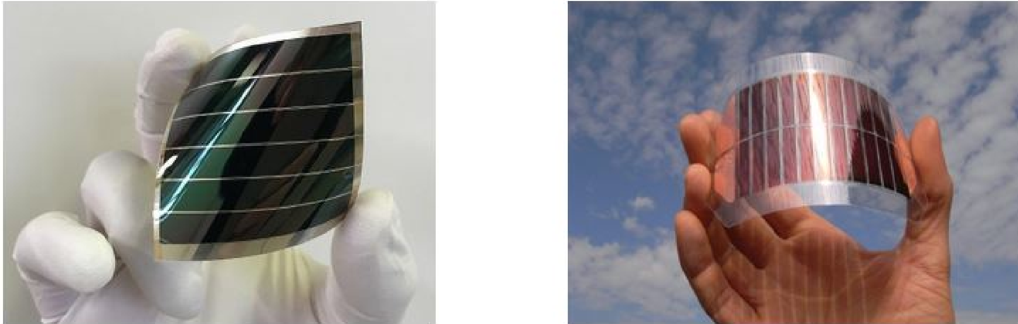

Figure 1.16: Organic solar panel sample.[34]

iii.Perovskite solar cell

The perovskite solar cell technology has a good reputation for enhancing efficiency overtime. At the beginning of this technology it had an efficiency of 3.8% and after rapid evolution 30% efficiency has been possible by 2020 [35]. Tunable bandgap ranging from 1.5 eV to 2.3 eV helps in enhancing the efficiency in perovskite solar cell.

Moreover, the most typical and well known perovskite solar cell is known as Methylammonium lead trihalide ($CH_3NH_3PbX_3$), where X represents as a halogen atom for example, chlorine, bromine, iodine. Lead is poisonous and possess a high risk to the eco-system which is found to be a major issue of producing perovskite solar cell. Besides, its instability issue is another prime concern. This issue is mainly caused by moisture, heating under applied voltage, heat, oxygen and photo degradation.

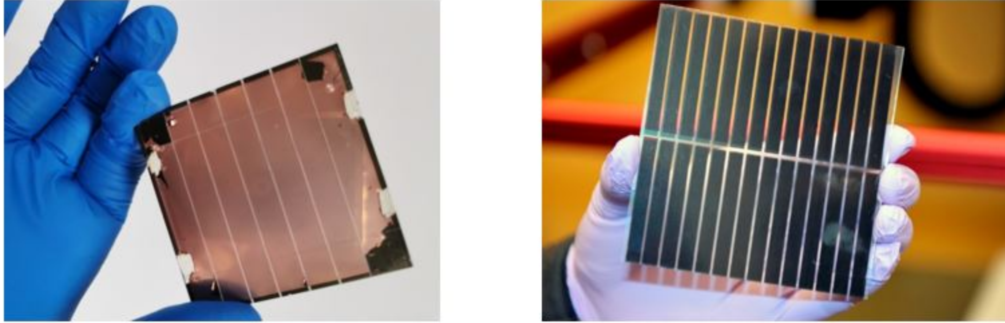

Figure 1.17: Perovskite solar panel sample.[35]

iv.Dye-sensitized solar cell

A dye-sensitized solar cell consists of a semiconductor which is placed in between a photo-sensitized anode and electrolyte. It is also known as Grätzel cell and considers roll-printing procedures to fabricate. This technique is more convenient comparing to other solar cell producing techniques. Less expensive materials are being used to produce this kind of solar cells. However, it has some major issues such as its temperature instability and low energy payback time. Highest efficiency listed for dye-sensitized solar cell till today is around 15%.

Figure 1.18: Dye-sensitized solar panel sample. [36]

1.10 Objective and Methodology

A brief discussion on theoretical aspects of tandem solar cell, its designing parameters and overall efficiency and fabrication difficulties is taken place. It is a tough job to commercialize and replace traditional power system with PV system yet because of having lower conversion efficiency and higher cost. However, effect of various

metallic nanoparticles of plasmonic structures having different size, shape, separation and material on tandem solar cell is reviewed. Besides, different plasmonic-photonic interaction over tandem solar cell performance is simulated and analyzed.

1.11 Thesis layout

The research paper has been divided into different sections, here mentioned as chapter. Each chapter consists of particular topic, mainly concentrated into enhancing the efficiency of a thin film tandem solar cell. To achieve this prime goal, it is required to apply different techniques and conduction both electrical and optical simulation.

At the beginning of the research paper, a literature review primarily focused on both theoretical and experimental different approaches has discussed. An overview of thin film tandem solar cell operation, its semiconductor junction, doping concentration and followed by overall features of the chosen material are given. Moreover, the main objective and relevant methodology of this thesis, a brief in general history of solar cell is added in end of this chapter 1.

In chapter 2, a theoretical discussion primarily focused on thin film tandem solar cell has reviewed. Here, various doping and light trapping mechanisms have been shown along with the theoretical analysis. This theoretical analysis has consisted of both electrical and optical parts of the simulation. These mentioned two electrical and optical simulation has performed in DEVICE and FDTD respectively. So, at the end, a simulation roadmap along with a general discussion about Lumerical Inc. software is given.

Chapter 3 demonstrated the model design of Gallium Arsenide (GaAs) thin film tandem solar cell. Its simulation parameters, simulation process and finally simulation results obtained both in FDTD and DEVICE are analyzed and compared with the theoretical value.

Chapter 4 shows another plant design namely Indium Phosphide (InP) thin film tandem solar cell. Here, different materials is used to enhance the efficiency of the

solar cell model. However, the simulation techniques and parameters are used same as the previous given solar cell design. The results got from both electrical and optical simulations are analyzed and compared with the expected value.

In the following chapter 5, a brief comparison of both thin film solar cell plant design has conducted side by side. This comparison has helped to show which model has successfully enhanced its overall absorption and efficiency. Furthermore, short-circuit current density, open circuit voltage, fill factor and photovoltaic efficiency have calculated for both of the model for various simulations which have analyzed and compared at the end of this chapter.

Chapter 6 summed up the whole thesis study by describing the remarkable achievement in terms of enhancing the overall photovoltaic efficiency in both of the tandem solar cell plant designs. However, the potential limitations and recommendations for the design drawbacks have also considered. To conclude this research paper, future opportunities has presented with strong remarks to develop further research so that it can play a vital role for enhancing the usage of solar power throughout the world.

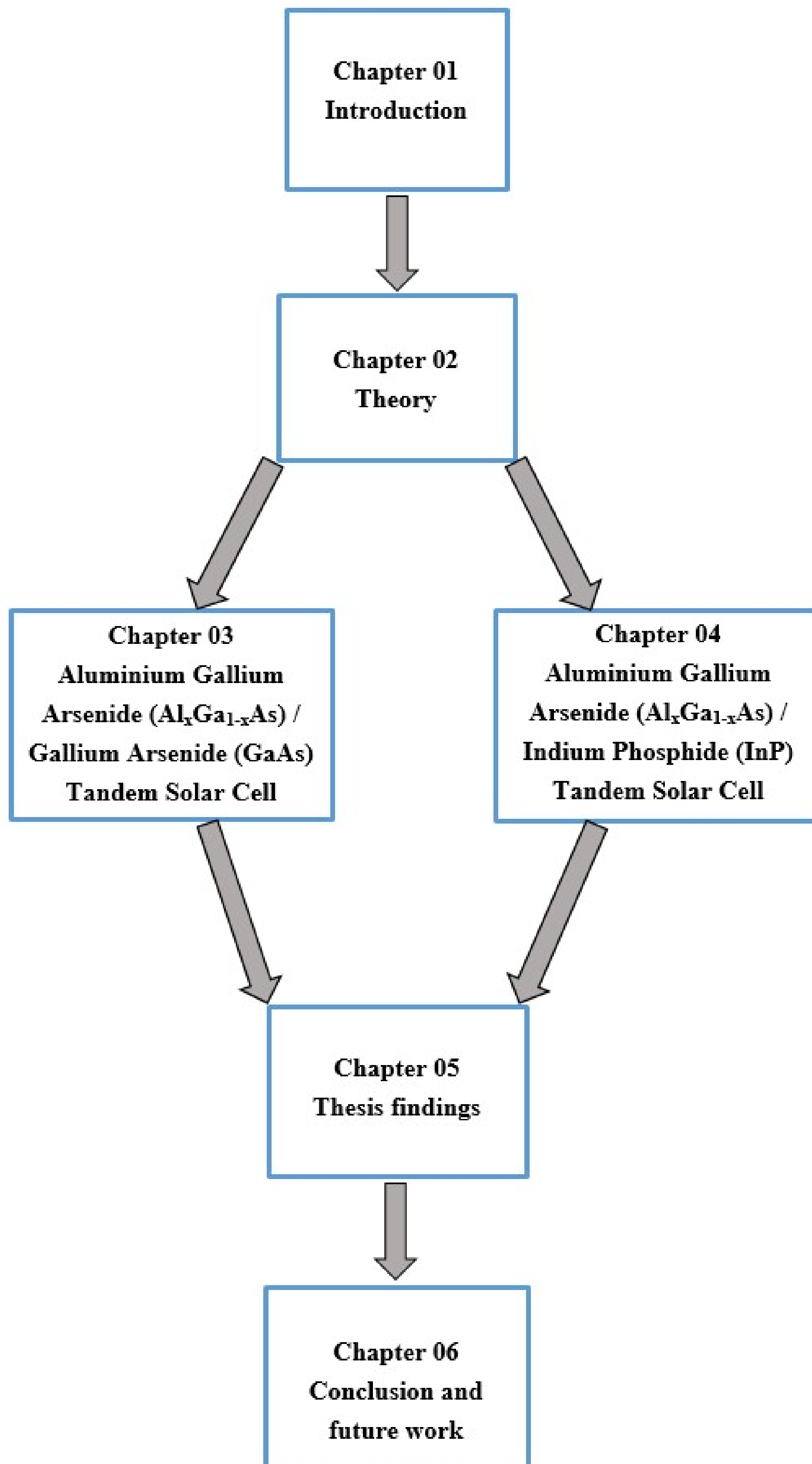

Figure 1.19: The thesis layout.

1.12 Conclusion

In this chapter, a discussion about the motivation and challenges that influenced to research in this field is given at the very beginning followed by a literature review. Some necessary information about semiconductor junction and how the solar cell mainly operates, are described here. Moreover, properties (general and optical) of the substrate material (InP) is necessary for designing the thin film tandem solar cell are short listed and analyzed. A brief discussion about doping, spectral and theoretical efficiency, history of solar cells are included. To conclude up this chapter, the objective and methodology of the whole research is added followed by a thesis layout at the very end of this section.

Chapter 2

Theory

2.1 Introduction

Solar cells are the future of the sustainable energy for human race and are the most optimistic and valuable technology in recent times. The toughest part of designing a solar cell technology is to enhance its efficiency by keeping the process economical. To achieve this higher efficiency and fabricate an economical solar cell, the Tandem Solar Cell (TSC) model has been applied (Two different TSC model will be discussed in the upcoming chapters of 3 and 4. In this following chapter, many theoretical prospects such as the ways of light-trapping, doping mechanism and different equations which are helpful for simulating electrical and optical part of tandem solar cell. Furthermore, a brief discussion about Lumerical Inc. software, mainly FDTD simulator and CHARGE solver will be provided. At end of this chapter, there will be a discussion about simulation road-map for successfully simulating and designing an economical tandem solar cell to enhance its efficiency.

2.2 Light trapping

Multi-junction solar cells fabricated from III-V semiconductors are more acceptable these days to obtain photo-voltaic (PV) conversion efficiency. Tandem junction solar cell having broad range of absorption in the solar spectrum makes it to use in research of achieving high efficiency [37][38][39]. Light could be trapped in TSC in many ways, which is necessary to increase absorption, and hence efficiency. Light trapping could be done by preventing light to escape from the material. As Aluminium is a good reflector, it could be placed at back side of the model to reflect back the escaping light. Besides, a back mirror could be used at backside to extend the optical path

length of higher wavelength. Furthermore, texturing procedure is favorable in solar cell, destructive interference caused by roughed surface increases transmittance of device [40]. Dielectric reflectors which disperse light in all direction are also a good approach for light trapping. A lot of research is happening for better method of light trapping in TSC.

2.3 Doping Mechanism

In a semiconductor, doping is the intentional introduction of impurities into an intrinsic semiconductor for the purpose of modulating its electrical, optical and structural properties. The doped material is referred to as an extrinsic semiconductor. A semiconductor doped to such high levels that it acts more like a conductor than a semiconductor is referred to as a degenerate semiconductor[41]. In other words, degenerate semiconductors are those materials where the electron or hole concentrations are approximately equal to the number of energy states available. In a degenerate semiconductor, also known as heavily doped semiconductor, p-type and n-type doped materials are represented as p^+ and n^+, respectively. This type of materials have Quasi-Fermi energy levels above and below the conduction band edge and the valence band edge for the n^+ and p^+ doped materials, respectively.

The region between the conduction band edge and the Quasi-Fermi energy level of electron (Qf_n) is completely filled with the electrons, while the region between the valence band edge and the Quasi-Fermi energy level of holes (Qf_p) is completely filled with holes.

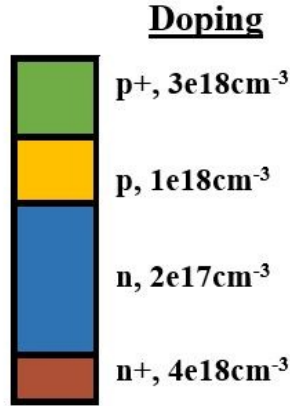

Figure 2.1: Doping concentration.

In the model, the base material is divided into two layers which are differently doped to be in contrast with its adjacent material. Here, the top surface is made of the material $Al_{0.3}Ga_{0.7}As$ which is heavily p^+ doped of concentration $3e18cm^{-3}$ and the junction it formed with the p- side of the base material is normally doped $1e18cm^{-3}$. On the back side of the structure, the material used is the $Al_{0.85}Ga_{0.15}As$ which is also heavily doped, but of opposite charge, that is n^+ doped of concentration $4e18cm^{-3}$ and the corresponding intersecting material is the n- type doped base material normally with dopant concentration of $2e17cm^{-3}$ shown in the Figure 2.1.

Moreover, the doping concentration is directly related to the work function of the material. Work function is the energy required to remove an electron from Fermi-energy level. It decreases for n-type material and increases for the p-type material with increasing dopant concentrations of electrons and holes on their respective sides.

Below is the general energy-band diagram of a photo-diode in PV cell mode operation. A conducting material Aluminium-CRC is used at either ends of the semiconductor (not shown in the figure) for the carrier to flow into the external circuit, generating photo-generated current, I_{ph}.

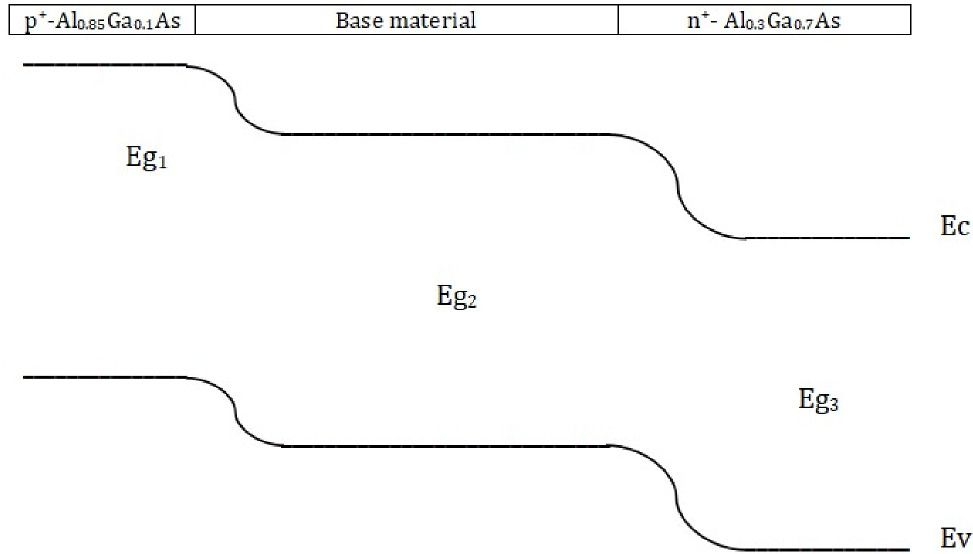

Figure 2.2: Energy-band diagram of a PV cell.

In the Figure 2.2, the base material or the substrate has a band-gap of E_{g_2}, while the adjacent heavily doped materials have band-gaps of E_{g_1} and E_{g_3}. The conduction band edge and valence band edge are given as E_c and E_v, respectively.

Light is incident from the p^+ side into the semiconductor and is absorbed in the base material. This generates electron-hole pair (E_{HP}) at the base material. The generated E_{HP} is separated by the existing Electric Field present caused by the depletion region within the base material due to different doping type in the base material. Both the electron and hole are separated and collected at either ends by the conductor placed on top of n^+ and p^+ sides respectively, as electrons act like solid objects and will roll down the slope on its own, whereas, holes act like bubbles in water and will move up the slope on its own.

2.4 Theoretical study of optical and electrical quantities

Electrical power is generated when a solar cell is illuminated producing current and voltage. Henceforth, a specific material is needed which will excite the electron to a higher energy state by the absorption of light. This excited electron is then ready to transport into an external circuit. The excited electron loses its energy in the external circuit and then returns back to the solar cell. Such criteria for photovoltaic energy transformation can be achieved by semiconductor materials in the

likes of a p-n junction. A solar cell operation implies the following steps:

- In the presence of light, carriers are generated.
- Photo current is produced due to the collection of these generated carriers.
- Voltage is induced across the solar cell.
- Power across the load is dissipated into the external circuit.

The “light-generated current” or photo-current in solar cells implies two main steps. The initial step is the absorption of the incoming light in the form of photons to generate electron-hole pairs (E_{HP}). The second process is the separation of the generated electron-hole pairs (E_{HP}). If the generated carriers are not separated, they may recombine and the E_{HP} generated will be lost without contributing to photo-current, thereby no power will be generated. If an electric load is connected across the base and emitter of the solar cell, then the separated carriers will flow in the external circuit in the form of photo-current.

Moreover, another significant phenomenon is the collection probability. It is the probability that in the contribution of photo-current, a charge absorbed in a specific location of the solar cell will be collected by the p-n junction. It relies upon the length that the transporter should venture out in relation to the diffusion length and the peripheral features of the cell.

Inside the depletion region, the collection probability is assumed to be one initially, since the E_{HP} are separated by the electric field present and are collected. Also, it is seen to reduce with increasing diffusion length when moved away from the junction. Thirdly, the collection probability will be lower if the carriers are generated in a region with higher recombination than the junction due to E_{HP} recombination.

The light-generated current density (J_L) is resolute by combination of the collection probability and the generation rate in the solar cell which is given as [42]:

$$J_L = \int_0^w eg(x)CP(x)dx \tag{2.1}$$

Where,
e=elementary charge,

W = thickness of the device,

g(x) = the arbitrary generation rate and

CP(x) = the collection probability.

2.4.1 Optical Simulation

A series of parameters are determined from optical simulation (FDTD):

1. Absorption per unit volume, Pabs
2. Generation rate, g
3. Short Circuit Current, Isc
4. Quantum Efficiency, QE and
5. Integrated Quantum Efficiency, IQE

i. Absorption per unit volume (Pabs)

Two separate methods are applied to compute the absorption per unit volume (Pabs). The initial one is to apply the divergence of a vector which is shown as [43]

$$Pabs = -0.5real(\overrightarrow{\nabla}.\overrightarrow{P}) \tag{2.2}$$

Nonetheless, divergence calculations is often to be very tactful to numerical problems. Therefore, a quite numerically stable form can be apply. The prior equation can be modified into [43] .

$$Pabs = -0.5real(i\omega^{\overrightarrow{E}.\overrightarrow{D}}) \tag{2.3}$$

This can be derived more into [43]

$$Pabs = -0.5\omega|E|^2 imag(\epsilon) \tag{2.4}$$

Absorption as a function of space and frequency can be computed, for this, electric field intensity and the imaginary part of the permittivity should be known. These two quantities can be calculated from FDTD simulation.

ii. Generation rate (g)

At any point within the solar cell and of any wavelength of light, an electron-hole pair generation can be found. Most of the light is absorbed at the surface of the material, hence highest generation take place there. The illumination used in PV applications, contains of various wavelengths from the whole standard solar spectrum. Therefore, while developing a solar cell, several generation rates should be taken into consideration. Generation rate can be found by integrating the g over simulation spectrum. Alternatively stated, generation rate is the ratio of number of absorbed photons per unit volume to energy per photon. In solar cell function, it is a major quantity and can be written as [44] :

$$g = \frac{Pabs}{\hbar\omega} = \frac{-0.5|E|^2 imag(\epsilon)}{\hbar} \tag{2.5}$$

iii. Short Circuit Current (I_{SC})

Considering ideal case, in which each absorbed photons generates an electron-hole pair, the photo-generation for this case can be found from I_{SC}= eg, in which e is the electron charge and current unit is in A/m. To achieve better result of short circuit current, the CHARGE solver can be used which will be discussed in the electrical simulation section. One more significant feature is the short current density. Considering all the electron-hole pair participates in photo current, the short circuit current density J_{sc} can be expressed as [44] :

$$J_{sc} = \int e\frac{\lambda}{hc}(\lambda)1.5(\lambda)d\lambda \tag{2.6}$$

iv.Quantum Efficiency (QE)

The quantum efficiency (QE) of a solar cell is defined as the ratio of number of carriers collected by the solar cell to the number of photons incident on the solar cell [39]. QE can be expressed as a function of either wavelength or energy. To illustrate, the quantum efficiency is unity for that specific wavelength of which all photons are absorbed, and the out coming minority carriers are collected.

The quantum efficiency (QE) of a solar cell is computed by [45] :

$$QE(\lambda) = \frac{P_{abs}(\lambda)}{P_{in}(\lambda)} \tag{2.7}$$

In which P_{abs} (λ) is the power of absorbed light, and $P_{in}(\lambda)$ is the power of the incident light, at a wavelength λ within the solar cell. Photons which have lower energy than band gap has zero quantum efficiency.

v. Integrated Quantum Efficiency (IQE)

Integrated quantum efficiency is expressed through the quantum efficiency [45]:

$$IQE = \frac{\int e\frac{\lambda}{\hbar c}QE(\lambda)IAM1.5(\lambda)d\lambda}{\int e\frac{\lambda}{\hbar c}IAM1.5(\lambda)d\lambda} \tag{2.8}$$

Where,

$I_{AM1.5}$ -AM 1.5 solar spectrum.

h- Planck's constant and

c- the speed of light in free space

In the aforementioned equation (2.8), the denominator represents the number of photons falling onto the cell whereas the numerator represents the number of photons absorbed by the cell.

2.4.2 Electrical simulation

Several parameters are calculated from electrical simulation (CHARGE). They are:

1. Short Circuit Current (I_{sc})
2. Open Circuit Voltage (V_{oc})
3. Photo-voltaic Energy Conversion Efficiency (η)
4. Fill Factor (FF)

1 **Short Circuit Current (I_{SC})**

As the name suggests, the short-circuit current is the current when the solar cell is short-circuited. In other words, it is the current present when the voltage across the solar cell is zero. This zero voltage occurs because of the generation and collection of light-generated carriers. The short circuit current (I_{SC}) and light-generated current (I_L) are equivalent in an ideal solar cell. Hence, it is assumed that the current obtained from the solar cell is maximum. The short-circuit current ((I_{SC})) relies upon several factors:

- The solar cell area

- Quantity of photons
- Spectrum of the incoming radiation
- Optical properties
- The collection probability

The diffusion length and surface stabilization are the vital material dependent parameters. The equation for the short-circuit current for a cell with uniform generation and perfectly stabilized surface can be represented as [42]:

$$I_{sc} = eg(L_n + L_p)$$

Where,
g- generation rate,
e- elementary charge,
L_n -electron diffusion length
L_p -hole diffusion length.
2 **Open Circuit Voltage** (V_{OC} **)**
Conversely, the highest voltage existing in the solar cell at zero current is known as the open-circuit voltage, (V_{OC}). It represents the value of forward bias cell which is due to the presence of solar cell bias junction with the help of photo-current. When the resultant current is set to zero, V_{OC} is found by the following equation [42]:

$$V_{OC} = \frac{kT}{q} \ln(\frac{J_L}{J_0} + 1) \tag{2.9}$$

Where,
J_L- photo-current density and
J_0 -dark current density or saturation current density.
It is seen from equation (2.9), the saturation current and photo-current affects V_{oc}. Open circuit voltage (V_{oc}) is also related with the number of recombination through the solar cell because the saturation current relies upon the recombination. Furthermore, since the dark current maintains linear relationship with the volume of the material, hence, reducing the thickness reduces the volume and thus, the dark current. If the photo-current can keep a large value across an ultra-thin solar cell due to efficient light trapping, thicker devices can be replaced with an ultra-thin material to enhance V_{oc}. However, the decreased of shunt resistance and surface

recombination have an impact on ultra-thin layers that should be considered.

3 **Photo-voltaic Energy Conversion Efficiency** (η)

Efficiency is a metric used to compare one solar cell's output to another. The ratio of the solar cell's output energy to the incident light's input energy is known as energy conversion efficiency. The quality relies on the incident light's strength and spectrum, as well as the solar cell's temperature. As a consequence, under particular conditions, it must be assessed. In basic terms, a solar cell's efficiency is calculated as the fraction of the incident power transferred to electricity. It needs to calculate the efficiency of photovoltaic energy conversion in order to determine the performance of solar cells [42]. The equation (2.10) shows below:

$$\eta = \frac{FF \times V_{\infty} \times J_{sc}}{S_{AM1.5G}} \tag{2.10}$$

Where,

FF- fill-factor

V_{OC} - open-circuit voltage,

$J_{SC} - short - circuitcurrentdensityand$

$S_{AM1.5G}$ - incident power.

The fill-factor equation (2.11) is dependent on the maximum power-point, in which the power (J×V) is maximum [44]:

$$FF = \frac{P_{max}}{V_{oc} \times J_{sc}} \tag{2.11}$$

4 **Fill Factor (FF)**

The fill factor (FF) is an electrical quantity. It measures the solar cell's maximum power with respect to open-circuit voltage and short-circuit current. The FF can be calculated by the fraction of the solar cell's maximum power and the product of open-circuit voltage and short-circuit current which shows in equation (2.12) [42]:

$$FF = \frac{P_{max}}{V_{oc} \times J_{sc}} \tag{2.12}$$

The fill factor determines the "squareness" of the solar cell graphically. Lengthiest rectangle's area that will adjust in the current vs voltage graph is considered in determining fill factor. It can also be expressed as the ratio of the maximum power to the product of V_{OC} and I_{SC}. Differentiating the power with respect to voltage

and solving this equation where it tends to zero can result the highest fill factor of a solar cell theoretically. This approach does not, however, provide a simple or closed solution. It only connects open-circuit voltage (V_{OC}) to maximum point voltage (V_{mp}) and additional measurements are required to measure maximum point current (I_{mp}) and FF [46].

The relationship of photo-current to various light trapping mechanisms was noticed. It was also mentioned that the overall cell efficiency is the V_{OC}, JSC, and FF product, with the effect on these amounts of nanophotonic light trapping. As previously mentioned, V_{OC} is associated with the photo current-dark current ratio and reducing the material volume reduces the dark current which improves V_{OC}. In such situations, however, fill factor will decrease because of the increased possibility of recombination in condensed volumes. The non-homogeneous absorption profiles have scope for expansion. The physics of a cell with nanophotonic light trapping can be different from either a flat cell or an arbitrarily textured surface if absorption varies [42]. Deposition of materials in various kinds of nano-structures can influence V_{OC}. The shunt resistance leading to void forming in the material which also deteriorate V_{OC} has been increased to special types of surfaces.

2.5 Fundamental of FDTD and CHARGE

2.5.1 FDTD

Electromagnetic investigation includes mathematical approach. The Finite Difference Time Domain (FDTD) system helps to calculate the electric and magnetic fields as a function of time. A well-defined characteristic of it can be obtained from FDTD's time-domain program. Fourier Transformation transforms the acquired outcome in frequency domain.

Other than time, a three-dimensional space result can also be procured from it, which is the function of Volume-based method in which the solution span is segregated into a uniform mesh [47].

The mesh consists of many cells, individual cell has a characterized E (electric) and H (magnetic) field part.

Maxwell's curl equations in non-magnetic materials can be solved using Finite Difference Time Domain. The mesh is made out of cells where every cell has a FDTD

solves Maxwell's curl equations in non-magnetic materials [48]:

$$\frac{\delta.\overrightarrow{D}}{(\delta.t)} = \nabla \times (\overrightarrow{H}) \tag{2.13}$$

H is the magnetic field.

$$\overrightarrow{D}(\omega) = \epsilon_0 \epsilon r(\omega) \overrightarrow{E}(\omega) \tag{2.14}$$

E is the electric field.

$$\frac{\delta.\overrightarrow{D}}{(\delta.t)} = -\frac{1}{\mu_0} \nabla \overrightarrow{E} \tag{2.15}$$

Here, ϵ r (ω) represents complex relative dielectric constant, and can be calculated from ϵ r $(\omega) = n^2$, using n as the refractive index.

For 3-Dimension, there are six electromagnetic parameters in Maxwell's equations i.e. $E_x, E_y, E_z, H_x, H_y, H_z$. Considering that the structure is infinite in z dimension and the fields do not depend on z, then [49]:

$$\epsilon r(\omega, x, y, z) = \epsilon r(\omega, x, y) \tag{2.16}$$

$$\frac{\delta \overrightarrow{E}}{\delta z} = \frac{\delta \overrightarrow{H}}{\delta z} = 0 \tag{2.17}$$

Afterwards, two independent equations come out from Maxwell's equation, each equation consist three vector quantities which can be resolved only for the x-y plane. One equation, Transverse Electric (TE), have components $E_x, E_y, E_z z$, second equation Transverse Magnetic(TM), have components H_x, H_y, H_z [50].

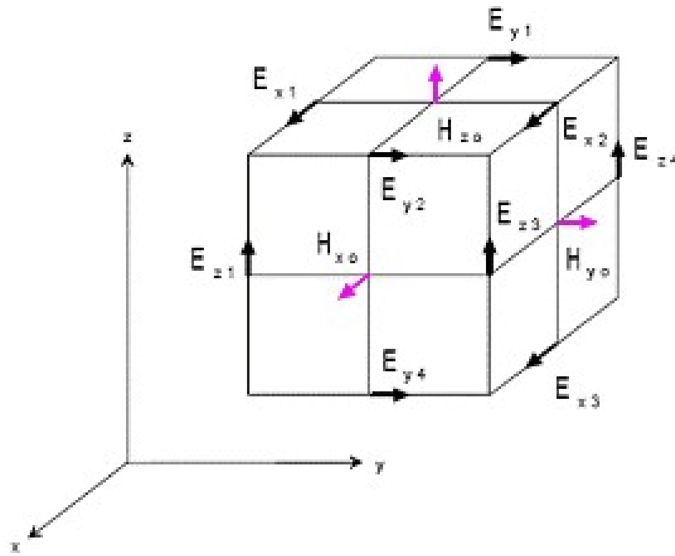

Figure 2.3: Grid cell, considering for solving field components.[51]

Maxwell equations can be resembled by illustrating TM condition as [49]

$$\frac{\delta D_z}{\delta t} = \frac{\delta H_y}{\delta x} - \frac{\delta H_x}{\delta x} \tag{2.18}$$

$$D_z(\omega) = \epsilon_0 \epsilon_r(\omega) E_z(\omega) \tag{2.19}$$

$$\frac{\delta H_x}{\delta x} = \frac{1}{\mu_0} \frac{\delta E_z}{\delta y} \tag{2.20}$$

$$\frac{\delta H_y}{\delta t} = \frac{1}{\mu_0} \frac{\delta E_z}{\delta x} \tag{2.21}$$

These above equations would be solve on a discrete spatial and temporal grid by FDTD function. From Figure 2.3, it can be seen that inside the grid cell, at marginally different location, every field component is resolved. By default, data collected from the FDTD solver is automatically interpolated to the origin of each grid point.

2.5.2 Implementing FDTD technique

Performing an FDTD solution of Maxwell equations, a physical calculative area must be established on which simulation will be carry out [47]. The E (electric) and H (magnetic) fields resolved at each point in space inside that area. Individual cell material inside the area should be designated generally as metal, free-space or dielectric. Permittivity, Permeability and Conductivity must be adjusted according to material chosen. Following the setup of computational area and the grid materials, a source is set out. The source can be either an applied electric field, current-carrying wire, or imposing plane wave or an incoming light from the typical solar radiation. FDTD can be used to model large periodic structures, illumination from random formed objects and planar periodic structures at various angles of incidents.

As the magnetic field and the electric field are resolved straightforwardly, the outcome simulation is normally the magnetic field (H) or the electric field (E) at a point or a range of points inside the calculative area.

The simulation develops the E and H fields forward in time as expected. Information preparation may likewise happen while the simulation is in progress. From near-to-far-field transformations, Scattered and radiated far fields can be acquired.

The FDTD solver has the following simulation objects:

1. General tab
2. Geometry tab
3. Mesh settings tab
4. Boundary conditions tab
5. Advanced options tab

Normally solar cells can be exhibit applying periodic structures. This requires only one-unit cell and periodic, symmetric or asymmetric boundary conditions are used mostly for simulation. In the frame work, a plane wave with wavelength spanning the full solar spectrum is used for the light source. In order to absorb reflected and transmitted fields, Perfectly Matched Layer (PML) boundary conditions are needed along the infusion direction [52]. In the place of genuine solar spectrum, the default source spectrum can be used. To decrease memory requirement, thus speeding up the simulation process, proper symmetry or anti-symmetry boundary conditions needs to be used. While doing sweep and optimization, inessential monitors such as movie monitors, should be disabled.

2.5.3 CHARGE

The Charge Transport (CHARGE) solver is a physics-based electrical simulation software for semiconductor devices. It self-consistently solves the system of equations describing electrostatic potential (Poisson's equations) and density of free carriers shown in equations (2.22 and 2.23). This is a powerful technique which produces precise results under equal working conditions for a broad range of semiconductor devices.

Several essential numerical and physics theories utilized for the CHARGE calculation is talked about in the accompanying section. The drift-diffusion equations (2.22 and 2.23) for electron carriers and hole carriers can be resolute by CHARGE and are given by **50**,

$$Jn = q\mu_n nE + qD_n\nabla_n \tag{2.22}$$

$$Jn = q\mu_p pE + qD_p\nabla_p \tag{2.23}$$

Where,
q - charge of the positron,

E - electric field,

$J_{n,p}$ - current density ($\frac{A}{cm^2}$),

$\mu_{n,p}$ - mobility,

$D_{n,p}$ - diffusivity,

n and p are the densities of the electrons and holes respectively

Every charge transports due to two forces acting on them: i) drift and ii) diffusion. The carriers drift because of the presence of the induced electric field and diffuse randomly in consequence of diffusion gradient present. Mobility ($\mu_{n,p}$) shows how simple transporters can pass through the semiconductor material and is connected to the diffusivity $D_{n,p}$ through Einstein equation [50],

$$D_{n,p} = \mu_{n,p} \frac{K_b T}{q} \tag{2.24}$$

Where:

K_b is the Boltzmann constant.

Mobility is an important parameter for a material which is modeled in terms of doping, temperature, electric field and carrier concentration. To resolute the equation of drift diffusion involving Poisson's equation, the electric field have to be defined [50],

$$-\nabla(\epsilon \nabla V) = qp \tag{2.25}$$

Here,

ϵ- is the dielectric permittivity,

V - the electrostatic potential ($E = -\nabla V$)

ρ -is the net charge density.

Lastly, in order to sustain the charge, the auxiliary continuity equations are required [50],

$$\frac{\delta n}{\delta t} = \frac{1}{q} \nabla J_n - R_n \tag{2.26}$$

$$\frac{\delta p}{\delta t} = \frac{1}{q} \nabla J_p - R_p \tag{2.27}$$

Here,

$R_{n,p}$ - the difference between the recombination rate and generation rate for electrons and holes respectively.

2.5.4 Implementing CHARGE technique

CHARGE solver breaks down and resolves Poisson's equations and drift-diffusion on a non-structured finite-element mesh in 1D and 2D. Simulation region is divided into several areas along the boundaries among materials, where the substance can be categorized as or insulators, semiconductors or conductors. Usually, specific multi-coefficient models are equipped with semiconductors depicting the major qualities intrinsic to the substance.

Aforementioned set of equations resolute both time-varying and steady-state output. The electrostatic potential and carrier density can be solved by executing the condition, $\frac{\delta_n}{\delta_t} = \frac{\delta_p}{\delta_t} = 0$ the continuity equations. The behavior of system could be analyzed and small-signal parameters could be derived with the help of steady-state simulations. On the other hand, it is necessary for electrostatic potential to solve equations and derive large-scale AC parameters in a series of discrete periods.

Boundary conditions plays an essential part for precise simulation of semiconductor substance. In CHARGE, there are two classes for boundary conditions. Firstly, it identifies the electrostatic potential (Poisson's equation).Secondly, it identifies with the transporter densities (the drift-diffusion equations). The boundary conditions are resolved from the actual properties of the interface between two domains that are not contacts at internal boundaries.

The CHARGE solver has the following simulation objects:

1. General tab Mesh tab
2. Transient tab
3. Small Signal AC tab
4. Results tab
5. Advanced tab

Appropriate voltage steps should be picked. The simulation may be difficult to converge when using a large voltage step, for example. Besides, a legitimate working temperature should be set which is T=300K by default. Moreover, there should not

be any vacuum in the whole simulation region, i.e. the simulation region must be occupied by materials other than vacuum, for example, GaAs. Lastly, all metals should be related with a contact.

2.6 Simulation road-map

Fabricate and define solar cells' characteristics are obtained through both electrical and optical simulation. Large number of effective charge carrying rate, output electrical power and high optical absorption are required parameters to determine the performance of any solar cell. To measure these required parameters, electrical and optical simulation are performed by using CHARGE and FDTD respectively.

The road-map for FDTD simulator:

1. Select materials from inventory
2. Define dimensions, geometry and then allocate them
3. Select plane source
4. Analysis group has been selected from object library
5. Meshing region must be defined
6. Run the simulation and check for any error
7. Collect the relevant data and locate the generated with the extension of (.mat) file
8. Finally analyze.

The road-map for CHARGE solver:

1. Select the materials from material library
2. Define geometry and set them
3. Select charge simulation region from solvers
4. Set boundary condition
5. Specify constant doping region and add band structure monitor

6. Define different electrical mesh constraint

7. Add optical generation rate as source

8. Run the simulation and check for any error

9. Collect the data and finally analyze.

The overall road-map of the simulations are shown in **Figure 2.4**:

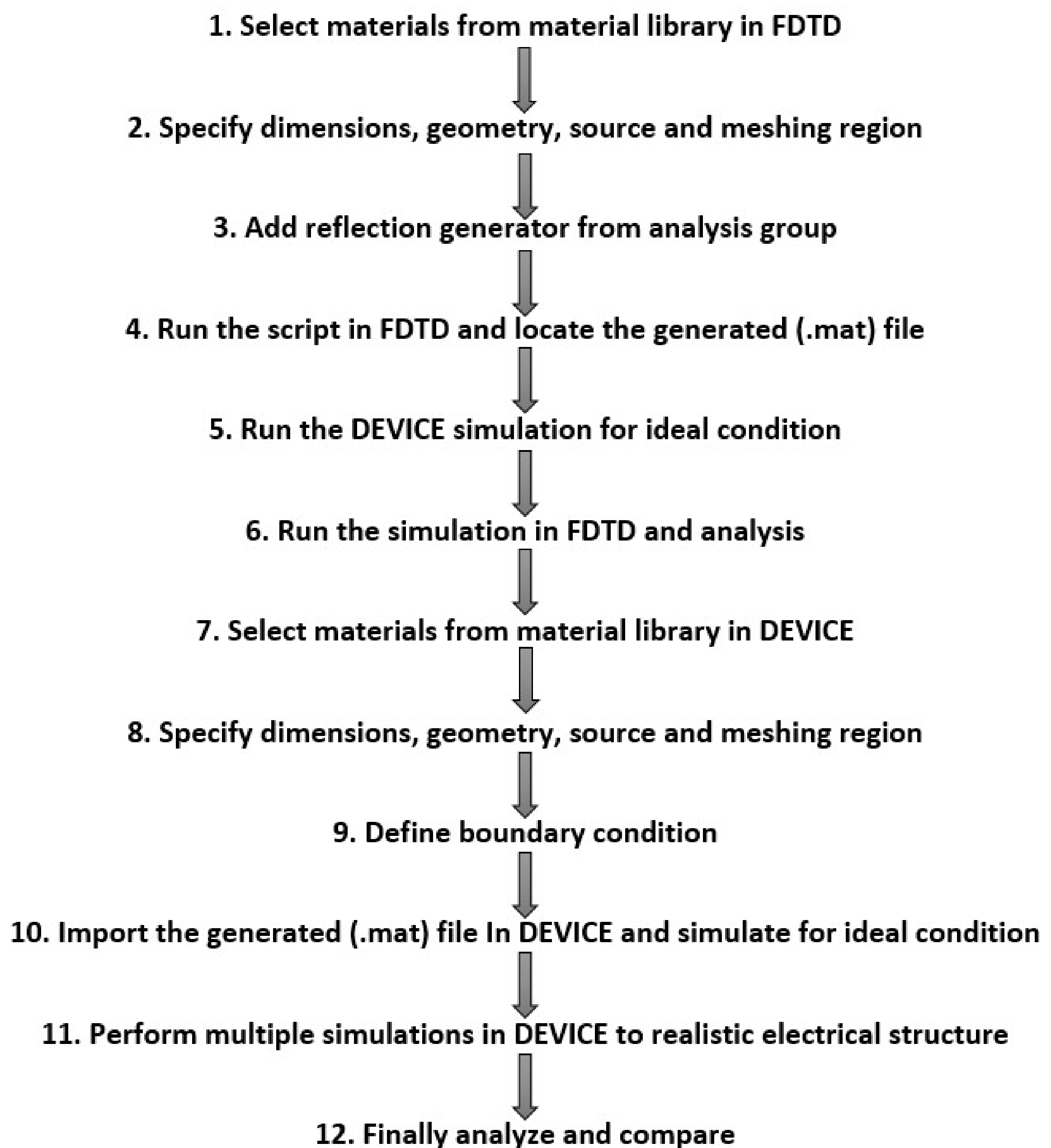

Figure 2.4: Simulation road-map.

2.7 Conclusion:

The above mentioned chapter carries the primary information about the theoretical prospects related to tandem solar cell especially light-trapping procedure, doping mechanism, different equations related to electrical and optical simulation, a brief discussion about FDTD simulator and CHARGE solver and at the end, the simulation road-map. For analyzing the TSC model in the coming chapters, these information will be essential.

Chapter 3

Aluminium Gallium Arsenide ($Al_xGa_{(1-x)}As$)/Gallium Arsenide ($GaAs$) Tandem Solar Cell

3.1 Introduction

It is vitally important to perform optical and electrical simulation to acquire the efficiency of a Photo-Voltaic(PV) solar cell. In this chapter, the outcomes of optical and electrical simulations will be analyzed, using FDTD and CHARGE of a 2-Dimensional(2D) planar Gallium Arsenide (GaAs) Tandem Solar Cell (TSC). The design of the 2D planar GaAs TSC is kept simple to get precise outcome, because with greater complexity, there is a high probability of errors.

Combining the optical and electrical methods are required as they provide separately the purpose of calculating the resultant PV efficiency. Taking into account each and every consequences of the substances participated to improve the absorption of illumination from the source, optical energy is absorbed in the GaAs TSC substrate. This is studied by monitoring the electron-hole pair generation in the optical simulation. The aforementioned generation rate is imported in the electrical simulation which happens to study the output electrical power. This is done by the accumulation of photo-generated electron-hole pair in the electrical contacts.

To overcome the Shockley-Queisser(S-Q) limitations, TSC which is a stacked of more than one sub-shell with dissimilar band gap can outstrip the S-Q limitations. In this chapter, GaAs has been taken as the base material in $Al_{0.8}Ga_{0.2}As/GaAs/Al_{0.3}Ga_{0.7}As$ to study TSC efficiency, optically and electrically.

3.1.1 Background study of GaAs Tandem Solar Cell

Shockley-Queisser Limitations with single sub-shell GaAs

GaAs efficiency subjected to S-Q limit for illumination of AM 1.5G solar spectrum is 32.8% (Figure 3.1). It is the highest theoretical efficiency for GaAs with the band gap of 1.424 eV.

When the AM1.5G spectrum is used as a source (with a total power density specified as 100 mW/cm^2), the total number of absorbed photons over all wavelengths would be capable of generating a current of

$$J_{AM1.5G} = \int_0^\infty \frac{\lambda}{\hbar c} S_{AM1.5G}(\lambda) d\lambda = 67.2707 mA/cm^2) \tag{3.1}$$

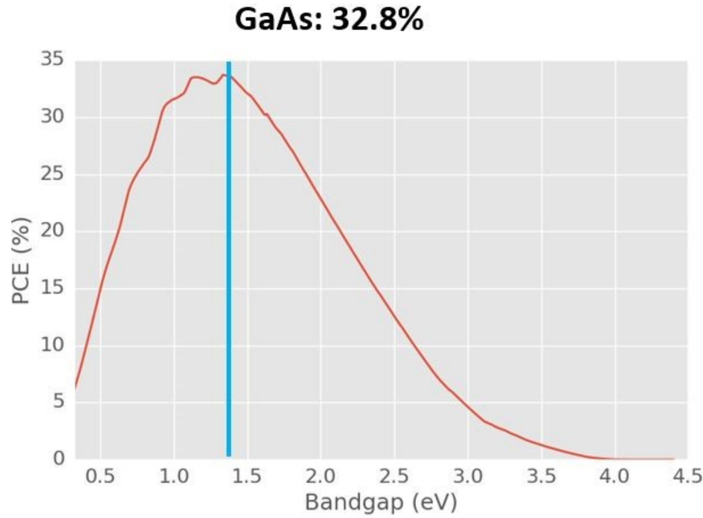

Figure 3.1: Efficiency vs Band-gap of a single junction solar cell.[24]

This efficiency is close to solo junction PV cell maximal efficiency which is 33.7% with the ideal band gap of 1.34ev, under S-Q limit accompanied by AM 1.5G solar spectrum.

3.2 Modeling and Simulation

3.2.1 FDTD Model

A pile of 2D TSC $Al_{0.3}Ga_{0.7}As$/GaAs/$Al_{0.8}Ga_{0.2}As$ has been fabricated in FDTD. $Al_{0.3}Ga_{0.7}As$ has a thickness of 0.03 μm, placed on top, works as a p^+-region. On

the bottom side, $Al_{0.3}Ga_{0.7}As/GaAs/Al_{0.8}Ga_{0.2}As$ As is placed performing as n^{+}-region. with thickness being 0.02 μm. The base material GaAs has a thickness of 1.65 μm and is sandwiched between the $Al_{0.3}Ga_{0.7}As$ and $Al_0.85Ga_0.15As.$, The depth of the structure is shown in the cross-section view in **Figure 3.2**.

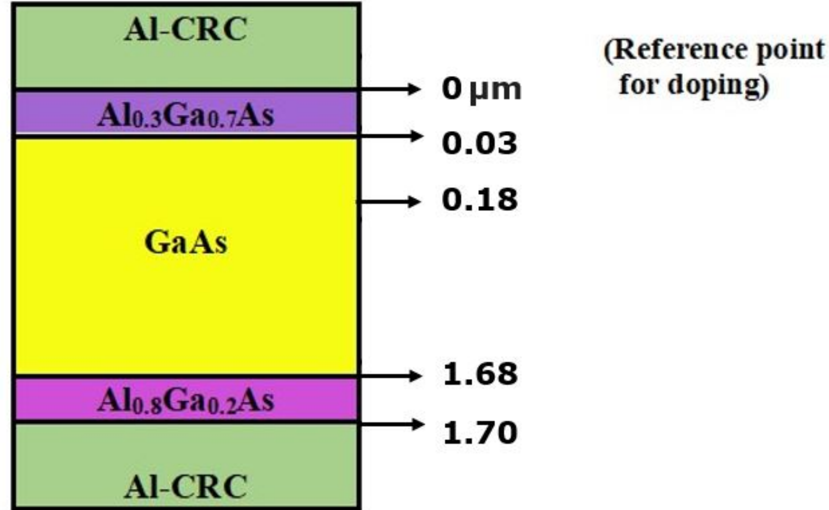

Figure 3.2: 2D Design of GaAs TSC.

While performing non ideal optical simulation of tandem solar cell, 4 phenomena must be taken into account. There will be some reflection from the front surface of the structure because Air reflective coating is non-ideal. Light from back side will not reflect entirely. The shadowing effect on solar cell, and partial absorption due to real refractive index.

To decrease the loss of efficiency due to reflection, Anti-reflective coating (ARC), which has a refractive index of 1.4, is joined at the front surface. Thickness of ARC has been varied till the maximum optical absorption (in GaAs) is observed at 0.1 μm. The back surface has been covered by aluminum contact layer. A plane wave source is used to provide light on FDTD region or simulation region. The region has been covered by solar generation rate analysis group. This will compute electron-hole pair generation rate and ideal short circuit current density under AM1.5G solar spectrum source.

Light of shorter wavelengths will be absorbed on the surface of GaAs, so a mesh

override is put on GaAs surface to enhance the resolution for the absorbed power calculations, which would have deteriorated otherwise.

The absorption band gap of GaAs is used as 1.424 eV.

The 2D and 3-Dimensional (3D) planar structure of the model in FDTD is shown in **Figure 3.3 and 3.4** respectively.

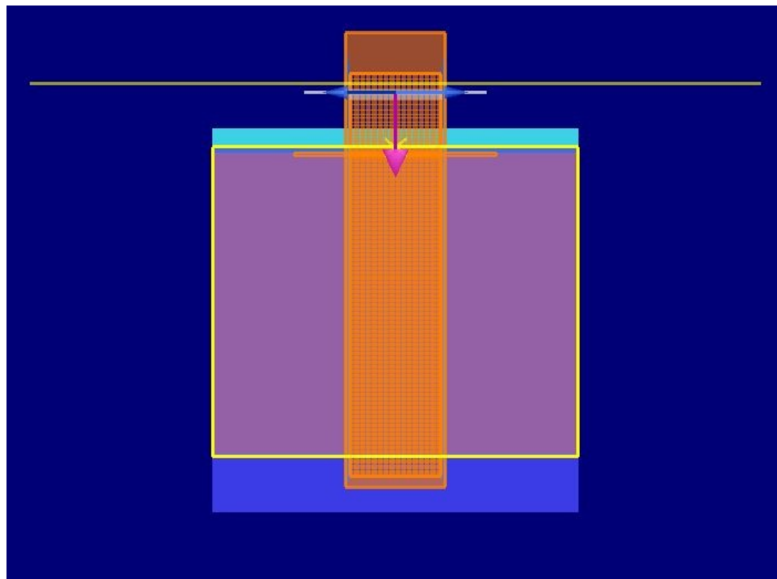

Figure 3.3: FDTD 2D Planar GaAs TSC design.

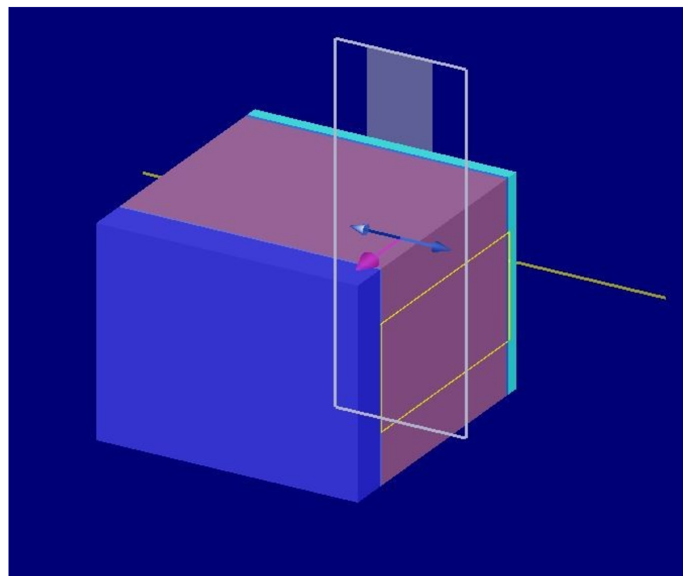

Figure 3.4: FDTD 3D Planar GaAs TSC design.

3.2.2 Device Model

The ideal electrical structure model of GaAs has been adjusted to the extent that all non-radiative recombination processes (Shockley-Read-Hall Auger) is disabled and the mobilities for both electron and hole are very high. Aluminium-CRC is used as base and emitter with a work function of 4.28 eV as well as the conductor. To achieve more proximate value with the theoretical reverse biased saturation current, the hole effective mass has been lessening a bit, which affects the open circuit voltage. The dimensions of CHARGE Transport model are equivalent to what has been set for optical structure.

The 2D and 3D planar structure of the model in DEVICE is shown in **Figure 3.5 and 3.6** respectively.

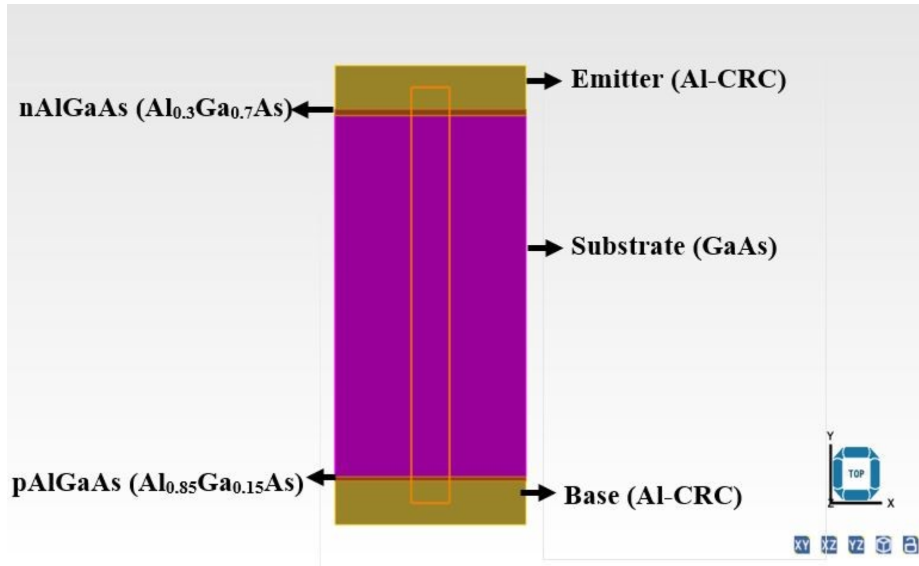

Figure 3.5: DEVICE 2D Planar GaAs TSC design.

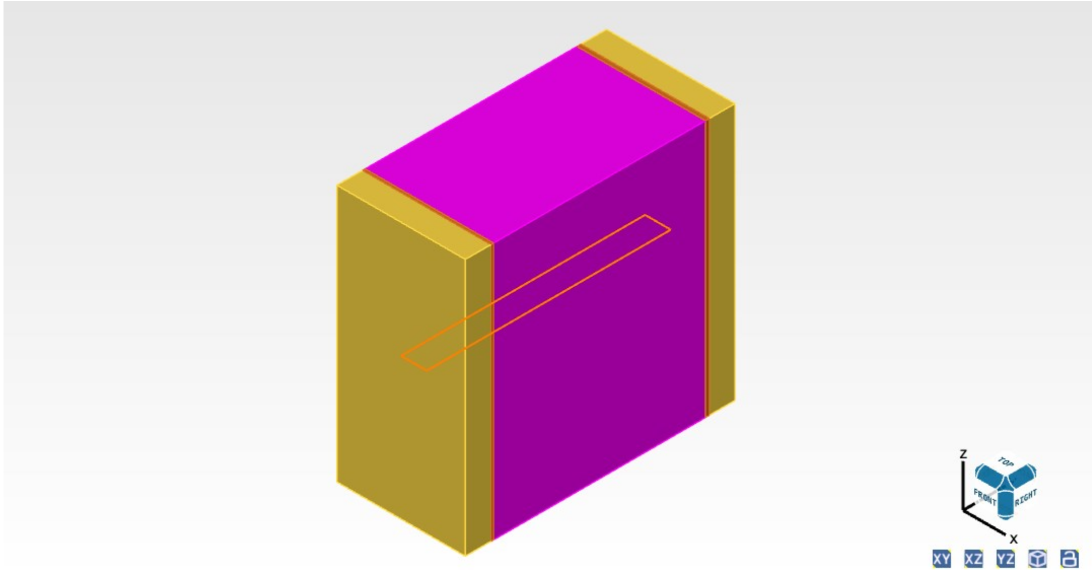

Figure 3.6: DEVICE 3D Planar GaAs TSC design.

3.3 Optical simulation

3.3.1 Introduction

In following segment, the optical simulation for determining the light absorbed by GaAs is carried out, considering that each photon will generate a single electron-hole pair. Under the FDTD method, the optical tandem solar cell model has run and computed Power absorbed, Total Power absorbed, Short-Circuit Current Density (J_{SC}), Generation rate(G) and Generation rate Export (G_ export). The simulation setup consists of a plane wave source whose wavelength is under solar spectrum. In the model, it has used the wavelength ranging from 300 nm to 1300 nm. This source transmit light in the direction of the surface of solar cell in negative direction of y-axis.

Besides, an artificial absorbing layer is setup as a Perfectly Matched Layer (PML) along the y-direction to prevent boundary reflection which is in excess. Periodic boundary condition is setup along the x-direction. The temperature was maintained at 300 Kelvin(K) and simulation time was kept at 1000 femto second (fs).

To confirm the AM1.5G spectral power is standardized to 100 mW/cm^2, the analysis object has been altered to some extent in the wavelength range of 0.3-2.6 μm.

The ideal (fully absorbed) optical simulation creates a source file for electron-hole pair generation. This file is loaded under ideal_ogr data, and simulation has been run.

3.3.2 Results and Discussions

The maximum short circuit current density is found to be 32.161 mA/cm^2, while the ideal current density of 32.0782 mA/cm^2. Maximum AM1.5G EHP generation is 67.2707 mA/cm^2. The maximum total absorption per unit volume is 0.96479 (arb. unit) with respect to 5.5E-07 m wavelength.

The Absorption per unit volume with respect to Wavelength **(Figure 3.7)** shows at locations ranging from approximately -250 nm to 250 nm and of depth ranging from surface to -1.6 μm is shown and the absorption in this volume is given as 1.05e+04 (arb. unit) approximately.

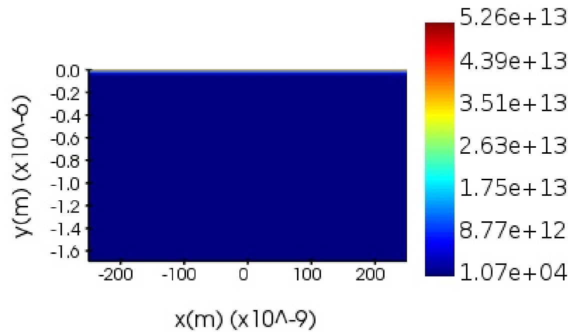

Figure 3.7: Absorption per unit volume vs Wavelength for GaAs.

In **Figure 3.8**, Total Absorption per unit volume is plotted with respect to the Wavelength. The graph starts from 0.3 μm wavelength and is seen an almost linear increase up to 0.54 μm Then the highest value is reached to 0.96 approximately at wavelength 0.55 μm The graph then starts to decrease up to 0.86μm with some spikes. On the contrary, there is a sharp decrease seen for the wavelength ranging from 0.86 μm to 0.89 μm. Finally, a parabolic spike is seen for the wavelength ending at 1.3 μm.

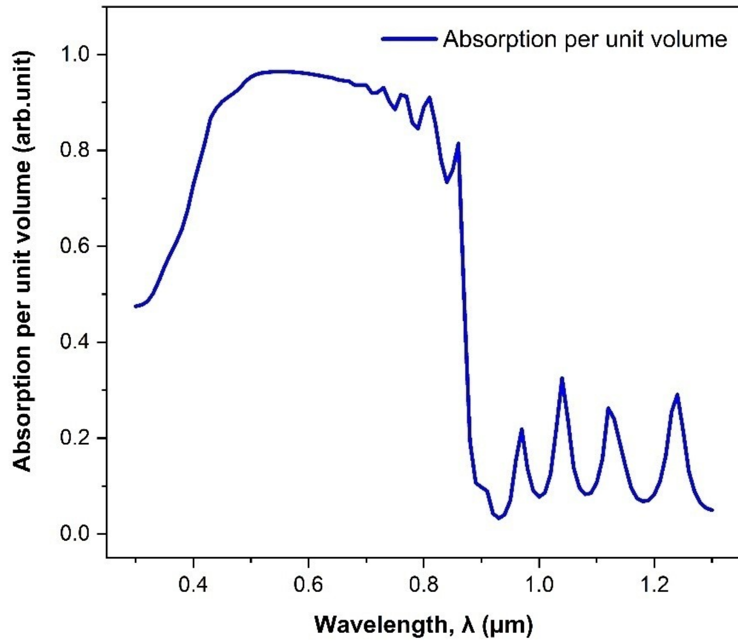

Figure 3.8: Total Absorption per unit volume vs Wavelength for GaAs.

Current density is plotted and is obtained to be 311.029 mA/cm^2 as shown in **Figure 3.9.**

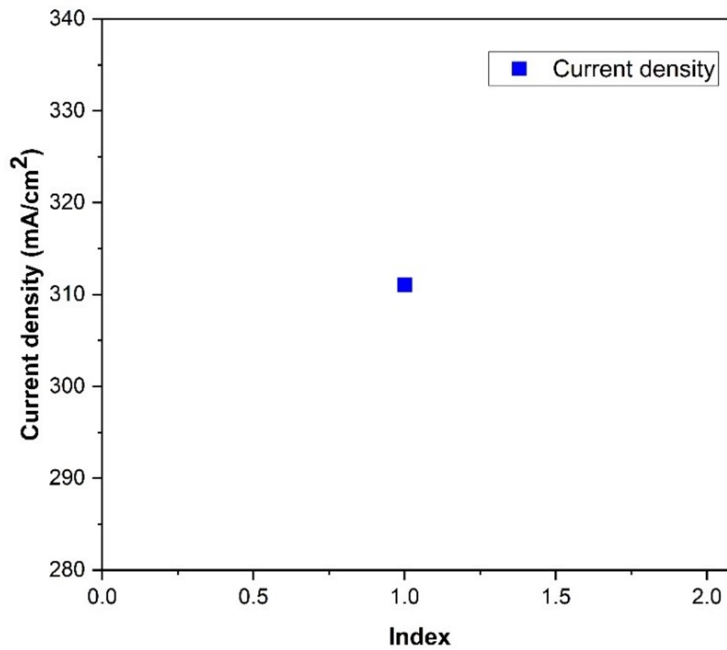

Figure 3.9: Current density (J_{SC}).

Next, the absorption enhancement factor is shown in **Figure 3.10.** The figure shows at locations of x = -250 nm to 250 nm, the absorption is seen to decrease from surface, that is y = 0.0 μm to y = -0.4 μm from 1.26e+28 (arb. unit) to 2.13e+27 (arb. unit) approximately. On the contrary, the absorption is then constant from y = -0.4 μm to -1.6 μm at a value of around 2.56e+25 (arb. unit) as shown in the figure.

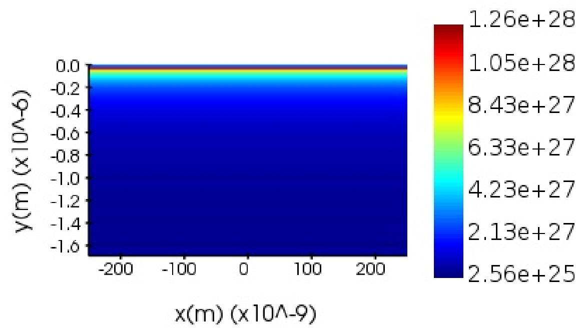

Figure 3.10: Absorption enhancement factor.

The following generation rate **Figure 3.11** shows at locations of x = -500 nm to 500 nm, the absorption is seen to decrease from surface, that is y = 0.0 μm to y = -0.4 μm from 1.26e+28 (arb. unit) to 2.13e+27 (arb. unit) approximately. However, the absorption is then constant from y = -0.4 μm to -1.6 μm at a value of approximately 2.56e+25 (arb. unit) shown in the figure.

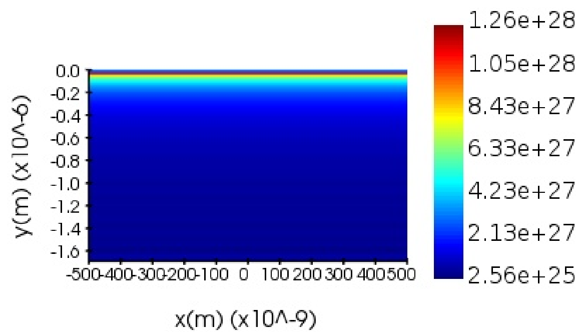

Figure 3.11: Generation Rate.

3.4 Electrical Simulation

3.4.1 Introduction

The boundary conditions have two groups, electrical boundary condition for base and emitter, and surface recombination for surface recombination. The CHARGE solver also consists of four Constant Doping Region: p, p^+, n and n^+.

The recombination rate process has been analyzed by running the code of recombination. From the recombination dataset of charge simulation, code will produce a plot showing three different recombination process.

1. Radiative Recombination: When an electron from higher energy level conduction band moves to lower energy level valence band, recombines with a hole, releases energy in the form of photon

2. Shockley-Read-Hall (SRH): It is non radiative recombination, in the transition of electron from valence band to conduction band, it may trap by an energy level which is in between of higher and lower energy level, and energy is released in the form of vibration. Such recombination also called as trap assisted recombination as electron has been trapped.

3. Auger Recombination: It occurs when instead of releasing photon after recombination, a third particle, either electron or hole moves to conduction band or valence band respectively.

3.4.2 Results and Discussions

1. Without contact shadow

   After running the necessary code for ideal recombination and plotting the result, the following graphs are obtained. The maximum short circuit current density (J_{SC}) is obtained 32.5941 mA/cm^2, and the open circuit voltage (V_{OC}) is close to 1.11 V **(Figure 3.12)** and also peak efficiency is found to be 32.2334 % **(Figure 3.13).**

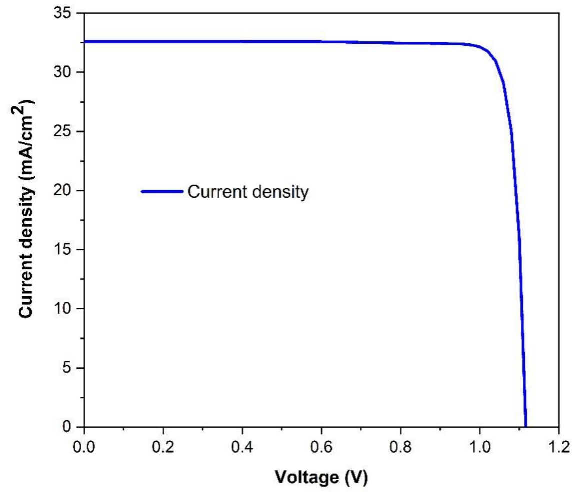

Figure 3.12: Current density vs Voltage for shadow less.

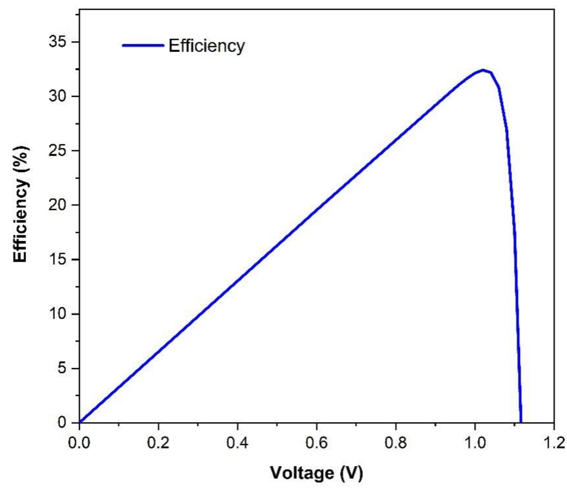

Figure 3.13: Efficiency vs Voltage for shadow less.

Band structure monitor shows the band diagram of conduction band, valence band, intrinsic Fermi-energy level, Quasi-Fermi energy level of electron and hole (in eV) with respect to depth as shown in **Figure 3.14.**

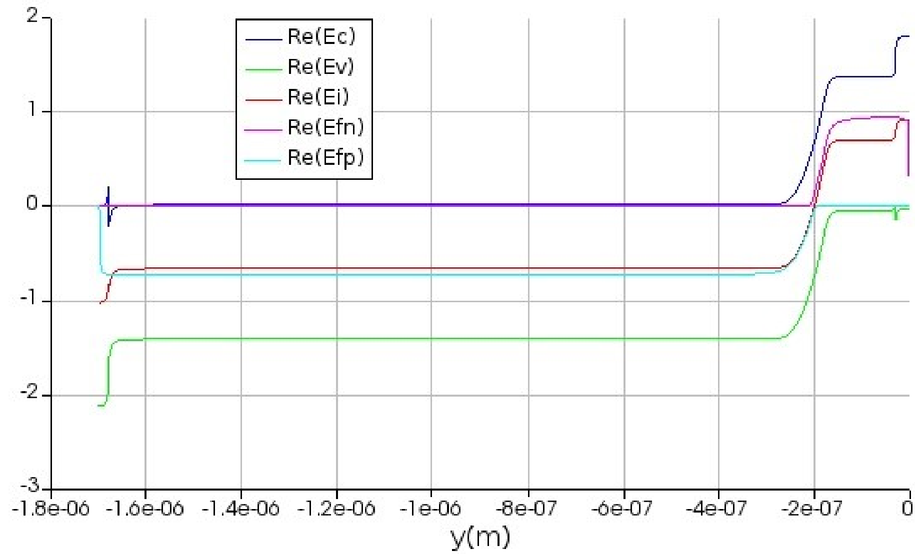

Figure 3.14: Total Absorption per unit volume vs Wavelength for GaAs.

2. <u>With contact shadow</u>

The ideal_ ogr has been disabled while its counterpart that is ogr (Optical Generation Rate) is enabled. Then the OGR_ AlGaAs_ fine.mat is imported into CHARGE and the simulation has been performed.

Then run the program code for contact shadow, and plotting the result, the following graphs are obtained. In **Figure 3.15,** maximum short circuit current density (J_{SC}) is obtained 28.5975 mA/cm^2, and the open circuit voltage (V_{OC}) is close to 1.11 V and the peak efficiency is found to be 28.1708 % **(Figure 3.16).**

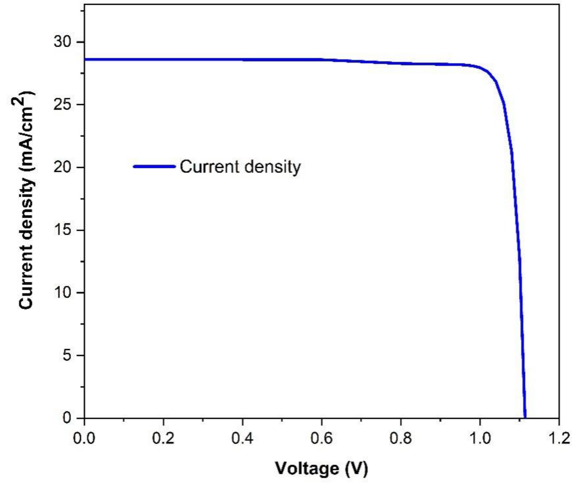

Figure 3.15: Current density vs Voltage with shadow loss.

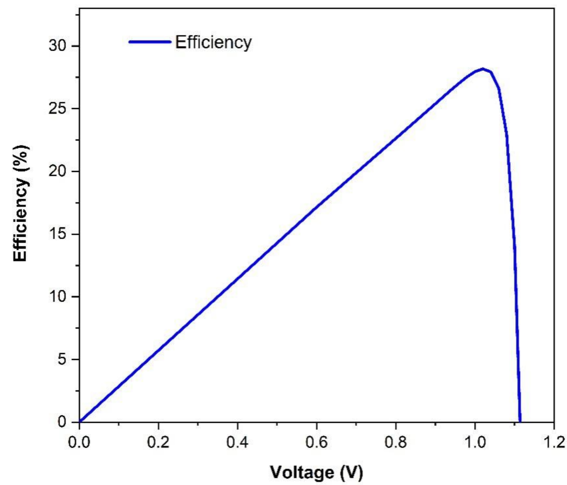

Figure 3.16: Efficiency vs Voltage with shadow loss.

In the following steps, all the semiconductor material models has been changed from ideal to their standard counterparts, and a series of charge simulation has been run:

The Trap-Assisted recombination function has been disabled for all 3 materials $Al_{0.8}Ga_{0.2}As$, GaAs and $Al_{0.3}Ga_{0.7}As$, while Radiative and Auger recombination are kept enabled. The contact shadow program code has run, and following graphs are obtained from data. In **Figure 3.17,** maximum short circuit current density (J_{SC}) is obtained 28.669 mA/cm^2, and the open circuit

voltage (V_{OC}) is close to 1.06 V. Besides, the peak efficiency is found to be 26.961% .

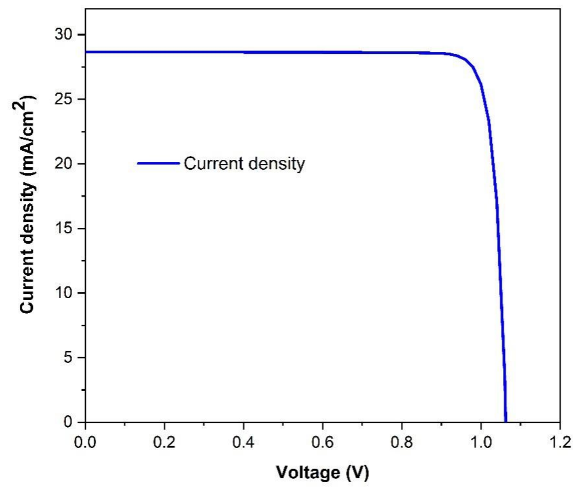

Figure 3.17: Current density vs Voltage when trap-assisted is disabled.

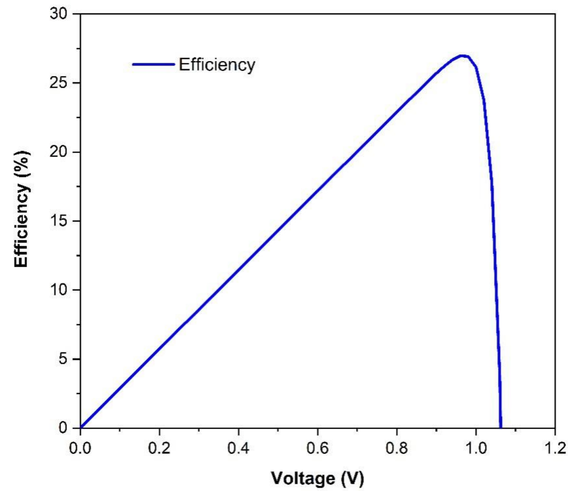

Figure 3.18: Efficiency vs Voltage when trap-assisted is disabled.

Now, the Trap-Assisted recombination has re-enabled for all 3 materials, and by running the contact shadow code another time, the following graphs are plotted. The maximum short circuit current density (J_{SC}) is obtained 28.6493 mA/cm^2, and the open circuit voltage (V_{OC}) is close to 1.06 V shown in **Figure 3.19** and its peak efficiency is found to be 26.8244% .

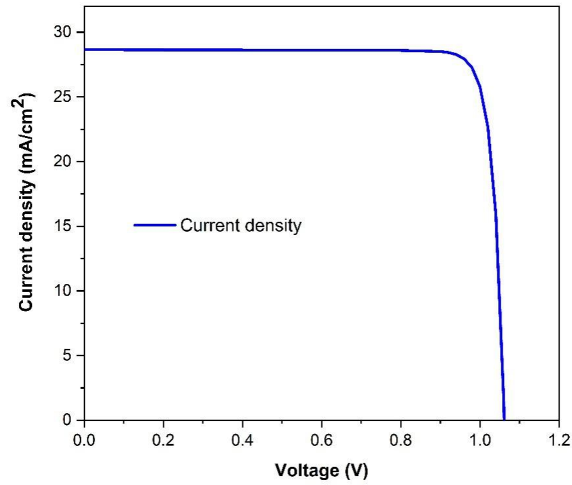

Figure 3.19: Current density vs Voltage with trap-assisted re-enabled.

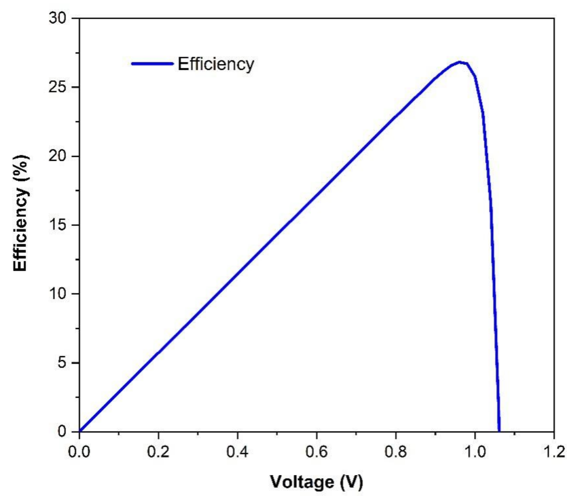

Figure 3.20: Efficiency vs Voltage with trap-assisted re-enabled.

Furthermore, the recombination program code has run and the following graph is obtained. In **Figure 3.21**, Radiative recombination rate is 91.6949% Auger recombination rate is the least which is 0.371643% and Shockley-Read Hall recombination rate is 7.93344%.

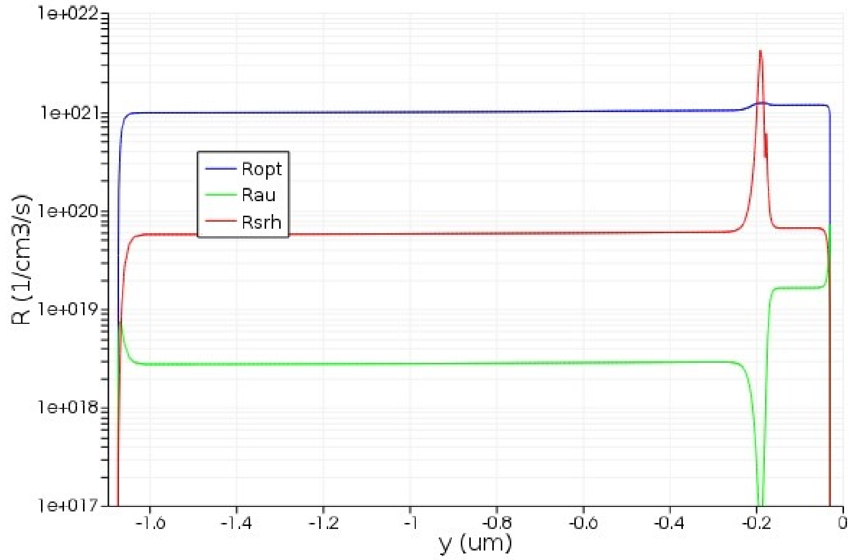

Figure 3.21: Recombination rate (Radiative, Auger, and Trap-Assisted) vs depth.

After successfully completing the previous simulation, the series resistance has been enabled and the value is set to 3.5E+04 to notice the effect in current density and in efficiency. After running the simulation, the shadow contact program has been run, and following graphs obtained. The maximum short circuit current density (J_{SC}) is obtained 28.6487 mA/cm^2, and the open circuit voltage (V_{OC}) is close to 1.07 V shown in **Figure 3.22** and its peak efficiency is attained to be 26.25 %.

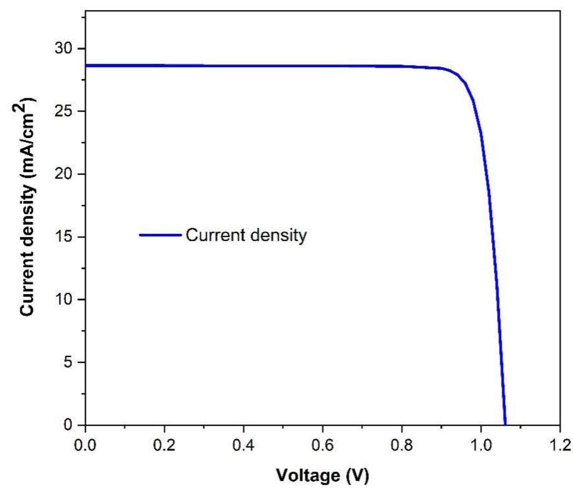

Figure 3.22: Current density vs Voltage with RSE enabled.

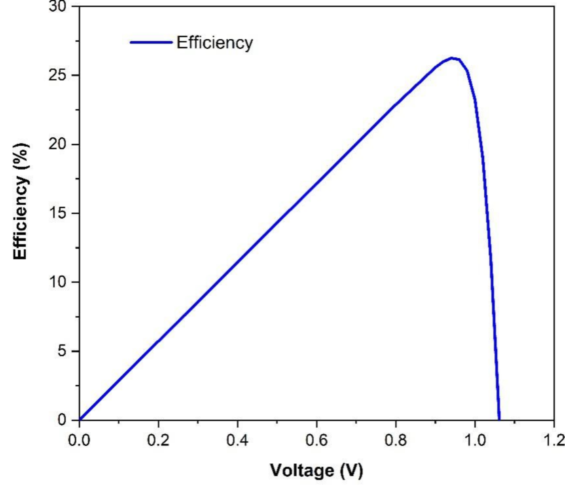

Figure 3.23: Efficiency vs Voltage with RSE enabled.

Finally, it is necessary to include the effects of photon recycling: that is when a photon is emitted with energy equal to the band gap, which might reabsorb, when the electrons and holes recombine radiatively. The coherent simulation of this process is difficult but can be approximated by the Asbeck coefficients by altering the radiative recombination rate coefficient.

The Asbeck coefficient is material dependent and is a function of depth. The Asbeck coefficient has a value of =4.6 for a 1.65μm thick layer of GaAs such that

$$\tilde{C}_{opt} = \frac{C_{opt}}{\phi} = 1.09 \times 10^{-10} cm^3 s^{-1} \tag{3.2}$$

Incorporating the altered value of radiative recombination rate coefficient, the current density and efficiency has been analyzed by changing the radiative recombination rate coefficient from $5e^{-10}cm^3s^{-1}$ to $1.09e^{-10}cm^3s^{-1}$. The changes have been simulated and shadow contact code has run. Then, following graphs plotted from the data obtained from the above mentioned simulation. In **Figure 3.24,** maximum short circuit current density (J_{SC}) is obtained 28.99 mA/cm^2, and the open circuit voltage (V_{OC}) is close to 1.0 V. Also, the peak efficiency is obtained to be 27.4635%.

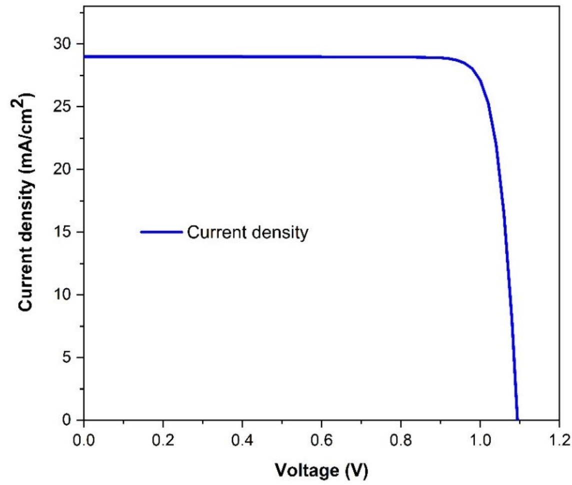

Figure 3.24: Current density vs Voltage with a decrease in radiative recombination rate.

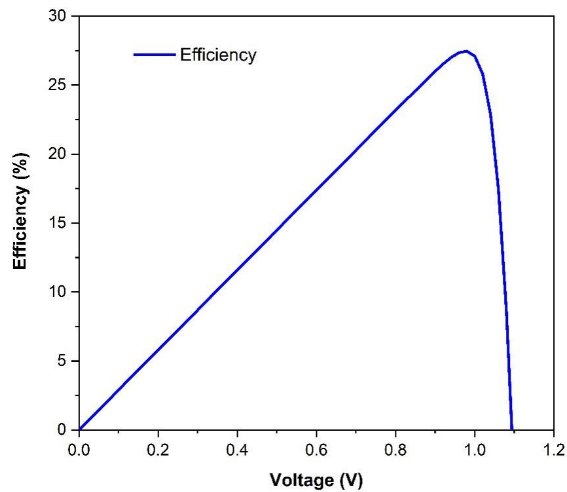

Figure 3.25: Efficiency vs Voltage with a decrease in radiative recombination rate.

To make comparison easier, all the graphs of current density against voltage and efficiency against voltage are plotted in the same axis in **Figure 3.26 and Figure 3.27**.

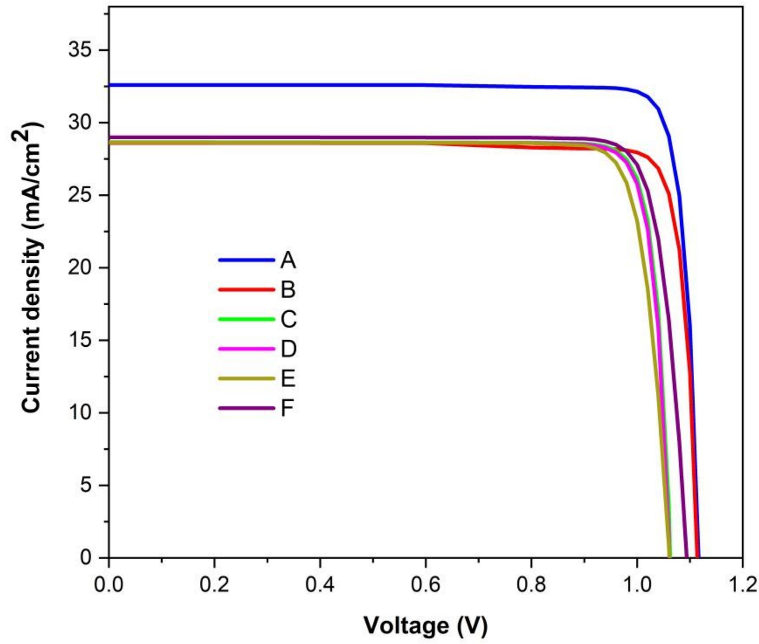

Figure 3.26: Comparison of Current Density vs Voltage.

Here,

- A: Ideal material without contact shadow
- B: Non- Ideal material with contact shadow
- C: Non- Ideal material with contact shadow and Trap-Assisted disabled
- D: Non- Ideal material with contact shadow and Trap-Assisted re-enabled
- E: Non- Ideal material with contact shadow and RSE enabled
- F: Non- Ideal material with contact shadow and changed value of Radiative Recombination Rate Coefficient

The maximum value of current density reached is 32.5941 mA/cm^2.

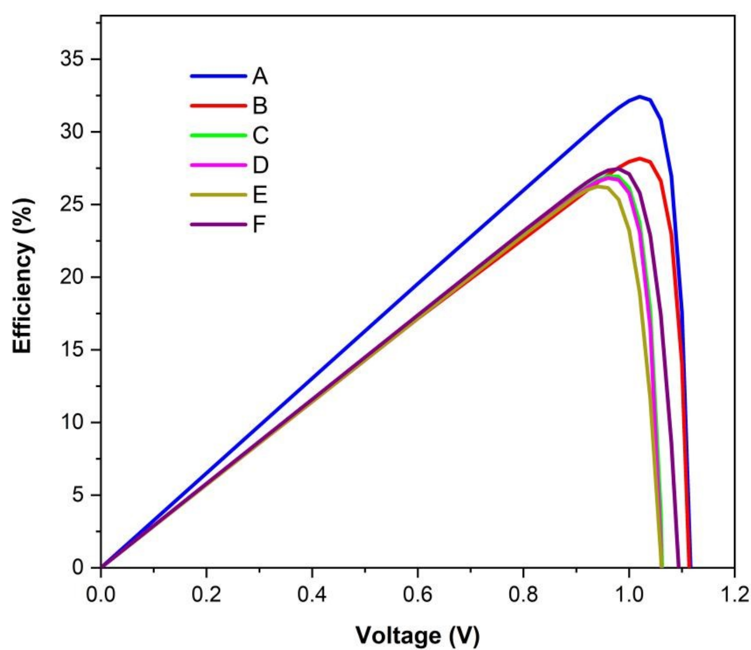

Figure 3.27: Comparison of Efficiency vs Voltage.

Here,

- A: Ideal material without contact shadow
- B: Non- Ideal material with contact shadow
- C: Non- Ideal material with contact shadow and Trap-Assisted disabled
- D: Non- Ideal material with contact shadow and Trap-Assisted re-enabled
- E: Non- Ideal material with contact shadow and RSE enabled
- F: Non- Ideal material with contact shadow and changed value of Radiative Recombination Rate Coefficient

The peak value of efficiency reached is 32.2334 %.

All the data of simulation results are summarized in the **Figure 3.28**

	Without Contact Shadow	**With Contact Shadow**				
Conditions	Default	Default	Trap-Assisted disabled	Trap-Assisted Re-enabled	Enabled series resistance with value 3.5E+04	Radiative Recombination rate reduced from 5E-10 to 1.09E-10
Maximum J_{sc}(mA/cm^2)	32.5941	28.5975	28.669	28.6493	28.6487	28.99
η (%) at Peak	32.2334	28.1708	26.961	26.8244	26.25	27.4635
V_{oc}(V)	1.11	1.11	1.06	1.06	1.07	1.00

Figure 3.28: Result obtained for different simulation settings.

3.5 Comment and Conclusion

All the simulation outputs have been listed in the figure below (Figure 3.28). The ideal maximum short circuit density (J_{SC}), open circuit voltage (V_{OC}) and peak efficiency (η) is found to be 32.5941 mA/cm^2, 1.11 V and 32.2334 % respectively as shown in the Figure 3.28.

On the other hand, Figure 3.28 shows the results for non-ideal maximum short circuit density (J_{SC}), open circuit voltage (V_{OC}) and peak efficiency is found to be 28.5975 mA/cm^2, 1.11 V and 28.1708 % respectively. To accomplish this, different settings were applied like disabling and re-enabling the trap-assisted recombination, enabling the series resistance, and changing the default value of radiative recombination rate coefficient with the calculated value. Hence, the same parameters were measured and compared.

After completing all the above mentioned simulations and their values listed in the table, it can be said that decreasing the value of Radiative Recombination rate coefficient gives the result closest to the non-ideal or practical values.

Lastly, the simulation results of optical and electrical parameters are recorded and compared in this chapter, along with the discussion on the outcome values.

Chapter 4

Aluminium Gallium Arsenide ($Al_xGa_{(1-x)}As$)/Indium Phosphide (InP) Tandem Solar Cell

4.1 Introduction

In this chapter, Indium Phosphide (InP) which is a III-V binary semiconductor, has been used as a base material. The III-V solar cells like Aluminium Gallium Arsenide (GaAs), Gallium Arsenide (GaAs), InP are prominent for producing higher efficiency. Therefore, InP has been selected, to do the analysis which has been done for GaAs in chapter 3.

Moreover, the design of InP Tandem Solar Cell(TSC) (both FDTD and DEVICE) is discussed along with optical and electrical simulation. Lastly, the chapter concludes with the brief discussion on the simulation results and analysis

4.1.1 Background study of InP Tandem Solar Cell

Shockley-Queisser Limitations with single sub-shell InP

In accordance with Shockley-Queisser limitations, maximum efficiency for InP with band gap of 1.35 eV, is achieved to be 33.2 % as shown in **Figure 4.1.** This efficiency is very close to Shockley-Queisser maximum efficiency of 33.7 % with band gap of 1.34 eV. Adding to this, the band gap of InP is close to 1.34 eV. Besides, the lattice constant of InP is 5.868 Å and 5.6533+0.0078x Å for $Al_xGa_{1-x}As$. Therefore.it was expected to obtain higher efficiency with InP in a TSC. The optical and electrical simulation has been performed on $Al_{0.85}Ga_{0.15}As/InP/Al_{0.3}Ga_{0.7}As$ TSC.

InP parameters has been set in the software data, and the results has been stored. The band-gap series of this $Al_{0.85}Ga_{0.15}As/InP/Al_{0.3}Ga_{0.7}As$ TSC stacked is 2.116 eV, 1.35 eV and 1.827 eV respectively. Hence, higher absorption is expected due to greater band-gap of top layer than the middle layer.

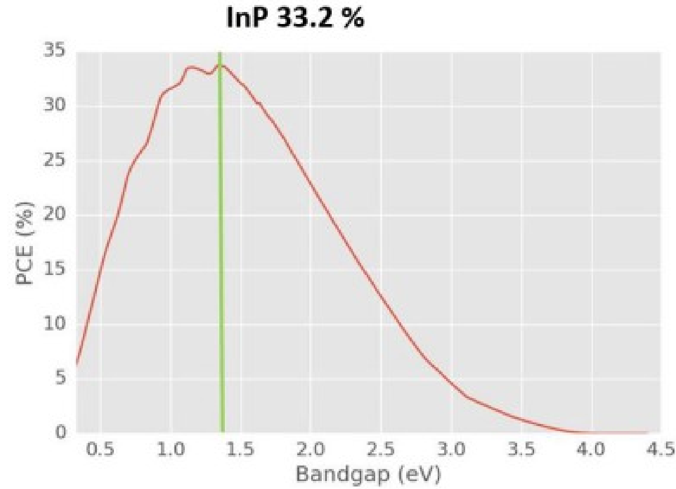

Figure 4.1: Efficiency vs Band-gap of a single junction solar cell.[24]

4.2 Modeling and Simulation

4.2.1 FDTD Model

The same pile of 2-Dimensional(2D) TSC is used with a different base material $Al_{0.85}Ga_{0.15}As/InP/Al_{0.3}Ga_{0.7}As$ in FDTD. $Al_{0.85}Ga_{0.15}As$ is kept the thickness of 0.03 μm and is placed on top working as a p^{+}-region. On the bottom side, $Al_{0.3}Ga_{0.7}As$ As is placed performing as n^{+}-region with thickness being 0.02 μm. The base material is now changed to InP which also has a thickness of 1.65 μm and is kept between the $Al_{0.85}Ga_{0.15}As$ and $Al_{0.3}Ga_{0.7}As$. The depth of the structure is shown in the cross-section view in **Figure 4.2.**.

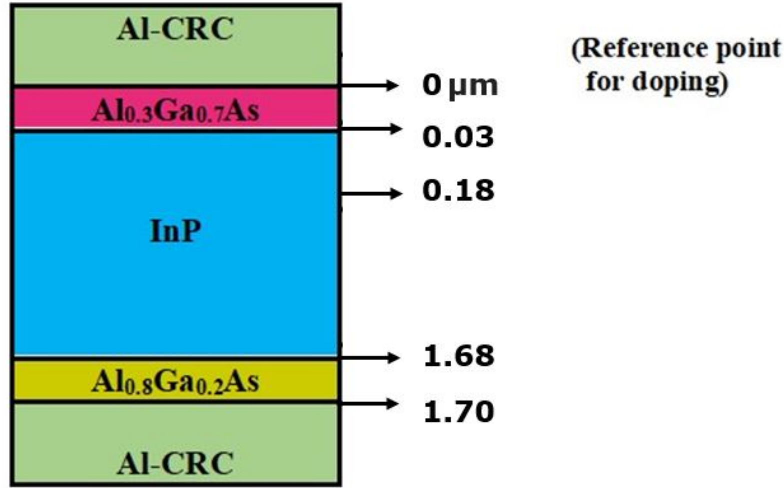

Figure 4.2: 2D Design of InP TSC.

While performing non-ideal simulation of TSC, 4 phenomena must be taken under consideration. They are:

1. Reflection from the front surface: Since Air Reflective Coating (ARC) is non-ideal, the front surface of the structure will experience some reflection
2. No TIR: There will not be Total Internal Reflection (TIR) in the back surface.
3. Shadowing effect: The effect on shadow must be taken into account.
4. Partial Absorption: There will be partial absorption due to the presence of real refractive index of the material.

ARC, which has refractive index of 1.4, is used at the front surface to reduce the loss of efficiency due to reflection. Thickness of ARC has been varied till the maximum optical absorption (in InP) is observed at 0.1 μm. The back surface has been covered by aluminum contact layer. Besides, a plane wave source is used to illuminate the FDTD/simulation region. This region has been covered by solar generation rate analysis group. This will compute Electron-Hole Pair(EHP) generation rate and ideal short circuit current density under AM1.5G solar spectrum source.

Light of shorter wavelengths will be absorbed on the surface of InP, so a mesh override is put on InP surface to enhance the resolution for the absorbed power calculations, which would have degraded otherwise.

The absorption band gap for InP is used as 1.35 eV.

The 2D and 3-Dimensional(3D) planar structure of the model in FDTD is shown in **Figure 4.3 and 4.4** respectively.

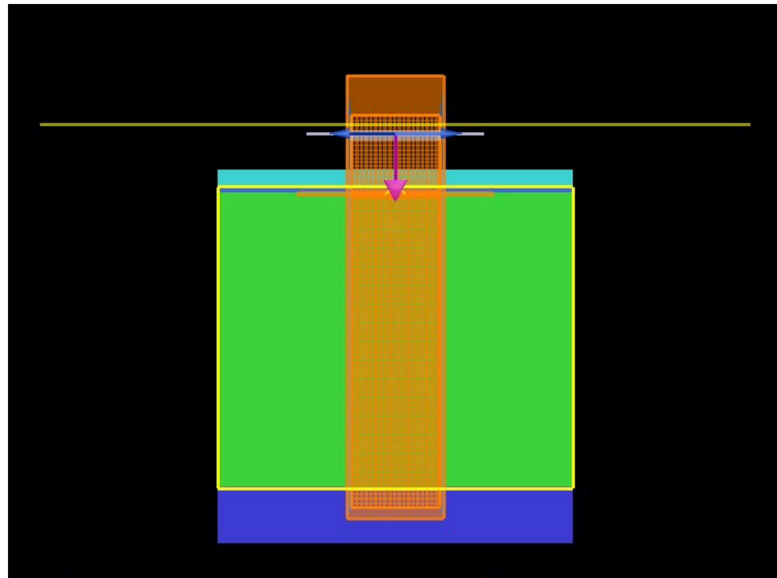

Figure 4.3: FDTD 2D Planar InP TSC design.

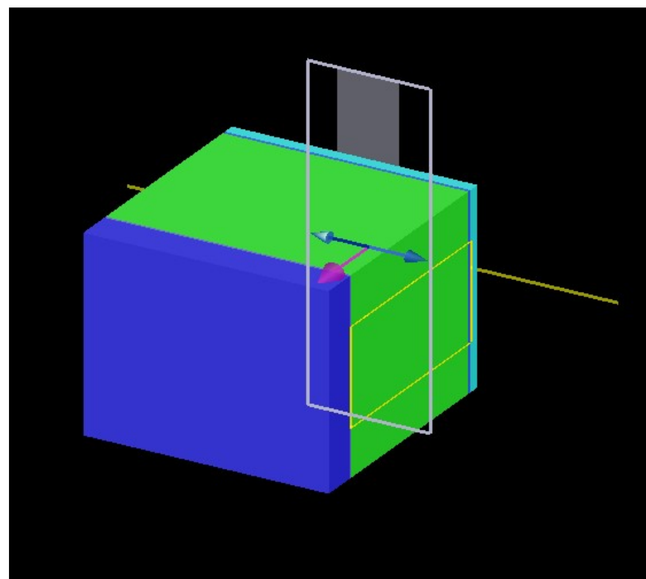

Figure 4.4: FDTD 3D Planar InP TSC design.

4.2.2 DEVICE Model

The ideal electrical structure model of InP has been adjusted to the extent that all non-radiative recombination processes (Shockley-Read-Hall Auger) is disabled and the mobilities for both electron and hole are very high. Aluminium-CRC, which has a work function of 4.28eV is used for both the base and emitter. It is also used as the conductor. To achieve value within the proximity of the theoretical reverse biased saturation current, the hole effective mass has been reduced slightly which affects the open circuit voltage. The dimensions of CHARGE Transport model are equivalent to what has been set for optical structure.

The 2D and 3D planar structure of the model in DEVICE is shown in **Figure 4.5 and 4.6** respectively.

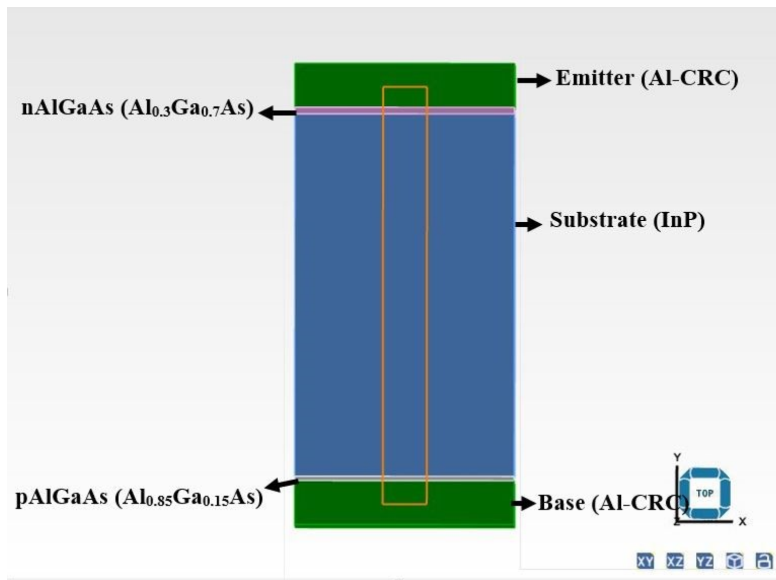

Figure 4.5: DEVICE 2D Planar InP TSC design.

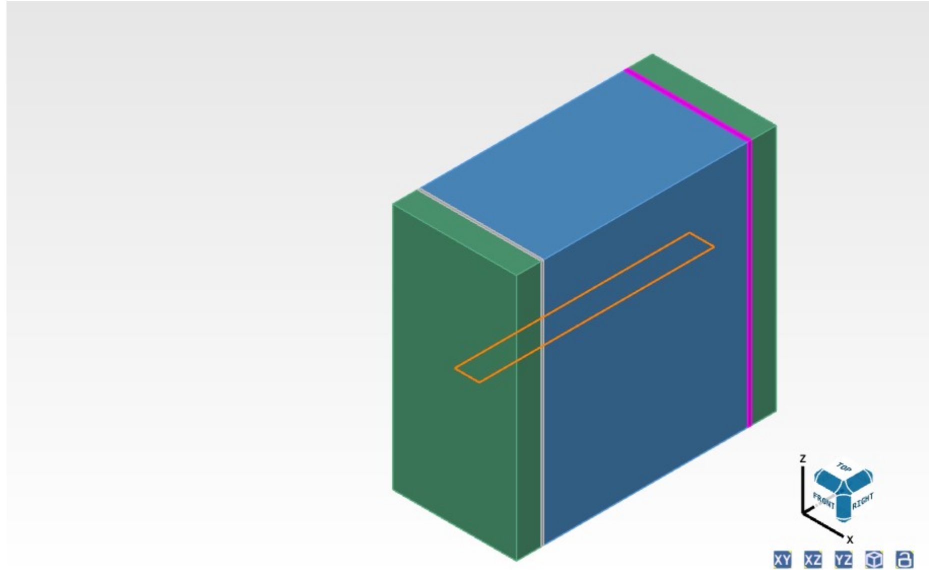

Figure 4.6: DEVICE 3D Planar InP TSC design.

4.3 Optical simulation

4.3.1 Introduction

In following section, the optical simulation in FDTD for determining the light absorbed by InP is carried out, assuming that each photon will generate a single EHP. Under the FDTD method, the optical tandem solar cell model has run and computed 5 quantities. They are the Power absorbed, Total Power absorbed, Short-Circuit Current Density (J_{SC}), Generation rate (G) and Generation rate Export (G_ export). The simulation setup is made of a plane wave source whose wavelength is varied within the solar spectrum. In the proposed model, it has used the wavelength ranging from 300 nm to 1300 nm. This source propagates light in the direction of the surface of solar cell in negative direction of y-axis.

Moreover, to prevent the excessive boundary reflection, an artificial absorbing layer is setup as a Perfectly Matched Layer (PML) along the y-direction. Periodic boundary condition is also setup along the x-direction. The temperature was maintained at 300K and simulation time was kept at 1000 fs.

To confirm the AM1.5G spectral power is normalized to 100 mW/cm^2, the analysis object has been altered to some extent in the wavelength range of 0.3-2.6 μm.

The ideal (fully absorbed) optical simulation creates a source file for electron-hole pair generation. This file is loaded under ideal ogr data, and simulation has been run.

4.3.2 Result and discussion

The maximum J_{SC} is found to be 34.9747 mA/cm^2, while the ideal current density of 34.8997 mA/cm^2. Maximum AM1.5G EHP generation is 67.2707 mA/cm^2. The maximum total absorption per unit volume is 0.960907 (arb. unit) with respect to 5.7E-07 m wavelength.

In **Figure 4.7,** at locations ranging from approximately -250 nm to 250 nm and of depth ranging from surface to -1.6 μm is shown and the absorption in this volume is given as 1.28e+03 (arb. unit) approximately.

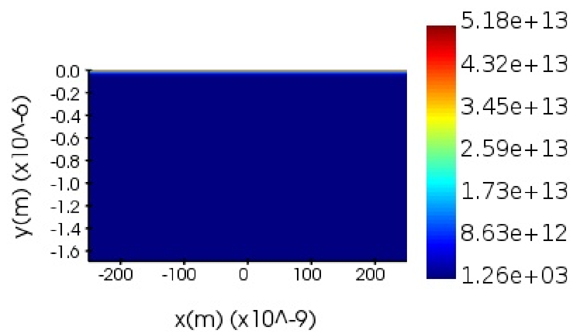

Figure 4.7: Absorption per unit volume vs Wavelength for InP.

Total Absorption per unit volume is plotted against the Wavelength **(Figure 4.8)**, the graph starts from 0.3 μm wavelength and is seen an almost linear increase up to 0.57 μm. Then the highest value is reached to is 0.96 approximately at wavelength 0.57 μm, then from 0.72 μm shown in the figure. However, the graph followed parabolic spikes pattern from 0.9 μm to 1.3 μm as shown below

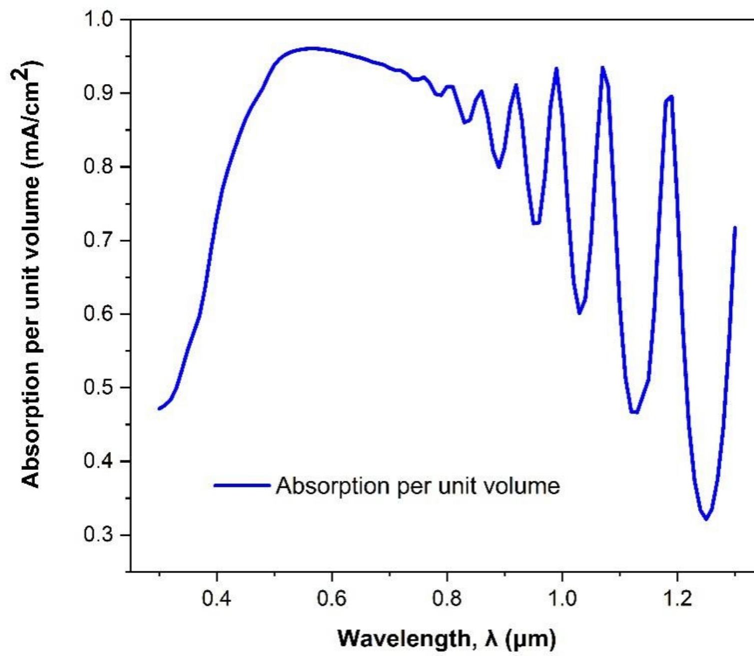

Figure 4.8: Total Absorption per unit volume vs Wavelength for InP.

In **Figure 4.9,** Current density is plotted and is found to be 421.717 mA/cm^2.

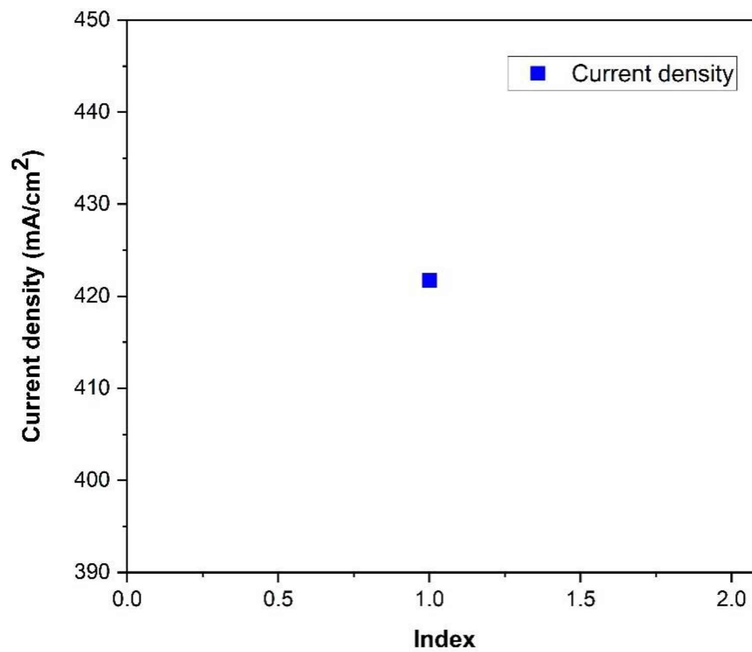

Figure 4.9: Current density (J_{SC}).

In the following **Figure 4.10,** Absorption enhancement factor is shown. At locations of x = -250 nm to 250 nm, the absorption is seen to decrease from surface, that is y = 0.0 μm to y = -0.4 μm from 1.41e+28 (arb. unit) to around 2.35e+27 (arb. unit). However, the absorption is then constant from y = -0.4 μm to -1.6 μm at a value of approximately 1.12e+25 (arb. unit) shown in the figure.

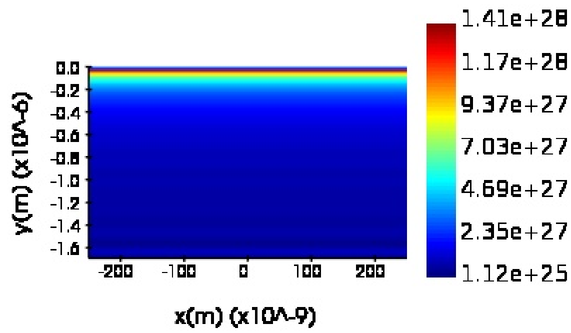

Figure 4.10: Absorption enhancement factor.

The following generation rate **Figure 4.11** shows at locations of x = -500 nm to 500 nm, the absorption is seen to decrease from surface, that is y = 0.0 μm to y = -0.4 μm from approximately1.41e+28 (arb. unit) to 2.35e+27 (arb. unit). On the contrary, the absorption is then constant from y = -0.4 μm to -1.6 μm at a value of about 1.12e+25 (arb. unit) as shown in the figure.

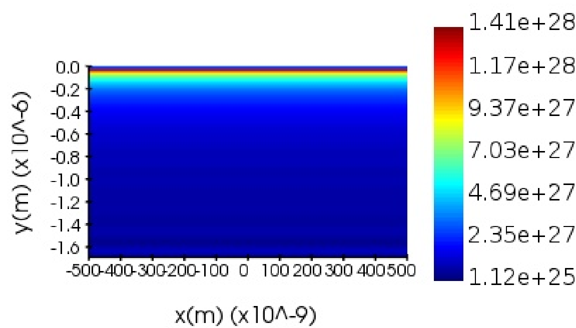

Figure 4.11: Generation Rate.

4.4 Electrical simulation

4.4.1 Introduction

The CHARGE solver has boundary conditions consisting of two different groups. Firstly, the electrical boundary conditions for the base and emitter. Secondly, the surface recombination for the surface recombination. The CHARGE Transport Solver also consists of 4 different Constant Doping Region, namely, p, p^+, n and n^+.

- The necessary code of recombination is run and the recombination rate process is analyzed. A plot will be generated showing three different recombination process from the recombination dataset.
- Radiative Recombination: It is the recombination when the electron recombines with the hole radiatively, i.e. when a photon is generated due to the recombination of electron and hole when the electron transit down in energy
- Shockley-Read-Hall (SRH): It is the non-radiative recombination process occurred when the electron gets trapped in the meta-stable energy state during its transition from valence band to conduction band and releases energy in the form of vibrations. Meta-stable state is the energy state between the higher energy and lower energy that is long-lived.
- Auger Recombination: It occurs when the third particle, either an electron or a hole is transited to conduction or valence band, respectively instead of releasing photon after recombining.

4.4.2 Result and discussion

1. Without contact shadow

   After running the program code for ideal recombination and plotting the result, the following graphs are obtained. In **Figure 4.12,** maximum (J_{SC}) is obtained 35.4157 mA/cm^2, and the open circuit voltage (V_{OC}) is close to 1.07 V and also the peak efficiency is found to be 33.5165%.

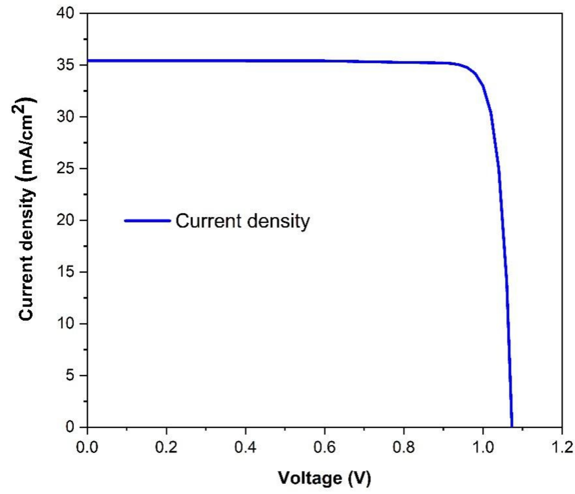

Figure 4.12: Current density vs Voltage for shadow less.

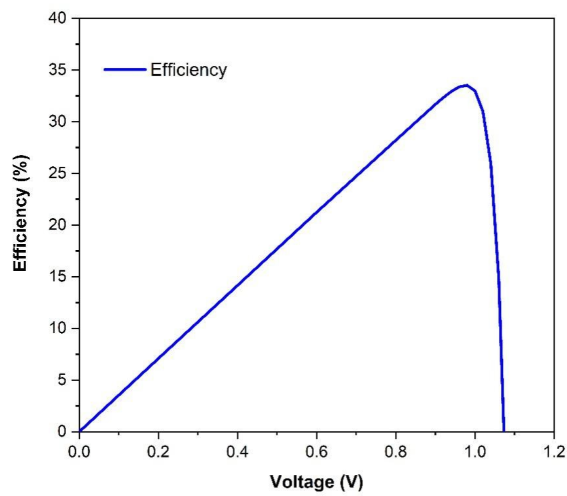

Figure 4.13: Efficiency vs Voltage for shadow less.

Band structure monitor shows the band diagram of conduction band, valence band, intrinsic Fermi-energy level, Quasi-Fermi energy level of electron and hole (in eV) with respect to depth as displayed in **Figure 4.14**.

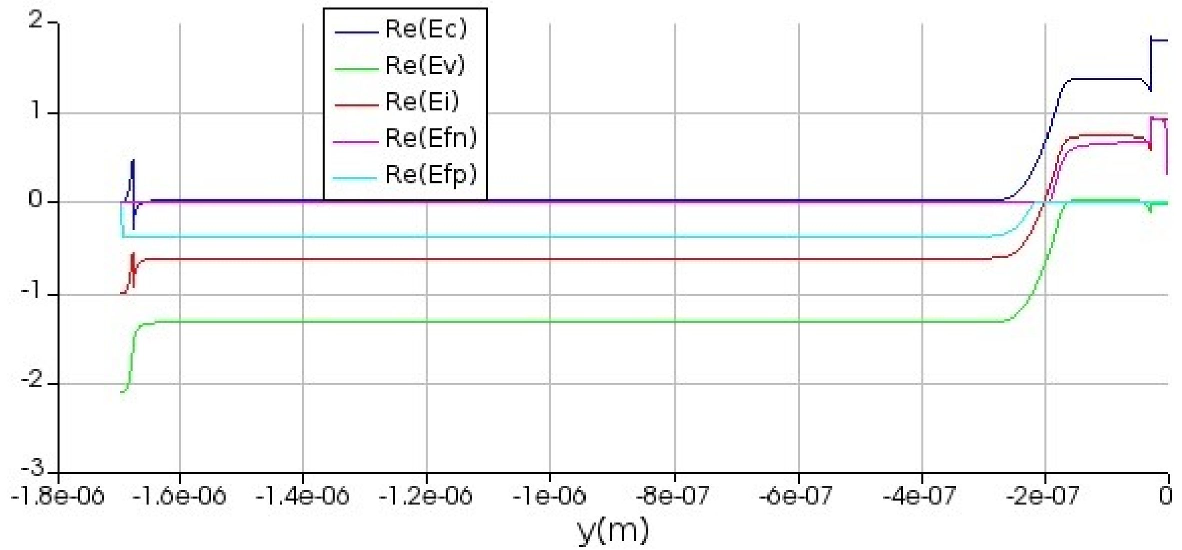

Figure 4.14: Band structure monitor.

2. With contact shadow

   The ideal_ ogr has been disabled while its counterpart that is ogr (Optical Generation Rate) is enabled. Then the OGR_ AlGaAs_ fine.mat is imported into CHARGE and the simulation has been performed.

   Then run the program code for contact shadow, and plotting the result, the following graphs are obtained. In **Figure 4.15** maximum (J_{SC}) is obtained 38.9771 mA/cm^2, and the (V_{OC}) is close to 1.079 V. In addition, the peak efficiency is obtained to be 36.9373 %.

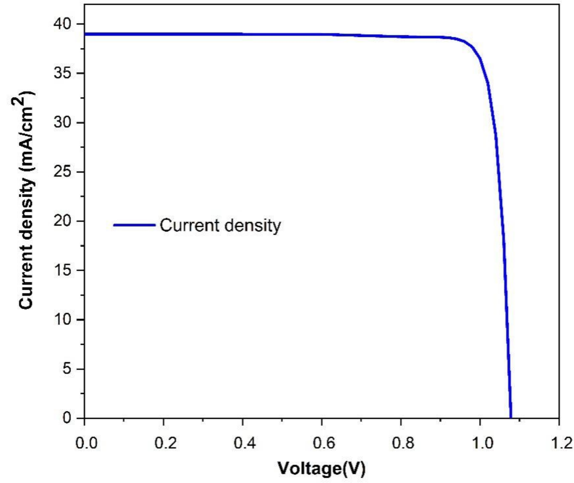

Figure 4.15: Current density vs Voltage with shadow loss.

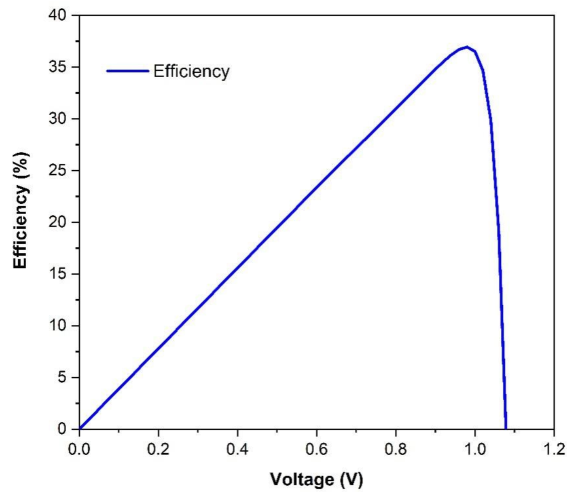

Figure 4.16: Efficiency vs Voltage with shadow loss.

In the upcoming steps, all the semiconductor material models has been changed from ideal to their standard counterparts, and a series of charge simulation has been run:

The Trap-Assisted recombination function has been disabled for all 3 materials $Al_{0.8}Ga_{0.2}As$, InP and $Al_{0.3}Ga_{0.7}As$, while Radiative and Auger recombination are kept enabled. The contact shadow program has run, and the following graphs are obtained from data. The maximum (J_{SC}) is obtained $38.188 mA/cm^2$, and the (V_{OC}) is close to 1.01 V **(Figure 4.17)**. Besides, in

Figure 4.18, peak efficiency is found to be 33.5316 %.

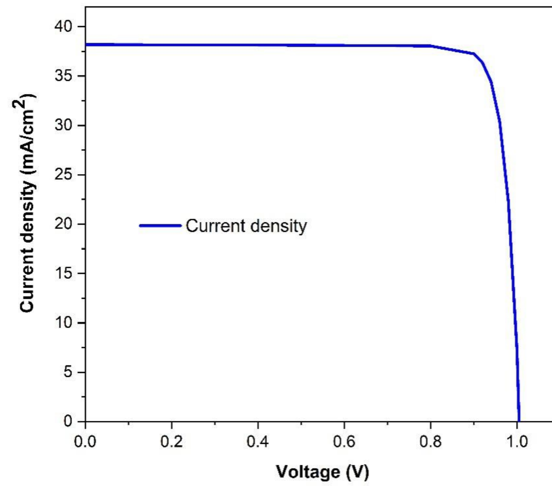

Figure 4.17: Current density vs Voltage when trap-assisted is disabled.

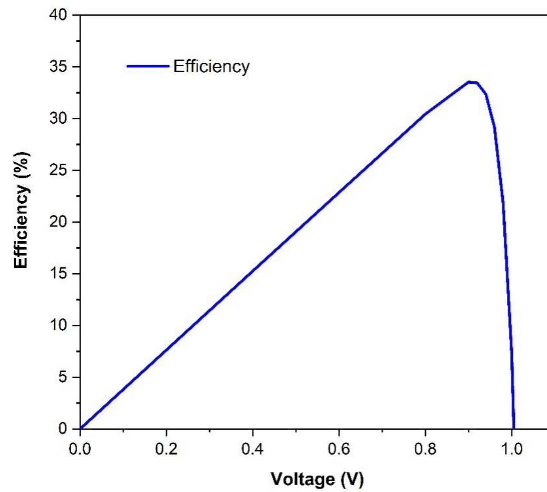

Figure 4.18: Efficiency vs Voltage when trap-assisted is disabled.

After attaining the previous results, the Trap-Assisted recombination has re-enabled for all 3 materials, and by running the contact shadow code again, the following graphs are plotted. In **Figure 4.19** maximum (J_{SC}) is obtained 38.175 mA/cm^2, and the (V_{OC}) is close to 1.01 V and its peak efficiency is found to be 33.3372 %.

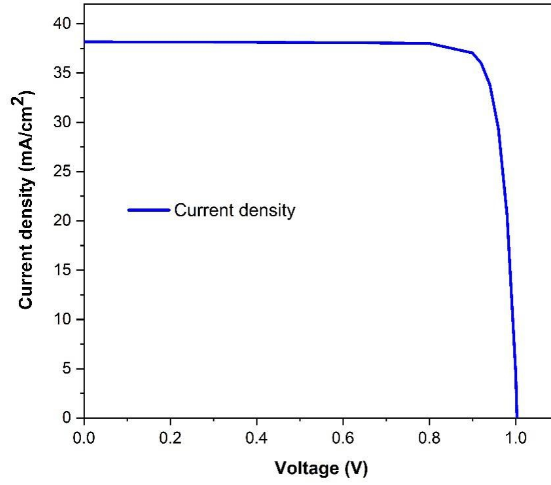

Figure 4.19: Current density vs Voltage with trap-assisted re-enabled.

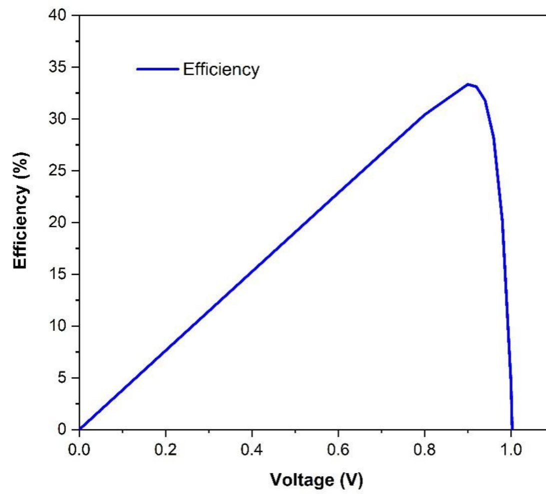

Figure 4.20: Efficiency vs Voltage with trap-assisted re-enabled.

Moreover, the recombination program code has run and the following graph is achieved. Radiative recombination rate is 92.3591 % Auger recombination rate is the least which is 0.0415341 % and Shockley-Read Hall recombination rate is 7.59933 %.

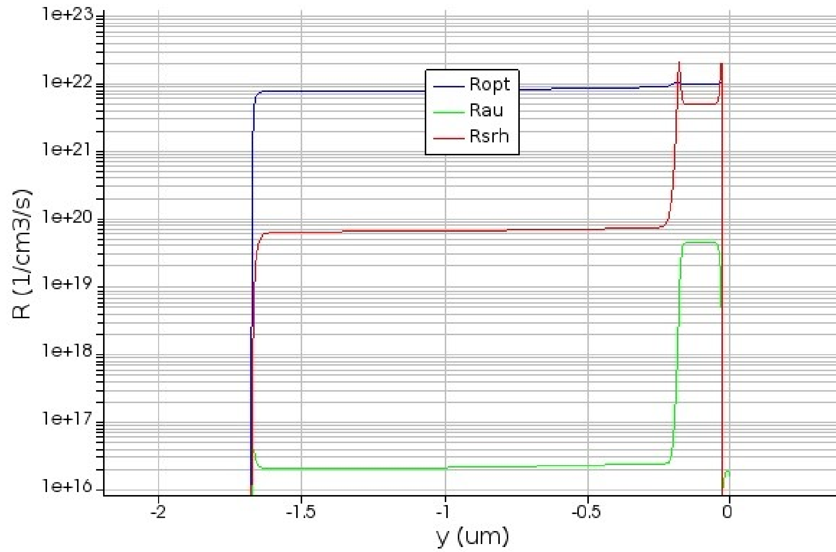

Figure 4.21: Recombination rate (Radiative, Auger, and Trap-Assisted) vs depth.

After attempting the previous simulation, the series resistance has been enabled, and the value is set to 3.5E+04 to observe the effect in current density and in efficiency. After running the simulation, the shadow contact program has been run, and following graphs are obtained. In **Figure 4.22** maximum (J_{SC}) is obtained 38.1687 mA/cm^2, and the (V_{OC}) is close to 1.01 V. The peak efficiency is found to be 31.9199 % after enabling the series resistance.

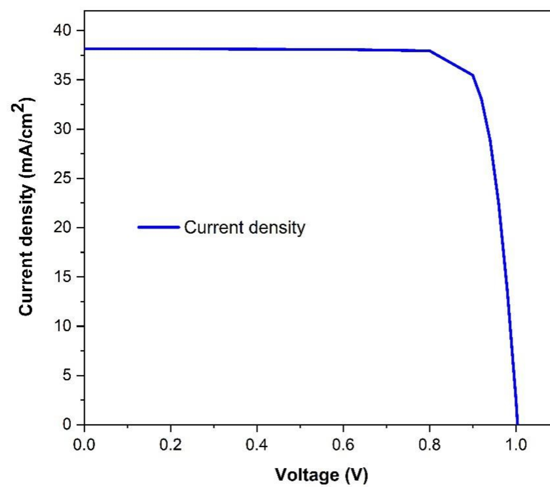

Figure 4.22: Efficiency vs Voltage with RSE enabled.

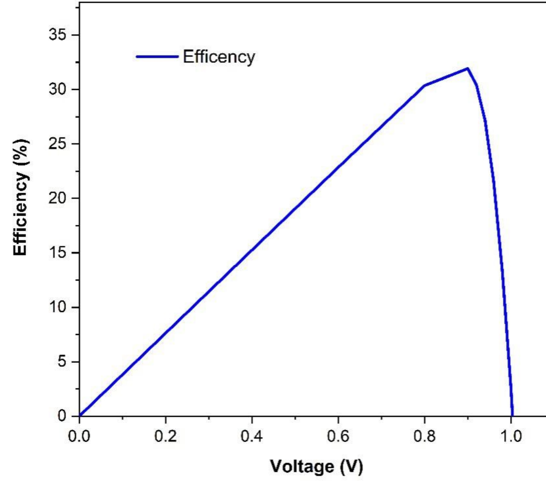

Figure 4.23: Efficiency vs Voltage with RSE enabled.

Finally, it is needed to consider the effects of photon recycling where a photon is emitted with energy equal to the band gap, which might reabsorb, when the electrons and holes recombine radiatively. The coherent simulation of this factor is difficult but can be approximated by the Asbeck coefficients by altering the radiative recombination rate coefficient.

The Asbeck coefficient is material dependent and is a function of depth. The Asbeck coefficient has a value of =4.6 for a 1.65um thick layer of InP such that.

$$\tilde{C}_{opt} = \frac{C_{opt}}{\phi} = 4.35 \times 10^{-11} cm^3 s^{-1} \tag{4.1}$$

Considering the newly calculated value of radiative recombination rate coefficient, the current density and efficiency has been measured by changing the radiative recombination rate coefficient from 2E-10 cm^3s^{-1} to 4.35E-11 cm^3s^{-1}. The changes have been simulated and shadow contact code has run, the following graph plotted from data. In **Figure 4.24** maximum (J_{SC}) is obtained 39.1479 mA/cm^2, and the (V_{OC}) is close to 1.03 V. Besides, the peak efficiency is found to be 34.3104 % shown in **Figure 4.25**.

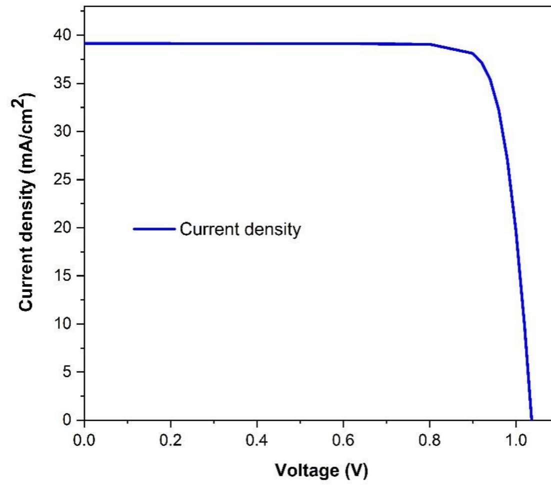

Figure 4.24: Current density vs Voltage with a decrease in radiative recombination rate.

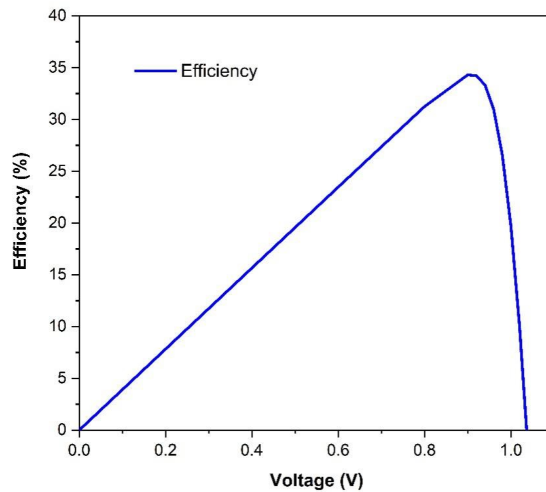

Figure 4.25: Efficiency vs Voltage with a decrease in radiative recombination rate.

Furthermore, to make comparison easier, all the graphs of current density against voltage and efficiency against voltage are plotted in the same axis in **Figure 4.26 and Figure 4.27**

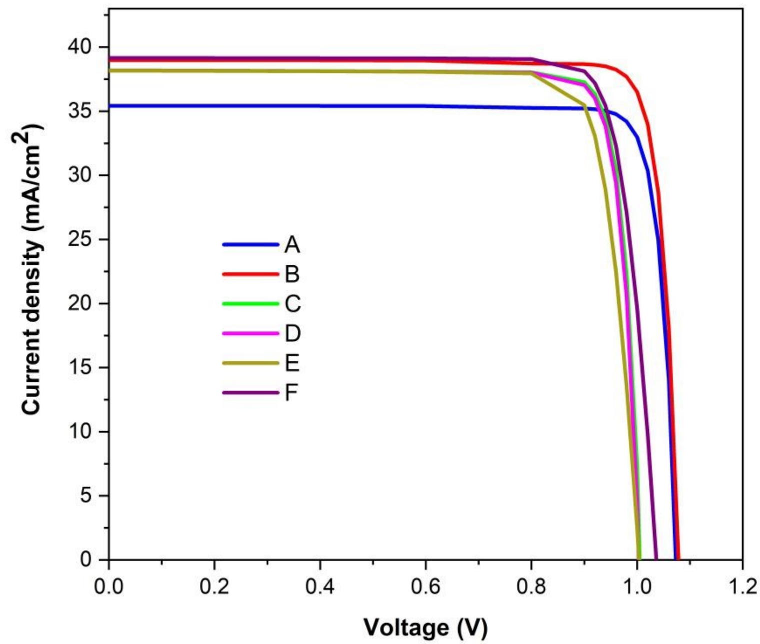

Figure 4.26: Comparison of Current Density vs Voltage.

Here,

A: Ideal material without contact shadow

B: Non- Ideal material with contact shadow

C: Non- Ideal material with contact shadow and Trap-Assisted disabled

D: Non- Ideal material with contact shadow and Trap-Assisted re-enabled

E: Non- Ideal material with contact shadow and RSE enabled

F: Non- Ideal material with contact shadow and changed value of Radiative Recombination Rate Coefficient

The maximum value of current density reached is 39.1479 mA/cm^2.

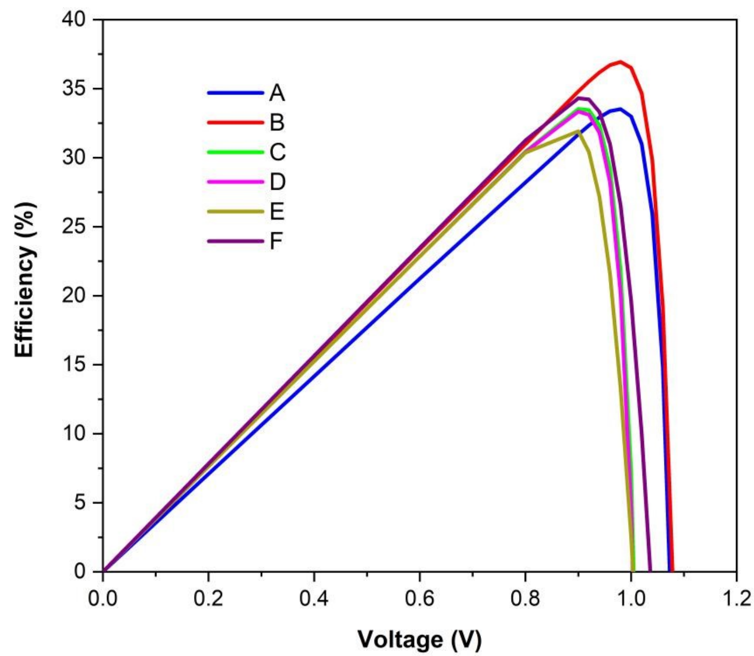

Figure 4.27: Comparison of Efficiency vs Voltage.

Here,

A: Ideal material without contact shadow

B: Non- Ideal material with contact shadow

C: Non- Ideal material with contact shadow and Trap-Assisted disabled

D: Non- Ideal material with contact shadow and Trap-Assisted re-enabled

E: Non- Ideal material with contact shadow and RSE enabled

F: Non- Ideal material with contact shadow and changed value of Radiative Recombination Rate Coefficient

The peak value of efficiency reached is 36.9373 %.

All the data of simulation results are summarized in the **Figure 4.28**

	Without Contact Shadow	**With Contact Shadow**				
Conditions	Default	Default	Trap-Assisted disabled	Trap-Assisted Re-enabled	Enabled series resistance with value 3.5E+04	Radiative Recombination rate reduced from 2E-10 to 4.35E-11
Maximum $J_{sc}(mA/cm^2)$	35.4157	38.9771	38.188	38.175	38.1687	39.1479
η(%) at Peak	33.5165	36.9373	33.5316	33.3372	31.9199	34.3104
V_{oc}(V)	1.07	1.079	1.01	1.01	1.01	1.03

Figure 4.28: Result obtained for different simulation settings.

4.5 Comment and conclusion

The InP TSC model simulation findings are summarized in the figure below (Figure 4.28). The ideal maximum (J_{SC}), (V_{OC}) and peak efficiency (η) is found to be 35.4157 mA/cm^2, 1.07 V and 33.5165 % respectively as listed in the Figure 4.28.

However, the non-ideal maximum (J_{SC}), (V_{OC}) and peak efficiency is found to be 39.1479 mA/cm^2, 1.079 V and 36.9373 % respectively as shown in the Figure 4.28. Different settings were applied such as disabling and re-enabling the trap-assisted recombination, enabling the series resistance, and changing the default value of radiative recombination rate coefficient with the calculated value to achieve this,. Finally, the same parameters were measured and compared with the previous obtained results.

From the findings listed in the Figure 4.28, reducing the value of Radiative recom-

bination rate coefficient gives the result closest to the non-ideal or realistic values for InP TSC.

To conclude, the simulation results of optical and electrical parameters are recorded and compared in this chapter, along with the discussion on the outcome values.

Chapter 5

Thesis Findings

5.1 Introduction

Since early 1950's, Gallium Arsenide (GaAs) has been substantially studied. Now, most of its optical and electrical properties, its processing and its growth are known and mastered. GaAs is widely used in Light Amplification by Stimulated Emission of Radiation (LASER) and infrared Light Emitting Diodes (LEDs), micro-technology and high speed electronic devices, fiber optic drivers and receivers. Most importantly, for designing high efficiency solar cell, GaAs is extensively used which has a direct band gap of 1.42 eV. However, InP has a band-gap energy of 1.35 eV. As a result, it is much more closely matched to optimum use of the solar spectrum than Silicon (Si) or GaAs. Fabricating different types of solar cell using InP has been a recent approach in sustainable energy which has shown significantly positive outcomes in terms of enhancing its efficiency.

In this paper, particularly this chapter, provides a brief comparison between GaAs Tandem Solar Cell(TSC) and InP TSC followed by their simulation results and dI_{SC}ussions. After an insightful analysis and rigorous dI_{SC}ussions, this chapter concludes with the comparison of both the structures and proved that the proposed model is better than the base model.

5.2 Comparison of GaAs and InP TSC

In this research, two models were studied and compared. They are Aluminium Gallium Arsenide ($Al_xGa_{(1-x)}As$)/Gallium Arsenide (GaAs) - (Chapter 3) and Aluminium Gallium Arsenide ($Al_xGa_{(1-x)}As$)/Indium Phosphide (InP) - (Chapter 4). In depth analysis of the aforementioned models yielded certain results. These results

were compared on the basis of best outcome. The following table (Table 5 and 6) provides the dimensions of the parameters used in the FDTD (optical simulation) and DEVICE (electrical simulation).

FDTD:

Parameters	GaAs Model	InP Model
Simulation Region	Xspan(μm) = 0.5 Yspan(μm) = 2.2 Zspan(μm) = 1.7 0.2 μm from the substrate surface	Xspan(μm) = 0.5 Yspan(μm) = 2.2 Zspan(μm) = 1.7 0.2 μm from the substrate surface
Emitter	Xspan(μm) = 2.0 Yspan(μm) = 0.1 Zspan(μm) = 2.0	Xspan(μm) = 2.0 Yspan(μm) = 0.1 Zspan(μm) = 2.0
Substrate	Xspan(μm) = 2.0 Yspan(μm) = 1.65 Zspan(μm) = 2.0	Xspan(μm) = 2.0 Yspan(μm) = 1.65 Zspan(μm) = 2.0
Base	Xspan(μm) = 2.0 Yspan(μm) = 0.3 Zspan(μm) = 2.0	Xspan(μm) = 2.0 Yspan(μm) = 0.3 Zspan(μm) = 2.0
p-AlGaAs	Xspan(μm) = 2.0 Yspan(μm) = 0.03 Zspan(μm) = 2.0	Xspan(μm) = 2.0 Yspan(μm) = 0.03 Zspan(μm) = 2.0
n-AlGaAs	Xspan(μm) = 2.0 Yspan(μm) = 0.02 Zspan(μm) = 2.0	Xspan(μm) = 2.0 Yspan(μm) = 0.02 Zspan(μm) = 2.0
DFT Monitor (linear X)	Xspan(μm) = 4.0 Yspan(μm) = 0.0 Zspan(μm) = 0.0	Xspan(μm) = 4.0 Yspan(μm) = 0.0 Zspan(μm) = 0.0
Plane Source	Xspan(μm) = 1.0 Yspan(μm) = 0.02 Zspan(μm) = 3.4	Xspan(μm) = 1.0 Yspan(μm) = 0.02 Zspan(μm) = 3.4

Continued on next page

Analysis Group	Xspan(μm) = 2.0 Yspan(μm) = 1.694 Zspan(μm) = 1.0	Xspan(μm) = 2.0 Yspan(μm) = 1.694 Zspan(μm) = 1.0
Mesh (directly defined)	Xspan(μm) = 1.10629 Yspan(μm) = 0.02 Zspan(μm) = 0.96	Xspan(μm) = 1.10629 Yspan(μm) = 0.02 Zspan(μm) = 0.96

Table 5.1: Comparing FDTD dimensions of each model.

DEVICE:

Parameters	**GaAs Model**	**InP Model**
Simulation Region	Xspan(μm) = 0.2 Yspan(μm) = 1.9 0.1 μm from the surface	Xspan(μm) = 0.2 Yspan(μm) = 1.9 Zspan(μm) = 1.7 0.1 μm from the substrate surface
Substrate	Xspan(μm) = 1.0 Yspan(μm) = 1.65 Zspan(μm) = 2.0	Xspan(μm) = 1.0 Yspan(μm) = 1.65 Zspan(μm) = 2.0
n-AlGaAs	Xspan(μm) = 1.0 Yspan(μm) = 0.03 Zspan(μm) = 2.0	Xspan(μm) = 1.0 Yspan(μm) = 0.03 Zspan(μm) = 2.0
p-AlGaAs	Xspan(μm) = 1.0 Yspan(μm) = 0.02 Zspan(μm) = 2.0	Xspan(μm) = 1.0 Yspan(μm) = 0.02 Zspan(μm) = 2.0
Base	Xspan(μm) = 1.0 Yspan(μm) = 0.2 Zspan(μm) = 2.0	Xspan(μm) = 1.0 Yspan(μm) = 0.2 Zspan(μm) = 2.0
Emitter	Xspan(μm) = 1.0 Yspan(μm) = 0.2 Zspan(μm) = 2.0	Xspan(μm) = 1.0 Yspan(μm) = 0.2 Zspan(μm) = 2.0

Continued on next page

Constant Doping Region (p^+)	Xspan(μm) = 1.0 Yspan(μm) = 0.04 Zspan(μm) = 2.0	Xspan(μm) = 1.0 Yspan(μm) = 0.04 Zspan(μm) = 2.0
Constant Doping Region (p)	Xspan(μm) = 1.0 Yspan(μm) = 0.1502 Zspan(μm) = 2.0	Xspan(μm) = 1.0 Yspan(μm) = 0.1502 Zspan(μm) = 2.0
Constant Doping Region (n)	Xspan(μm) = 1.0 Yspan(μm) = 1.502 Zspan(μm) = 2.0	Xspan(μm) = 1.0 Yspan(μm) = 1.502 Zspan(μm) = 2.0
Constant Doping Region (n^+)	Xspan(μm) = 1.0 Yspan(μm) = 0.03 Zspan(μm) = 2.0	Xspan(μm) = 1.0 Yspan(μm) = 0.03 Zspan(μm) = 2.0
Optical Generation Rate (ogr)	Xspan(μm) = 1.0 Yspan(μm) = 1.69196 Zspan(μm) = 2.0	Xspan(μm) = 1.0 Yspan(μm) = 1.69196 Zspan(μm) = 2.0
Optical Generation Rate (ideal$_o gr$)	Xspan(μm) = 2.0 YYspan(μm) = 2.0 Zspan(μm) = 2.0	Xspan(μm) = 2.0 YYspan(μm) = 2.0 Zspan(μm) = 2.0
Band-structure Monitor (linear y)	Yspan(μm) = 2.021	Yspan(μm) = 2.021
Electrical Mesh Constraint (gen surf) Directly defined	Xspan(μm) = 1.0 Yspan(μm) = 0.02 Zspan(μm) = 1.0 Max edge length(μm) = 0.002	Xspan(μm) = 1.0 Yspan(μm) = 0.02 Zspan(μm) = 1.0 Max edge length(μm) = 0.002
Electrical Mesh Constraint (gen surf 1) Directly defined	Xspan(μm) = 1.0 Yspan(μm) = 0.004 Zspan(μm) = 1.0 Max edge length(μm) = 0.0005	Xspan(μm) = 1.0 Yspan(μm) = 0.004 Zspan(μm) = 1.0 Max edge length(μm) = 0.0005
Electrical Mesh Constraint (scl) Directly defined	Xspan(μm) = 1.0 Yspan(μm) = 0.16 Zspan(μm) = 0.72 Max edge length(μm) = 0.005	Xspan(μm) = 1.0 Yspan(μm) = 0.16 Zspan (μm) = 0.72 Max edge length(μm) = 0.005

Continued on next page

Table 5.2: Comparing DEVICE dimensions of each model.

5.3 Results and Discussions

5.3.1 Results from Optical Simulation

From the optical simulation in FDTD, Power absorbed (P_{abs}),Total absorbed power ($P_{abs_}$ total), Short-Circuit Current Density (J_{SC}), Absorption enhancement factor (G) and Exported Generation rate (G_ export) was observed and recorded. The following section dI_{SC}ussed these results in details separately.

1. Power absorbed (P_{abs}):

   The spectra in the 5.1 and 5.2 gives the power absorbed in the structure with the base material being GaAs and InP respectively.

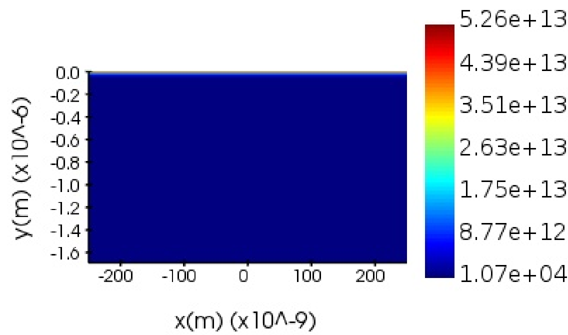

Figure 5.1: Power absorbed when GaAs is the base material.

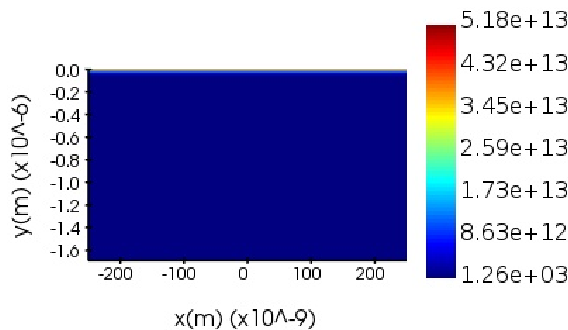

Figure 5.2: Power absorbed when InP is the base material.

Both thes are kept in the same axis for ease of comparison. At locations of approximately x = -250 nm to 250 nm, the power absorbed for both the structures seem to stay constant from the surface to the depth of y = -1.6 μm but differs in values. The power absorbed for the GaAs structure is around 1.07e+04 (arb.unit), while that for InP is approximately 1.28e+03 (arb.unit).

2. Total absorbed power ($P_{abs-total}$):
   Absorption is an important parameter in photo-voltaic devices, hence the total power absorbed within the structure is recorded for the determination of the efficiency of the device. The below compares the total power absorbed for both the structures.

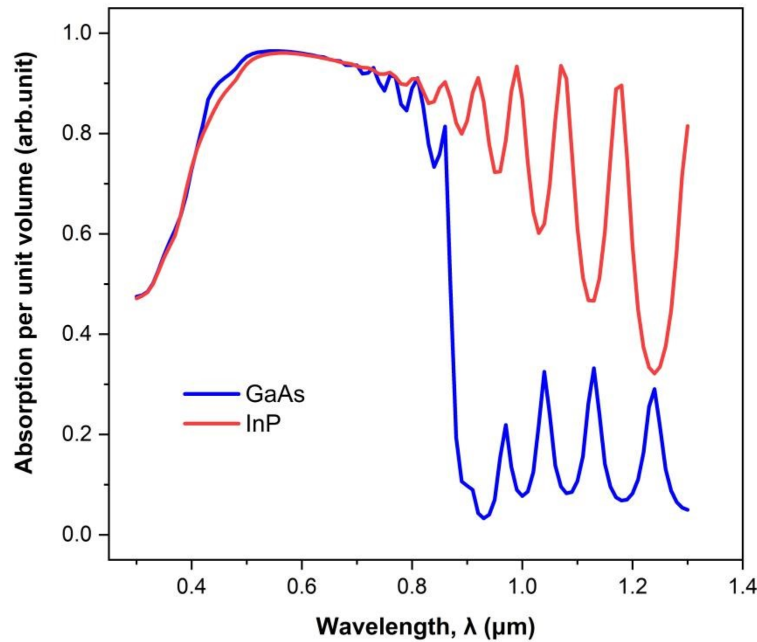

Figure 5.3: Total power absorbed for GaAs and InP.

In the shown, total power absorbed is plotted as a function of wavelength(λ). The graphs are seen to start from $0.3\mu m$ and almost linear increase are observed until the peaks are reached for their respective graphs. The peak for GaAs occurs at $\lambda = 0.55$ μm and is a value of 0.96479, while the peak for InP has a value of 0.960907 with the corresponding $\lambda = 0.57\mu m$. As expected, both the graphs then continue to decrease, but the abrupt fall of the GaAs is somewhat unexpected. The gradual decrease of the absorption for the InP

is what stands out, as the total overall absorption is higher than the GaAs structure. The minimum value reached by the GaAs graph is 0.0326675 for the corresponding $\lambda = 0.93\mu m$ while the minimum for InP graph occurs at $\lambda = 1.24\mu m$ with the value of 0.32133. The minimum values for either of the graphs indicates that InP structure has a greater absorption for even greater wavelength of light.

3. Short-Circuit Current Density(J_{SC}):

   The following (Figure 5.4) plotted give the values of the short-circuit current density for both the GaAs and InP structure.

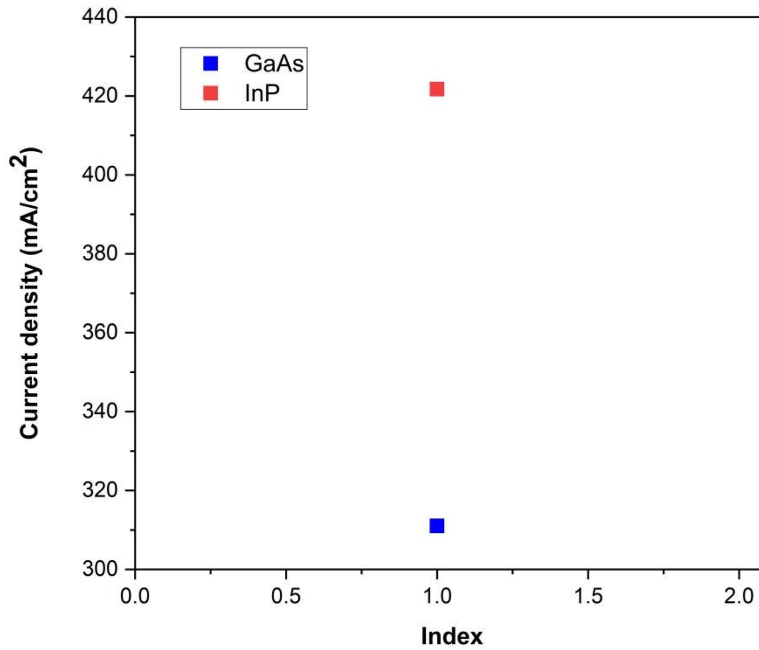

Figure 5.4: Short-Circuit Current Density for GaAs and InP.

   The Short-Circuit Current Density (J_{SC}) for GaAs is 311.029 mA/cm^2 and that for InP is 421.717 mA/cm^2.

4. Absorption Enhancement Factor (G):

   Moreover, the absorption enhancement factor is recorded for both the structure in 5.4 for GaAs and 5.5 for InP.

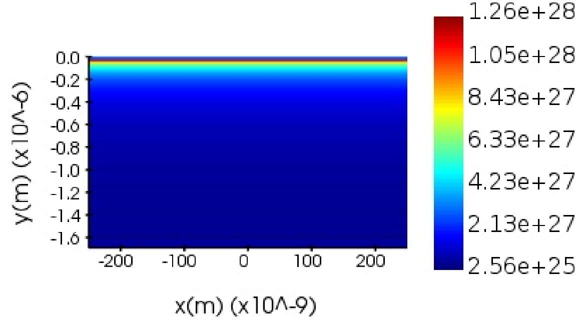

Figure 5.5: Absorption Enhancement Factor for GaAs.

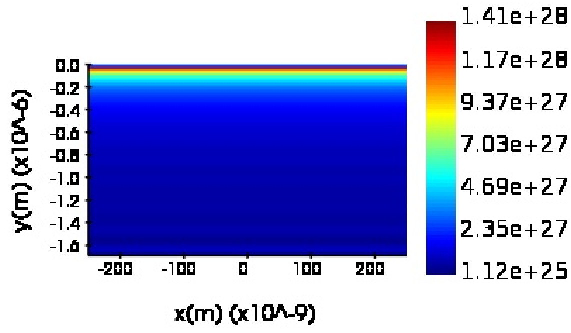

Figure 5.6: Absorption Enhancement Factor for InP.

The spectra gives the absorption enhancement factor for GaAs and InP and are observed to be identical, yet differ in values only. At locations x = -250 nm to 250 nm, the absorption enhancement factor is observed to decrease for both the structures with the values ranging from 1.26e+28 (arb. unit) to 2.13e+27 (arb. unit) approximately for GaAs and around 1.41e+28 (arb. unit) to 2.35e+27 (arb. unit) for InP for the depth up to y = -0.4μm from the surface. This parameter then stays constant for either of the structures with the value of 2.56e+25 (arb.unit) for GaAs and 1.12e+25(arb.unit) for InP.

5. Exported Generation Rate (G_ export):

   Lastly, the exported generation rate is recorded and the following spectra is observed (Figure 5.7 for GaAs and 5.8 for InP).

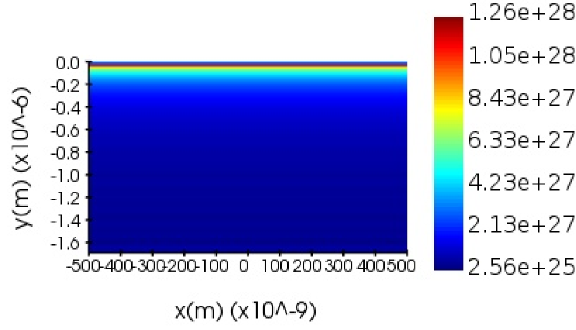

Figure 5.7: Exported Generation Rate for GaAs.

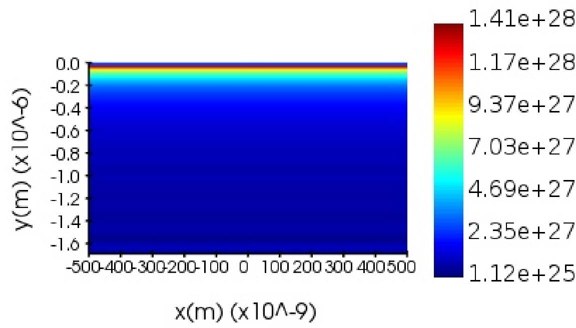

Figure 5.8: Exported Generation Rate for InP.

Finally, the spectra shown in the gives the absorption enhancement factor for GaAs and InP and are seen to be identical yet different than the absorption enhancement factor in values of locations only. At locations x = -500 nm to 500 nm, the absorption enhancement factor is observed to decrease for both the structures with the values ranging from approximately 1.26e+28 (arb. unit) to 2.13e+27 (arb. unit) for GaAs and 1.41e+28 (arb. unit) to 2.35e+27 (arb. unit) approximately for InP for the depth up to y = -0.4μm from the surface. This parameter then stays constant for either of the structures with the value of around 2.56e+25 (arb.unit) and 1.12e+25(arb.unit) for GaAs and InP, respectively.

5.3.2 Results from Electrical Simulation

The electrical simulation in DEVICE, particularly, the CHARGE Transport Solver solves the drift-diffusion equations and provides the electrical parameters like Short-Circuit Current Density(J_{SC}), Short-Circuit Current(I_{SC}), Open-Circuit Voltage(V_{OC}),

Fill Factor(FF) and Peak Efficiency. The detailed comparison of the mentioned parameters are discussed for both the structures with different base materials in the following section.

- <u>Without contact shadow</u>

  The script for ideal recombination has been run and the Current Density-Voltage and Efficiency-Voltage graphs are obtained (Figure 5.9 and 5.10).

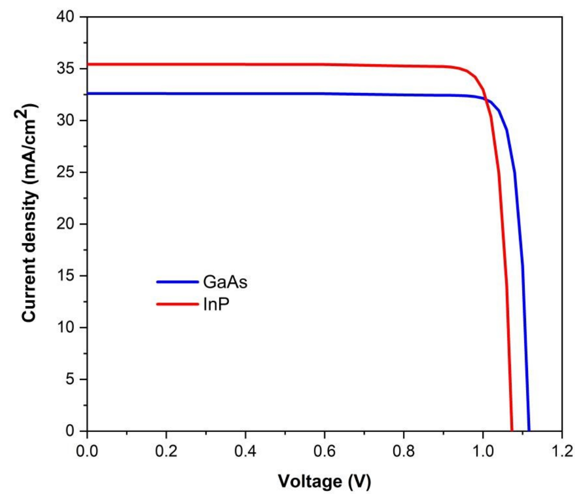

Figure 5.9: Current-Density vs Voltage for GaAs and InP.

From the, the highest current density for GaAs obtained is 32.5941 mA/cm^2 while that for InP is 35.4157 mA/cm^2. The open-circuit voltage for GaAs is close to 1.11 V and that for InP is close to 1.07 V.

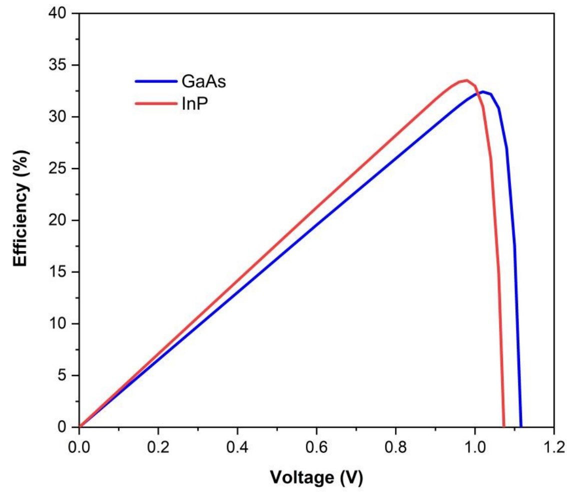

Figure 5.10: Efficiency vs Voltage for GaAs and InP.

The maximum peak efficiency reached by the GaAs structure is 32.2334 % while that by the InP structure is 33.5165 % as shown in the above.

The band structure monitor shows the energy band diagram of Conduction Band(Ec), Valence Band(Ev), Intrinsic Fermi-Energy Level(Ei), Quasi-Fermi Energy Level for Electron(EFn) and Hole(EFp) in eV as a function of depth as shown in the 5.11 for GaAs and 5.12 for InP.

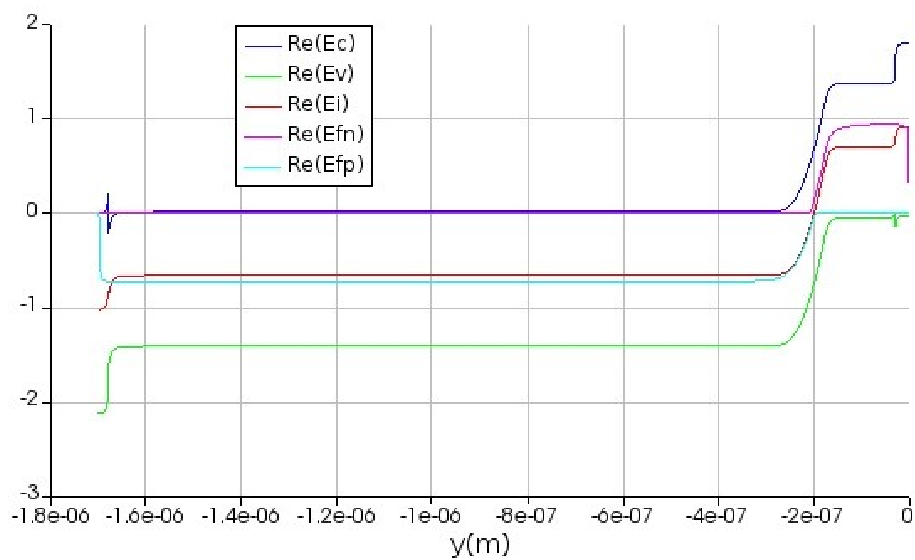

Figure 5.11: Band Structure for GaAs.

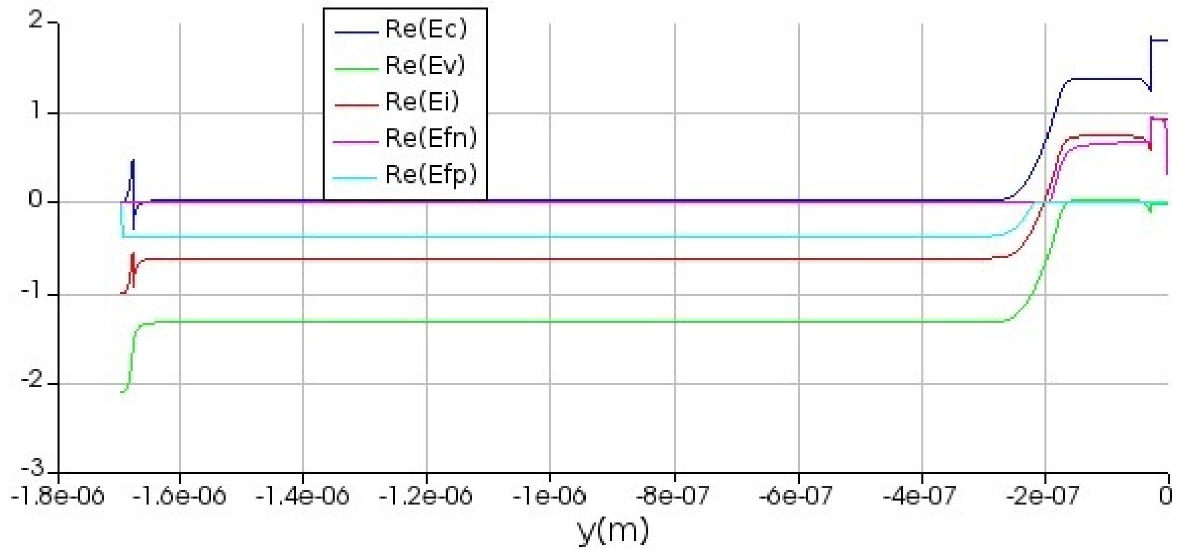

Figure 5.12: Band Structure for InP.

- <u>With contact shadow</u>

The ideal_ogr is disabled while the ogr (Optical Generation Rate group) is enabled and the generated file from FDTD (.mat file) is imported into the CHARGE Solver and simulations are performed.

The script for contact shadow has been opened and the plot results the Current Density-Voltage and Efficiency-Voltage graphs (Figure 5.13 and 5.14).

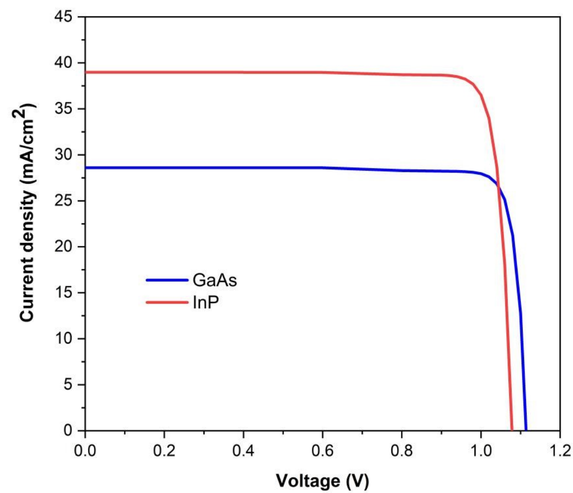

Figure 5.13: Current Density vs Voltage for GaAs and InP.

From the, the highest current density for GaAs obtained is 28.5975 mA/cm^2 while that for InP is 38.9771 mA/cm^2. The open-circuit voltage for GaAs is close to 1.11 V and that for InP is close to 1.079 V.

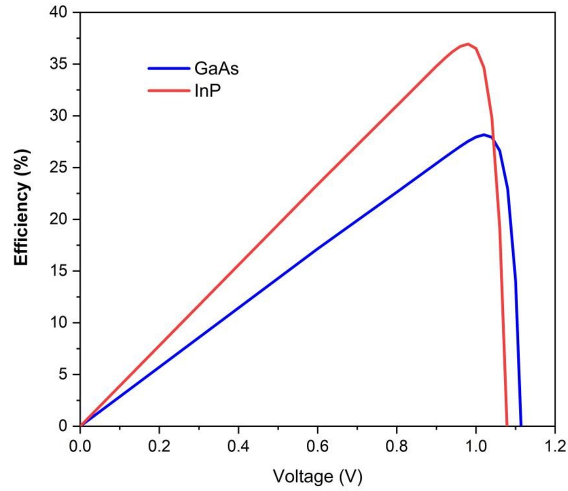

Figure 5.14: Efficiency vs Voltage for GaAs and InP.

The maximum peak efficiency reached by the GaAs structure is 28.1708 % while that by the InP structure is 36.9373 % as shown in the above.

In the forthcoming steps, the materials are changed to standard materials from the ideal materials and an iterative simulations are run with different settings as dI_{SC}ussed below.

Firstly, the Trap-Assisted function is disabled for all the materials for both the structures, while the Radiative and Auger recombination are kept enabled for all the materials and the script for contact shadow has been run. The graphs obtained are compared in 5.15 and 5.16.

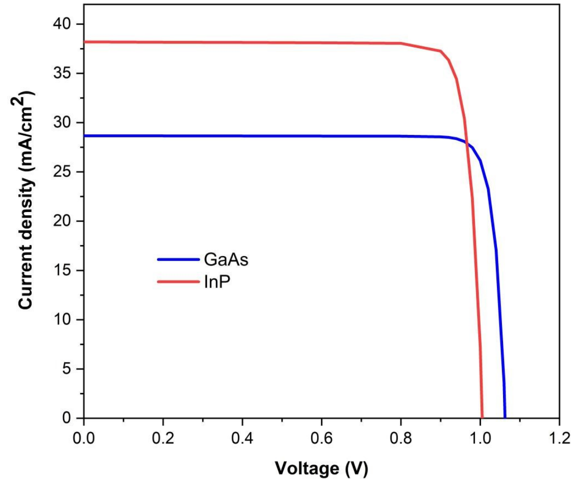

Figure 5.15: Current Density vs Voltage for GaAs and InP when Trap-Assisted is disabled.

From the, the highest current density for GaAs obtained is 28.669 mA/cm^2 while that for InP is 38.188 mA/cm^2. The open-circuit voltage for GaAs is close to 1.06 V and that for InP is close to 1.01 V.

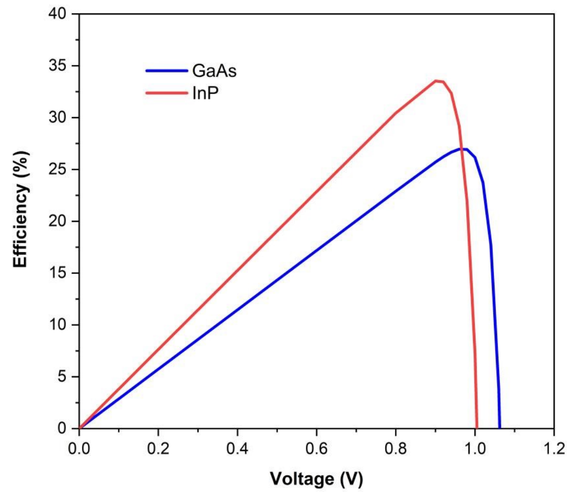

Figure 5.16: Efficiency vs Voltage for GaAs and InP when Trap-Assisted is disabled.

The maximum peak efficiency reached by the GaAs structure is 26.961 % while that by the InP structure is 33.5316 % as shown in the above.

Alternately, the Trap-Assisted function is re-enabled for all the materials and

the script is run again. The graphs obtained are compared in the 5.17 and 5.18 for both the GaAs and InP structures.

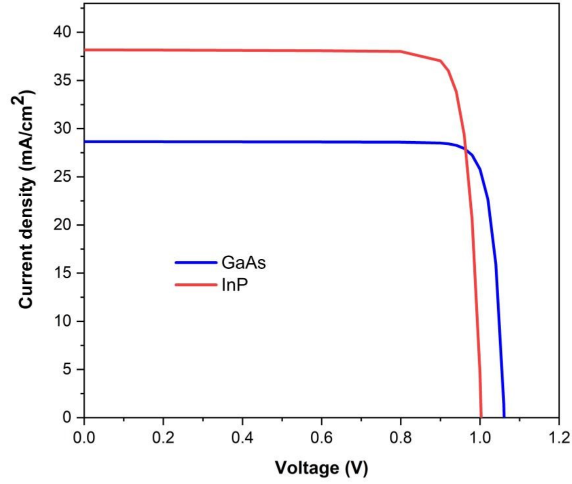

Figure 5.17: Current density vs Voltage for GaAs and InP with Trap-Assisted re-enabled.

From the, the highest current density for GaAs obtained is 28.6493 mA/cm^2 while that for InP is 38.175 mA/cm^2. The open-circuit voltage for GaAs is close to 1.06 V and that for InP is close to 1.01 V.

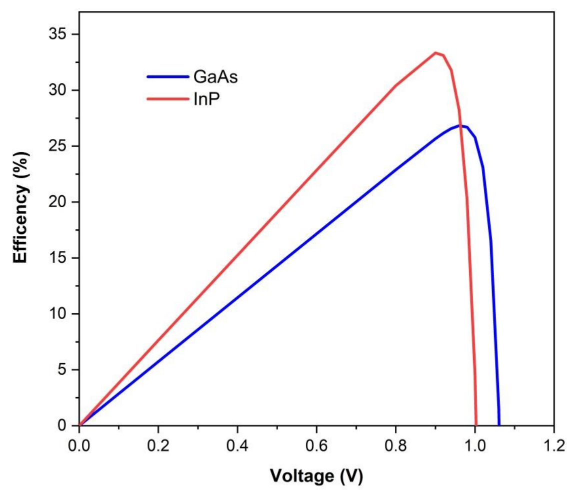

Figure 5.18: Efficiency vs Voltage for GaAs and InP with Trap-Assisted re-enabled.

The maximum peak efficiency reached by the GaAs structure is 26.8244 %

while that by the InP structure is 33.3372 % as shown in the above.

Besides, the recombination code for GaAs and InP are run for their corresponding structures and the results are plotted in 5.19 for GaAs and 5.20 InP.

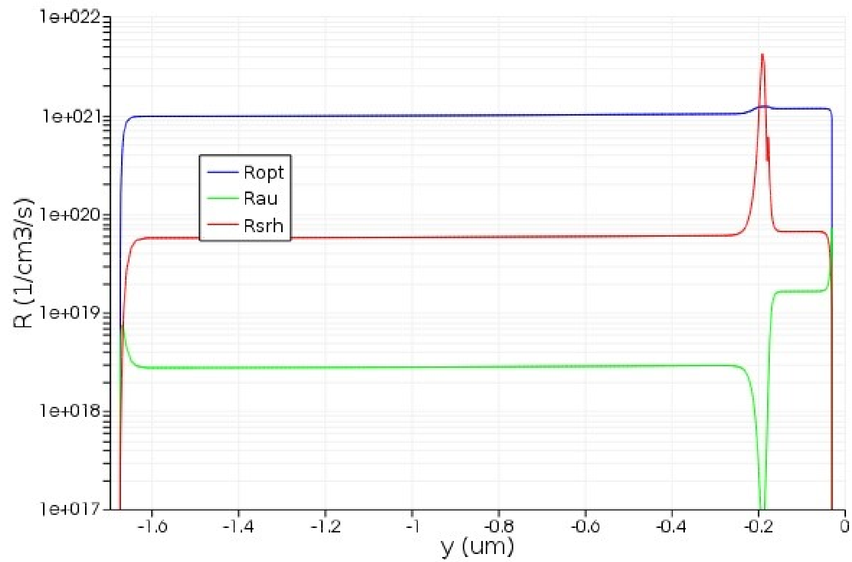

Figure 5.19: Recombination rate (Radiative, Auger, and Trap-Assisted) vs depth for GaAs.

From the, Radiative recombination rate is 91.6949% Auger recombination rate is the least which is 0.371643% and Shockley-Read Hall recombination rate is 7.93344%.

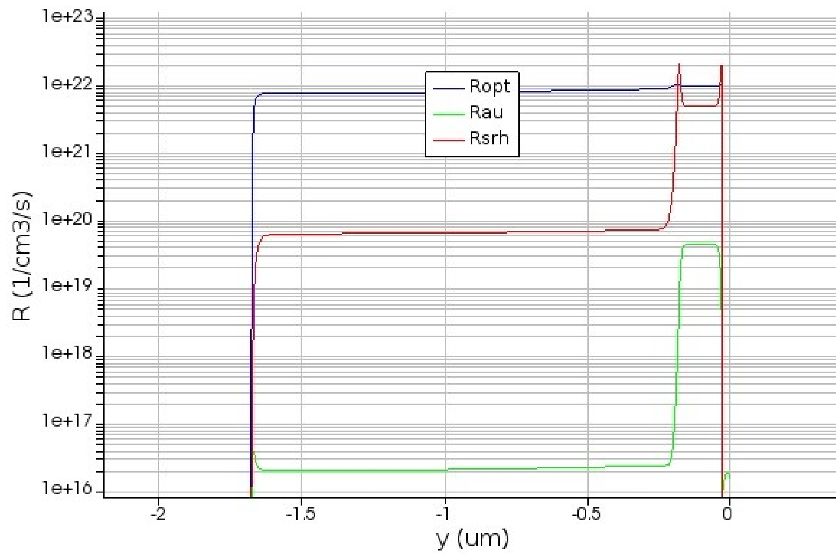

Figure 5.20: Recombination rate (Radiative, Auger, and Trap-Assisted) vs depth for InP.

Radiative recombination rate is 92.3591 % Auger recombination rate is the least which is 0.0415341 % and Shockley-Read Hall recombination rate is 7.59933 % as shown in the.

After successfully completing the previous simulations, the Series Resistance(RSE) has been enabled and the value is set to 3.5E+04 to observe the effect in current density and in efficiency.The code for contact shadow is run again and the graphs are plotted in 5.21 and 5.22.

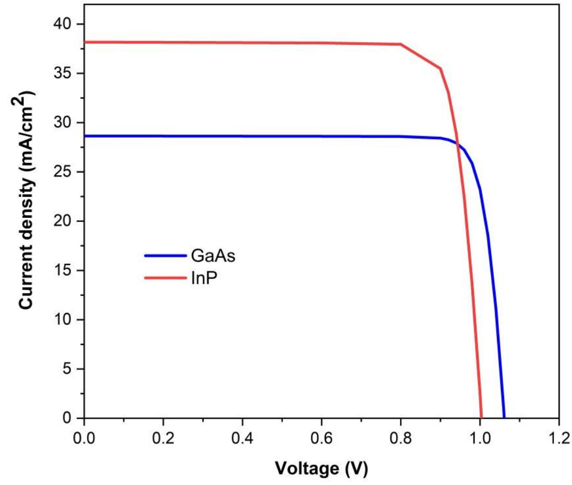

Figure 5.21: Current Density vs Voltage for GaAs and InP with RSE enabled.

From the, the highest current density for GaAs obtained is 28.6487 mA/cm^2 while that for InP is 38.1687 mA/cm^2. The open-circuit voltage for GaAs is close to 1.07 V and that for InP is close to 1.01 V.

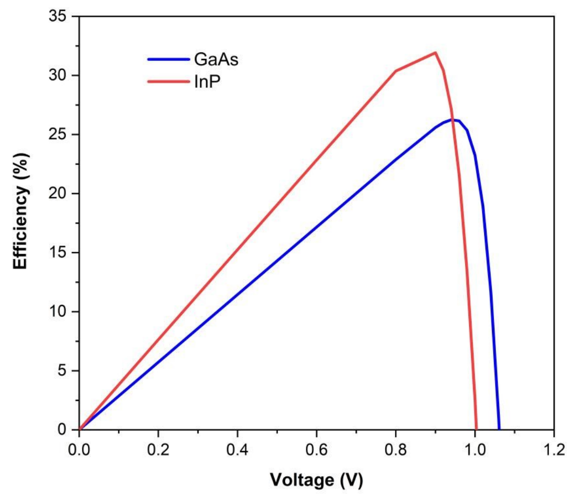

Figure 5.22: Efficiency vs Voltage for GaAs and InP with Rse enabled.

The maximum peak efficiency reached by the GaAs structure is 26.25 % while that by the InP structure is 31.9199 % as shown in the above.

Lastly, incorporating the altered value for the radiative recombination rate

coefficient brings about the effect of photon recycling and script is run again one more time for both the structures. The difference between the structures are shown in the 5.23 and 5.24.

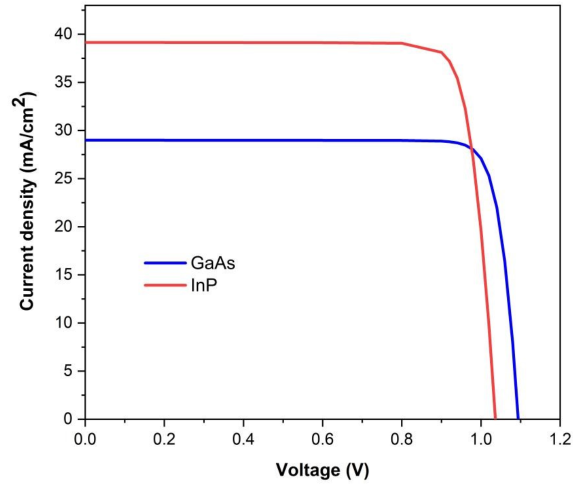

Figure 5.23: Current Density vs Voltage for GaAs and InP incorporating radiative recombination rate coefficient.

From the, the highest current density for GaAs obtained is 28.99 mA/cm^2 while that for InP is 39.1479 mA/cm^2. The open-circuit voltage for GaAs is close to 1.0 V and that for InP is close to 1.03 V.

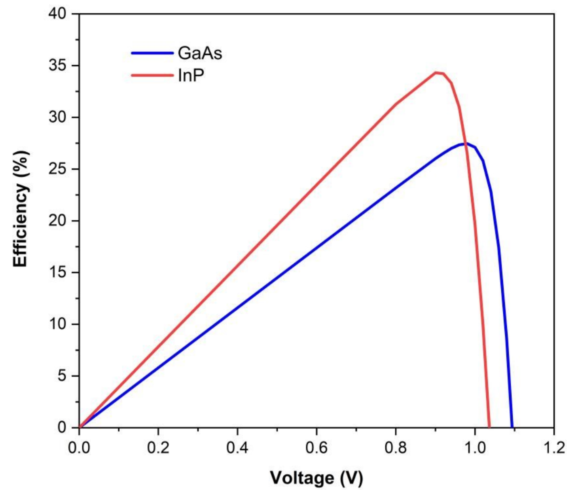

Figure 5.24: Efficiency vs Voltage for GaAs and InP incorporating radiative recombination rate coefficient.

For the ease of comparison and look-up at one place, the graphs are current density against voltage and efficiency against voltage are provided herein, 5.25 and 5.26.

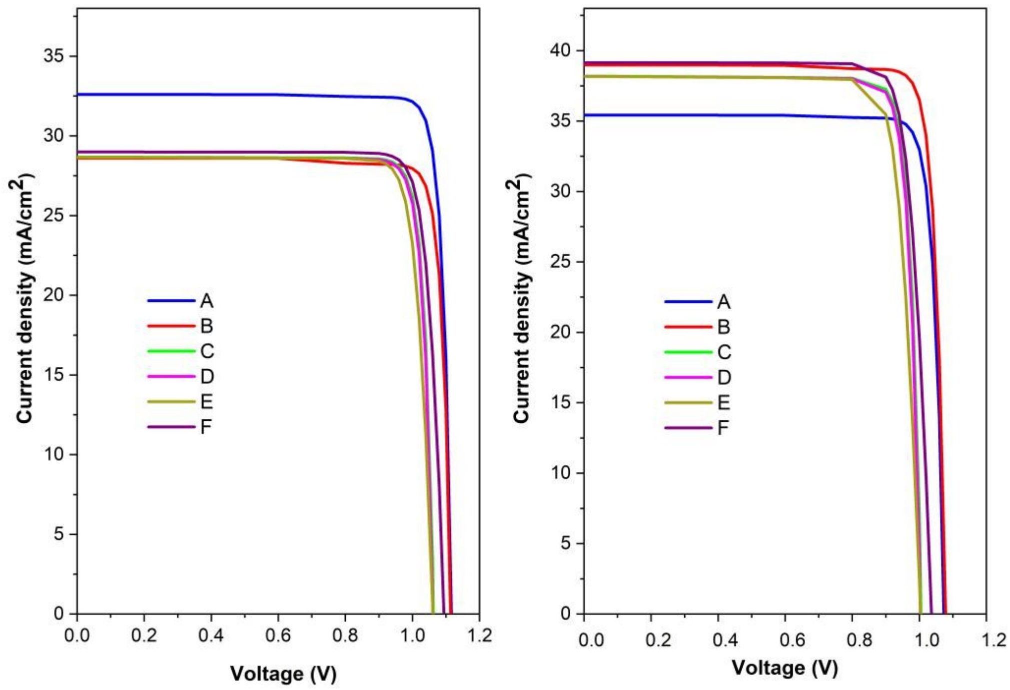

Figure 5.25: Current Density vs Voltage for both the models.

Here,

A: Ideal material without contact shadow

B: Non- Ideal material with contact shadow

C: Non- Ideal material with contact shadow and Trap-Assisted disabled

D: Non- Ideal material with contact shadow and Trap-Assisted re-enabled

E: Non- Ideal material with contact shadow and RSE enabled

F: Non- Ideal material with contact shadow and changed value of Radiactive Recombination Rate Coefficient

The maximum value of current density reached is 32.5941 mA/cm^2 for GaAs while that for InP is 39.1479 mA/cm^2 as shown in the 5.25.

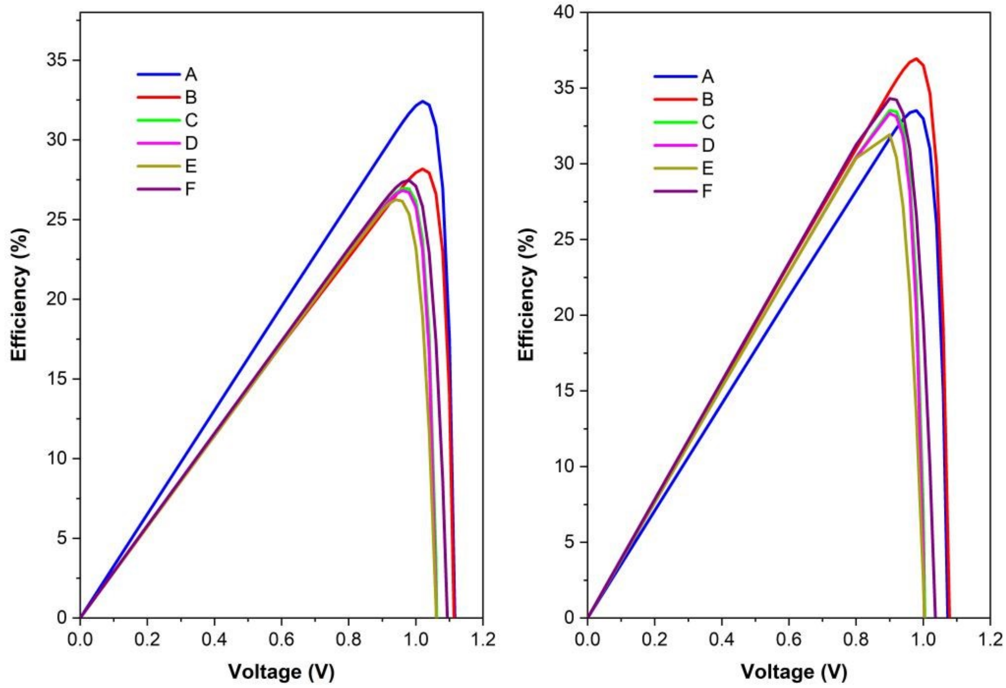

Figure 5.26: Efficiency vs Voltage for both the models.

Here,

- A: Ideal material without contact shadow
- B: Non- Ideal material with contact shadow
- C: Non- Ideal material with contact shadow and Trap-Assisted disabled
- D: Non- Ideal material with contact shadow and Trap-Assisted re-enabled
- E: Non- Ideal material with contact shadow and RSE enabled
- F: Non- Ideal material with contact shadow and changed value of Radiative Recombination Rate Coefficient

The maximum peak efficiency reached by the GaAs structure is 32.2334 % while that by the InP structure is 36.9373 % as shown in the above (Figure

5.26).

Finally, the maximum value of the key parameters obtained through out the research are summarized in the Table 5.3.

Parameters	$Al_xGa_{(1-x)}As/GaAs$	$Al_xGa_{(1-x)}As/InP$
Current Density (mA/cm^2)	32.5941	39.1479
Open Circuit Voltage (V)	1.11	1.079
Efficiency (%)	32.2334	36.9373

Table 5.3: Comparison of key parameters.

5.4 Conclusion

All the results obtained from both the FDTD and DEVICE. It has been observed that the proposed InP TSC model has 20.1% higher (J_{SC}) than GaAs TSC model. In addition to that, the open circuit voltage for InP TSC has a reduction of around 2.8% than GaAs TSC. Most importantly it has 14.6% higher efficiency and higher overall absorption rate than GaAs TSC. This significant result has been achieved because InP has much more closely matched to optimum use of solar spectrum and InP solar cell is more resistant to radiation degradation than GaAs solar cell.

Chapter 6

Conclusion and Future Work

6.1 Introduction

After successfully designing and analyzing the multi-junction thin film solar cell structures and comparing between the two models, the research have come to a ground where the summary of the research is discussed. In the preceding section, alongside the challenges faced during the whole research, the potential use and extension of the research is also discussed.

6.2 Thesis Summary

The main goal of this thesis is about to examine the usefulness of various structure, material, and dimensions to enhance the electrical and the optical properties of thin-film tandem solar cells to apply in an economical manner and give priority to the feasibility in the long run. After the procedure of ultimate development with Indium Phosphide(InP) as the base material, the finest result is achieved and hence shown. The mathematical and graphical outcomes on the basis of the FDTD simulation depicts that the proposed model shows greater absorption than the previous model due to the capability of the material itself to absorb the wide range of solar spectrum incident on the structure. The proposed model with InP as the substrate shows a current density of 39.1479 mA/cm^2 which is approximately 20.1% greater than that of the Gallium Arsenide (GaAs) as the base material. Moreover, the open circuit voltage (Voc) for InP structure is 1.079V which is a reduction of around 2.8% from the GaAs structure. In comparison of efficiency, which is our main concern, the value of efficiency of InP structure is 36.9373% which is roughly 14.6% higher than that of GaAs structure. To conclude, the design of the solar cell would now be composed of the proposed model, in order to substitute the less effective thin film Aluminium

Gallium Arsenide($Al_xGa_{(1-x)}As$)/Gallium Arsenide($GaAs$) tandem solar cell model. This design would not only open doors in terms of performance and efficiency only, but rather be compact and cost-effective.

6.3 Challenges

During the course of the research, several challenges were encountered. However, some were overcome, but many were left yet to be met which could have been possible in the long run. The challenges includes the following:

1. Selecting the desired model and the material. The research started from scratch, hence it was at ground zero. No light of direction was visible for the research to start primarily. However, with utmost literature review, this was overcome and the research was at a position to be carried out further.

2. After selecting the model and the material, it was a long and tiring process to fix the dimensions of each material of the structure.

3. Conversion of theory in the form of equations into the necessary code was needed for the simulation to take place. Incorporating the theory from various sources into couple of codes was troublesome. In the end, this challenge was completed with effective literature review.

4. The code was completed at this stage, but the simulation seemed to be the main barrier between the theory and the expected outcome. Various attempt was made to fix the simulation along with some modification of the code. Lastly, after trial and error method, the simulation was completed with each steps being carried out very carefully.

5. Next, various material would yield different outcomes, hence, changing the material, its properties and modifying the code accordingly was also one of the biggest challenge faced during the research.

6. Lack of resources. The software lacked the desired material which would fit best with the base material. The material library lacked these complementary materials in either of the software. As a result, this problem is not yet met. For example, when using InP as the base material, the complementary or adjacent materials required for simulation would be Indium Gallium Phosphide

(InGaP). Even the Internet of Things (IoT) failed to provide relevant data to create the material InGaP within the software. Hence, the research uses the next best available material to complement the base material.

7. Varying the mole fraction of the in-built alloy was next to impossible, let alone creating one. This problem still exists and might be solved in near future.

6.4 Future Work

The challenges which are yet to be overcome are discussed here as they may prove to provide better results and hence improve efficiency of the proposed model.

Firstly, plasmonic light trapping mechanism can be used which will absorb greater amount of light. Hence power absorbed would increase which would result greater generation of Electron-Hole Pair (EHP) and this may lead to greater photo current if proper steps are followed. Secondly, increasing the depth of the degenerately doped material might increase active area and hence greater absorption region. This would further lead to greater photo current and hence improved efficiency. Lastly, if one can change the doped material with the one that would fit best as explained earlier, he/ she might yield better results. To conclude, incorporating the mentioned steps may prove to be efficient, but care need to be taken on the overall cost as one would not want to manufacture the solar cell with such high cost. Lastly, one must balance the increasing cost and improved result when designing the cost-effective solar cell that would prove to be efficient.

Bibliography

[1] J. Wang, S. Jia, Y. Cao, W. Wang, and P. Yu, "Design principles for nanoparticle plasmon-enhanced organic solar cells," *Nanoscale research letters*, vol. 13, no. 1, pp. 1–6, 2018.

[2] J. A. Duffie and W. A. Beckman, *Solar engineering of thermal processes*. John Wiley & Sons, 2013.

[3] D. Friedman, J. Olson, and S. Kurtz, *Chapter 8 of handbook of photovoltaic science and engineering. chichester*, 2011.

[4] S. Hossain, N. Amin, M. Martin, M. M. Aliyu, T. Razykov, and K. Sopian, "A numerical study on the prospects of high efficiency ultra thin zn x cd 1-x s/cdte solar cell.," *Chalcogenide Letters*, vol. 8, no. 4, 2011.

[5] M. M. Rana, S. M. F. Khan, and M. S. Shafayat, "Design and optimization of algaas/inp multi-junction solar cell," in *2019 1st International Conference on Advances in Science, Engineering and Robotics Technology (ICASERT)*, IEEE, 2019, pp. 1–5.

[6] Z. J. Yu, M. Leilaeioun, and Z. Holman, "Selecting tandem partners for silicon solar cells," *Nature Energy*, vol. 1, no. 11, pp. 1–4, 2016.

[7] F. Dimroth, M. Grave, P. Beutel, U. Fiedeler, C. Karcher, T. N. Tibbits, E. Oliva, G. Siefer, M. Schachtner, A. Wekkeli, *et al.*, "Wafer bonded four-junction gainp/gaas//gainasp/gainas concentrator solar cells with 44.7% efficiency," *Progress in Photovoltaics: Research and Applications*, vol. 22, no. 3, pp. 277–282, 2014.

[8] V. Raj, *J.Phys.* D:Appl.Phys, 2018.

[9] K. K. Likharev and D. B. Strukov, "Cmol: Devices, circuits, and architectures," in *Introducing Molecular Electronics*, Springer, 2006, pp. 447–477.

[10] *Semiconductor materials*. [Online]. Available: https://www.pveducation.org/pvcdrom/pn-junctions/semiconductor-materials.

[11] S. O. Kasap *et al.*, *Optoelectronics and photonics*. Pearson Education UK, 2013.

[12] *This month is physics history*, 2019.

[13] M. A. Green, E. D. Dunlop, J. Hohl-Ebinger, M. Yoshita, N. Kopidakis, and A. W. Ho-Baillie, "Solar cell efficiency tables (version 55)," *Progress in Photovoltaics: Research and Applications*, vol. 28, no. 1, pp. 3–15, 2020.

[14] A. R. Jeong, S. B. Choi, W. M. Kim, J.-K. Park, J. Choi, I. Kim, and J.-h. Jeong, "Electrical analysis of c-si/cgse monolithic tandem solar cells by using a cell-selective light absorption scheme," *Scientific reports*, vol. 7, no. 1, pp. 1–10, 2017.

[15] V. Shrotriya, G. Li, Y. Yao, T. Moriarty, K. Emery, and Y. Yang, "Accurate measurement and characterization of organic solar cells," *Advanced functional materials*, vol. 16, no. 15, pp. 2016–2023, 2006.

[16] Q. J. Daigle, "Applications of luminescent solar concentrators," 2020.

[17] F. A. Lindholm, J. G. Fossum, and E. L. Burgess, "Application of the superposition principle to solar-cell analysis," *IEEE transactions on electron devices*, vol. 26, no. 3, pp. 165–171, 1979.

[18] W. b. A. 1. 2013, *Indium phosphide (inp) semiconductors*, Jun. 2013. [Online]. Available: http://www.azom.com/article.aspx?ArticleID=8364.

[19] *Basic parameters*, 2017. [Online]. Available: www.ioffe.ru/SVA/NSM/Semicond/InP/bandstr.html.

[20] T. S. Chao, C. L. Lee, and T. F. Lei, "The refractive index of inp and its oxide measured by multiple-angle incident ellipsometry," *Journal of materials science letters*, vol. 12, no. 10, pp. 721–723, 1993.

[21] [Online]. Available: http://www.iue.tuwien.ac.at/phd/palankovski/node32.html.

[22] U. G. I. J. O. AKINLAMI*, *Optical properties of indium phosphide*, 2014.

[23] *Doping*. [Online]. Available: http://www.pveducation.org/pvcdrom/pn-junctions/doping.

[24] G. L. Araujo, "Limits to efficiency of single and multiple band gap solar cells," *Physical Limitations to Photovoltaic Energy Conversion*, vol. 106, 1990.

[25] V. Raj, *J.Phys.* D:Appl.Phys, 2018.

[26] [Online]. Available: https://g2voptics.com/photovoltaics-solar-cells/types-of-solar-cells/.

[27] B. Roberts, "Photovoltaic solar resource of the united states," *National Renewable Energy Laboratory*, 2008.

[28] S. M. -, By, -, S. Mag., and here, *[comparison] monocrystalline vs polycrystalline solar panels*, Nov. 2020. [Online]. Available: https://solarmagazine.com/solar-panels/monocrystalline-vs-polycrystalline-solar-panels.

[29] L. G. s. A. 19 and L. G. says: *Innovation: Thin film solar cells at mx2016*, Jan. 2016. [Online]. Available: https://materialdistrict.com/article/innovation-thin-film-solar-cells-at-mx2016/.

[30] *Thin film solar cell*, Aug. 2015. [Online]. Available: https://en.wikipedia.org/wiki/Thin_film_solar_cell.

[31] J. M. Roman, "State-of-the-art of iii-v solar cell fabrication technologies, device designs and applications," *Advanced Photovoltaic Cell Design*, 2004.

[32] *Thin film solar cell*, Aug. 2015. [Online]. Available: https://en.wikipedia.org/wiki/Thin_film_solar_cell.

[33] H. Shirakawa, E. J. Louis, A. G. MacDiarmid, C. K. Chiang, and A. J. Heeger, "Synthesis of electrically conducting organic polymers: Halogen derivatives of polyacetylene,(ch) x," *Journal of the Chemical Society, Chemical Communications*, no. 16, pp. 578–580, 1977.

[34] C. Rollet, *An organic solar cell with 25% efficiency*, Mar. 2020. [Online]. Available: http://www.pv-magazine.com/2020/03/24/an-organic-solar-cell-with-25-efficiency/.

[35] [Online]. Available: https://physicsworld.com/a/metallic-tin-reduces-limitations-of-perovskite-solar-cells/.

[36] *Sustainable product innovation using dye-sensitized solar cells*, Dec. 2020. [Online]. Available: http://www.borderstep.org/projects/sustainable-product-innovation-using-dye-sensitized-solar-cells/.

[37] M. Yamaguchi, "Iii–v compound multi-junction solar cells: Present and future," *Solar energy materials and solar cells*, vol. 75, no. 1-2, pp. 261–269, 2003.

[38] *Best research-cell efficiency chart.* [Online]. Available: https://www.nrel.gov/pv/cell-efficiency.html.

[39] J. F. Geisz, R. M. France, K. L. Schulte, M. A. Steiner, A. G. Norman, H. L. Guthrey, M. R. Young, T. Song, and T. Moriarty, "Six-junction iii–v solar cells with 47.1% conversion efficiency under 143 suns concentration," *Nature energy*, vol. 5, no. 4, pp. 326–335, 2020.

[40] J. Zhao, A. Wang, M. A. Green, and F. Ferrazza, "19.8% efficient "honeycomb" textured multicrystalline and 24.4% monocrystalline silicon solar cells," *Applied physics letters*, vol. 73, no. 14, pp. 1991–1993, 1998.

[41] *Semiconductor*, Jan. 2021. [Online]. Available: https://en.wikipedia.org/wiki/Doping/semiconductor.

[42] Y. Baghzouz, "Basic photovoltaic theory," *Handbook of Clean Energy Systems*, pp. 1–13, 2015.

[43] H. Kim, S.-Y. Ahn, S. Kim, G. Ryu, J. H. Kyhm, K. W. Lee, J. H. Park, and W. J. Choi, "Inas/gaas quantum dot infrared photodetector on a si substrate by means of metal wafer bonding and epitaxial lift-off," *Optics express*, vol. 25, no. 15, pp. 17 562–17 570, 2017.

[44] D. A. Clugston and P. A. Basore, "Modelling free-carrier absorption in solar cells," *Progress in Photovoltaics: Research and Applications*, vol. 5, no. 4, pp. 229–236, 1997.

[45] *Quantum efficiency.* [Online]. Available: http://www.pveducation.org/pvcdrom/solar-cell-operation/quantum-efficiency.

[46] *Finite-difference time-domain method*, Jan. 2021. [Online]. Available: https://en.wikipedia.org/wiki/Finite-difference_time-domain_method.

[47] A. S. Mohsin and M. B. Salim, "Probing the intracellular refractive index and molecular interaction of gold nanoparticles in hela cells using single particle spectroscopy," *International journal of nanomedicine*, vol. 13, p. 6019, 2018.

[48] D. Sullivan, J. Liu, and M. Kuzyk, "Three-dimensional optical pulse simulation using the fdtd method," *IEEE transactions on microwave theory and techniques*, vol. 48, no. 7, pp. 1127–1133, 2000.

[49] S. D. Gedney, "Introduction to the finite-difference time-domain (fdtd) method for electromagnetics," *Synthesis Lectures on Computational Electromagnetics*, vol. 6, no. 1, pp. 1–250, 2011.

[50] A. Taflove and S. C. Hagness, *Computational electrodynamics: the finite-difference time-domain method.* Artech house, 2005.

[51] K. Yee, "Numerical solution of initial boundary value problems involving maxwell's equations in isotropic media," *IEEE Transactions on antennas and propagation*, vol. 14, no. 3, pp. 302–307, 1966.

[52] E. Lindman, "
free-space" boundary conditions for the time dependent wave equation," *Journal of computational physics*, vol. 18, no. 1, pp. 66–78, 1975.